Evaluation of a NEMO model of the Strait of Georgia and insights into mixing and transport of the Fraser River plume

by

Jie Liu

B.Sc., Ocean University of China, 2014

A THESIS SUBMITTED IN PARTIAL FULFILLMENT OF
THE REQUIREMENTS FOR THE DEGREE OF

MASTER OF SCIENCE

in

The Faculty of Graduate and Postdoctoral Studies

(Oceanography)

THE UNIVERSITY OF BRITISH COLUMBIA

(Vancouver)

April 2017

Abstract

The goals of this modeling study of the Fraser River plume, located in the Strait of Georgia, British Columbia, are twofold. Firstly, it aims at improving the Fraser River plume properties by evaluating the model results with various available observations. Secondly, mixing and transport processes within the plume, driven by different forcing factors, are investigated with the improved configuration to understand the plume dynamics in the model. The problems found by comparing with ferry-based salinity data, drifter data and CTD data in the modeled Fraser River properties are: (1) too weak cross-strait velocities; (2) too strong along-strait flows; (3) too salty surface water. To fix the problems, a longer and deeper river channel was created and added into the model. The results show promising improvements with stronger cross-strait motions. Background vertical eddy viscosity was reduced from 1×10^{-4} to 1×10^{-5} m^2s^{-1}, which tends to reduce the along-strait velocities. In addition, background vertical eddy diffusivity was reduced to 1×10^{-6} m^2s^{-1} which reduced the surface salinity. Furthermore, effects of river discharge, tides, winds and the Coriolis force are explored on plume mixing and transport. As expected, plume size increases with increasing river outflow. Tides are important in mixing at the river mouth and inside the river channel during low and moderate river flow periods with wind magnitude smaller than 5 m s^{-1}, whereas winds become the dominant factor in mixing over almost the entire plume domain when wind speed is greater than 5 m s^{-1}. The Coriolis force strengths the northward flux across a transect north of

the river mouth when winds are not strong, resulting in a fresher plume in English Bay, north of the City of Vancouver. This thesis provides both a guide to accurately modeling the Fraser River plume and insight into plume dynamics.

Preface

This thesis contains detailed numerical experiments and analysis conducted and undertaken primarily by the author, Jie Liu. Susan Allen was my supervisor on this project and contributed substantially on suggesting modeling techniques, interpreting the results and editing the manuscript. This work is previously unpublished, although a manuscript version of Chapter 2 is prepared to submit for publication in the future.

Table of Contents

Appendices

List of Tables

List of Figures

List of Acronyms

SoG Strait of Georgia

SJDF Juan de Fuca Strait

GLS Generic Length Scale

CTD Conductivity Temperature Depth

IOS Institute of Ocean Sciences

NEMO Nucleus for European Modelling of the Ocean

CGRF Canadian Meteorological Centre's 33 km Global Atmospheric Reforecasting Model

HRDPS High Resolution Deterministic Prediction System

ROMS Regional Ocean Modeling System

POM Princeton Ocean Model

TKE Turbulent Kinetic Energy

Acknowledgements

I would really like to thank Susan Allen, my supervisor, who gave me such an interesting and well-structured project as well as countless encouragement and suggestions during my masters study. Susan is an organized, well-respected, humorous and knowledgeable professor who always cares the most about her graduate students. I enjoy the regular weekly individual meeting with you, and all the guidance and assistance that you provide. I also appreciate the many conference opportunities I have had that you supported, which both broadened my research horizons and made me more social.

I would like to thank my committee members, Nancy Soontiens and Mark Halverson. Thank you for committing your time, enthusiasm and useful suggestions throughout my whole master program. In particular, Nancy, thank you for always being so patient and helpful whenever I turn to you and always encouraging me no matter how silly the mistake I made.

Thank you to Richard Pawlowicz for examining my thesis carefully and the suggestions and comments during the physical oceanography seminar.

I consider myself very lucky to be in the Salish Sea modeling group and thank you to every team member for discussing the modeling issues during each group meeting and being in such harmony. Thanks to Ben Moore-Maley, for providing your movie of surface currents to help me understand the circulation pattern and listening to my pre-defense as well as my pre-talk for seminar with patience

and many helpful tips. Also thanks to you, Doug Latornell, for teaching and fixing Mercurial and web-related problems for me.

Last but not the least, thank you to my enlightened parents for supporting me to study abroad and to my husband Tony for your consistent companionship, encouragement and love.

Chapter 1

Introduction

1.1 The Strait of Georgia and the Fraser River Estuary-Plume System

The Strait of Georgia (hereafter SoG) is a strongly stratified, semi-enclosed ocean basin located between Vancouver Island and the mainland coast of British Columbia, Canada, constituting one of Canada's major ecological marine environments (Thomson, 1981). It is part of the larger Strait of Georgia-Juan de Fuca-Puget Sound system, collectively known as the Salish Sea. The SoG is around 220 km long and 28 km wide and 155 m deep on average, with a maximum depth exceeding 400 m in the central strait. The SoG connects to the Pacific Ocean via Juan de Fuca Strait (hereafter SJDF) at the south and narrow but relatively long Johnstone Strait at the north. At the south, Haro Strait is the largest passage connecting with SJDF and is a strong tidal mixing region due to the complex bathymetry and steep topographic slopes (Thomson, 1981; Soontiens et al., 2016).

Prevailing winds in the SoG are predominately from the northwest in summer, when clockwise motion of air around the North Pacific High centred west of California dominates and southeast in winter, which is driven by the strong anticlockwise flow of air around the Aleutian Low that develops just south of Alaska. In general, winds are channeled along the SoG by the mountainous terrain (Stronach, 1981; Halverson, 2009). Winds are typically lighter and more variable in direction in

summer when southeasterlies and southwesterlies dominate the southern Strait while northwesterlies dominate the northern Strait (Thomson, 1981).

Mixed semi-diurnal and diurnal tides are found throughout most of the Salish Sea, although tides are mainly semi-diurnal. The tidal range undergoes a bi-weekly variation due to the spring/neap (i.e., lunar phase) and tropic/equatorial (i.e., lunar declination) cycling (Thomson, 1981; Halverson, 2009). The minimum daily tidal range at Pt. Atkinson is around 1.9 m while the maximum reaches about 5.0 m (Halverson, 2009).

The barotropic tides form a standing wave in the SoG, produced by a combination of northward progressive ocean tides that enter from the SJDF and southward reflected waves that are reflected from the northern end of the SoG. The characteristics of the standing wave affect the timing of maximum flood and ebb within the SoG, where maximum flood occurs roughly 3 hrs before high water and maximum ebb around 3 hrs before low water. The standing wave is more pronounced in the northern SoG and river channels and weakens slightly southward where the progressive tides becomes more prevalent (Thomson, 1981).

The Fraser River is the largest single source of freshwater that empties into the SoG, supplying up to 50-85% of total freshwater in the Strait (Crean et al., 1988; Pawlowicz et al., 2007). It originates in the Rocky Mountains near Jasper, Alberta, descends rapidly until Hope, BC, and starts a 160 km journey through the Fraser valley to the SoG (Thomson, 1981). The Fraser River plume is formed by discharge from each of its three arms and Canoe Pass, with the southern (main) arm carrying roughly 75% of the total river flow, located 15 km south of Vancouver, with the remaining outflow divided among the North Arm (15%), the Middle Arm (5%) and Canoe Pass (5%) (Thomson, 1981). The plume thickness varies within the upper 10 m (Stronach, 1981) and was selected as 7 m by Halverson and Pawlowicz (2011).

The Fraser River estuary is considered a salt-wedge type estuary (Geyer and Farmer, 1989) (Figure 1.1). The location of salt-wedge depends on river discharge and tides (Crean et al., 1988; Geyer and Farmer, 1989; Kostaschuk and Atwood, 1990). Through an observational-based parametrization, Kostaschuk and Atwood (1990) predict that the tip of salt-wedge (practical salinity of 10) can propagate upstream of the mouth at Steveston by 30 km at high tides and by 22 km at low tides during low river flow (around 700 m^3s^{-1} at Hope). During high river flow (freshet period, flows around 8000 m^3s^{-1} at Hope), the salt-wedge position is at the mouth at low tides and 10 km upstream at high tides.

Similar with tides in the SoG, tides in the estuary are mixed, mainly semi-diurnal. Tides in the estuary channel are influenced by the amount of freshwater carried downstream. For example, the tides can be detected at Chilliwack, 100 km upstream of Steveston during the winter period of low flows. During the freshet, the tides cannot be detected beyond Mission, around 60 km upstream (Thomson, 1981).

Geometry in the river mouth region is complex (Stronach, 1981). Beyond the mouth at Steveston, a rock jetty breakwater protects a 9 km channel through tidal mud flats to Sand Heads, a meteorological station. The depth of the channel is about 12 m on average (Halverson, 2009).

The volume of Fraser River discharge varies considerably from year to year and also seasonally (Thomson, 1981). Annual discharge peaks in late May and early June due to snow-melt. This maximum, called the freshet, discharge ranges from 6000-10000 m^3s^{-1} between 2014-2016 at Hope. River discharge decreases significantly to about 2000 m^3s^{-1} by the end of August and reaches about 800 m^3s^{-1} by early December which continues until the following spring. However, winter rain storms can cause river discharge at the mouth to more than double over the span of a few days (Halverson and Pawlowicz, 2011).

1.2 Past Modeling Studies on the Fraser River Plume

The Fraser River plume is distinct from most previously studied river plumes that are located on the shelf, such as Columbia River plume, Changjiang River plume and Merrimack River plume. The Fraser River plume thickness is less than 10 m (Stronach, 1981). Compared to the Columbia River plume which is typically 20 m thick (MacCready et al., 2009), Changjiang River plume with thickness around 18 m at maximum ebb during spring tide (Wu et al., 2011), the Fraser River plume is thinner. The Fraser River plume surface area was estimated with a combination of ferry-based data and satellite images and it varies from around 400 km^2 during low river flow periods and to 1700 km^2 during freshets, when the plume may span the SoG (Tabata, 1972; Halverson and Pawlowicz, 2008). The Fraser River plume depth in the plume surface area is not a constant and it changes in space. For instance, S2-3 station and S3 station of STRATOGEM observation project are considered in the Fraser River plume area [Figure 1, (Halverson and Pawlowicz, 2011)], but the difference of plume depth is about 1 m during low river discharge ($<$3500 m^3s^{-1}) and up to 4 m during high river discharge ($>$3500 m^3s^{-1}) assuming plume salinity threshold is 25 as an example (Figure 3 in (Halverson and Pawlowicz, 2011)). Recent CTD profiles in October, 2014 in the region directly influenced by the Fraser River discharge (Figure 1.2) show salinity stratification occurs mostly in the upper 10 m with salinity values below about 30, which are generally in agreement with the study of Stronach (1981).

Previous modeling studies of the SoG, in particular the Fraser River plume date back to the 1980s. Stronach (1981) developed an upper-layer model using a control-volume approach to simulate the plume although sufficient calibration and verification were not done due to lack of observations. This model did not include wind stress. Based on Stronach (1981), Royer and Emery (1985) further calibrated the same model with measured salinity from ferry data (Royer and Emery, 1982),

added wind stress and found the effect of the varying river discharge on salinity in the model was minimal. They improved model performance by modifying entrainment velocities to be dependent on stratification and reducing the newly included wind stress term for regions with high salinity. They found plume salinity along the northern ferry route, which is between Horseshoe Bay and Nanaimo (Royer and Emery, 1982), was more sensitive to changes in the entrainment velocity due to the stronger influence of discharge fluctuations but the salinity of southern ferry route between Tsawwassen and Swartz Bay was more affected by the change of wind stress. However, the northern end of the SoG was not included, which would influence the freshwater circulation (Royer and Emery, 1985). Marinone et al. (1996) used a three-dimensional baroclinic model which was forced by tides, winds and runoff, to study the residual current in the central SoG generated by these forcing agents and by interaction among them. They discovered that the one-year mean residual at the first layer (0-5 m) showed the river discharge enters the Strait and is deflected northward by the Coriolis force. Wind stress pushes this layer northward as a slab. They defined the residual current as the flow remaining after low pass filtering with a 2-day cut-off. This residual contains both a time-averaged and a fluctuating component. The total residual maximum speed can reach 0.4 m s^{-1} at the surface. Time-averaged residual speed is about 0.1 m s^{-1} at the surface away from the river mouth. More recently, Masson and Cummins (2004) evaluated time-averaged salinity in the surface freshwater plume, including the Fraser River plume, produced by the Princeton Ocean Model (POM) with observed CTD salinity. They found the surface plume is more trapped in the south compared to the observations, and they argued this problem was caused by inadequate representation of runoff in the northern Strait and also inaccurate salinity values at the northern end of SoG.

In summary, past modeling studies discovered some plume characteristics, such as the modeled averaged residual current speed in the central SoG is about 0.1 m s^{-1} at the surface away from the

river mouth (Marinone et al., 1996). However, there are a number of limitations in the previous studies. One example is that runoff in the northern Strait is not represented appropriately in the study of Masson and Cummins (2004), which affects the surface plume location. In this thesis, a three-dimensional baroclinic ocean model, which solves the three-dimensional hydrostatic equations of motion for an incompressible fluid under the Boussinesq approximation on a structured computational grid (Madec, 2012; Soontiens et al., 2016), will be used to simulate the Fraser River plume. The focus will be on improving small-scale dynamical features with high spatial and temporal variability and understanding the impact of forcings on plume dynamics, such as river flows, tides, winds and the Coriolis force. The ultimate goal is to predict the plume movement and properties.

1.3 The Model Configuration

In this study, the Nucleus for European Modelling of the Ocean (NEMO) framework version 3.4 in its regional configuration (Madec, 2012) has been employed to model the whole Salish Sea. The model domain extends from the SJDF at the west to Puget Sound at the south to Johnstone Strait at the north. The curvilinear orthogonal numerical domain has been divided into 398 by 898 grid points horizontally and 40 levels vertically, with around 500 m resolution horizontally. Vertical spacing is unequal. It is 1 m for the upper 10 m and increases smoothly to a maximum of 27 m starting from around 150 m to the bottom (Soontiens et al., 2016). The purpose of this spacing is to better resolve the surface plume structure. The initial model used a crude representation of the Fraser River. It was 10 km long, up to 2 km wide and depths were set to 4 m. This representation is not realistic. As will be shown, lengthening and deepening the river channel affects tidal propagation in the river, and thus influences the cross-strait velocity at the river mouth. Similar river treatment was performed for the Columbia River in Regional Ocean Modeling System (ROMS), where a straight

river channel was added and extended 300 km to the east (MacCready et al., 2009). This river geometry was considered as the most realistic one for tidal energy dissipation (MacCready et al., 2009).

This NEMO model in the Salish Sea region was spun up for 15.5 months, starting on September 16, 2002, with initial uniform horizontal conditions for temperature and salinity from a CTD cast in the middle of the SoG taken in September, 2002. Velocity was initialized at zero. The atmospheric forcing from 2002 to 2003 is the Canadian Meteorological Centres 33 km global atmospheric reforecasting model (CGRF) (Smith et al., 2014). Temperature, salinity and sea surface height at the boundaries are climatologies, as well as tides and climatology river discharge (Soontiens et al., 2016). Using the September 7, 2003 temperature and salinity field, the model was restarted from zero velocities on September 10, 2014. Since then, the model has run operationally producing daily nowcasts for the current day and up to two 30 hr forecasts across the whole domain, with forcing of daily Fraser River runoff, eight tidal constituents at the west and north open boundaries and daily operational model winds employing the western Canada component of the High Resolution Deterministic Prediction System (HRDPS, `https://weather.gc.ca/grib/grib2_HRDPS_HR_e.html`).

1.4 Vertical Turbulence Scheme

The surface currents in the plume are sensitive to two model physical parameters: vertical eddy viscosity and diffusivity. These two turbulence coefficients are used to model the vertical turbulent fluxes of momentum and tracers. The coefficients are calculated by the $k - \varepsilon$ configuration of the generic length scale (hereafter GLS) turbulence scheme (Umlauf and Burchard, 2003) and then the maximum of these values and the background vertical eddy viscosity and diffusivity parameters values are used.

The GLS turbulence closure scheme computes the vertical eddy viscosity and diffusivity using (1.1). The mixing length l and turbulent kinetic energy k are calculated through a set of differential equations and the stability functions C_μ and C'_μ are derived from the Reynolds stress equations and depend on shear and buoyancy numbers. Consequently, the turbulent coefficients are calculated and updated using the equations below:

$$\begin{aligned} \nu_t &= C_\mu \sqrt{k} l, \\ \kappa_t &= C'_\mu \sqrt{k} l \end{aligned} \tag{1.1}$$

where ν_t and κ_t are vertical viscosity and diffusivity, respectively (Reffray et al., 2015). Most frequently used closures available in the GLS scheme are : $k-kl$, $k-\varepsilon$ and $k-w$ (Reffray et al., 2015). In a comparison of several turbulence closures, including $k-\varepsilon$, $k-w$ and $k-kl$, Reffray et al. (2015) found that the $k-\varepsilon$ configuration had the smallest salinity bias in a modelling study covering the North Pacific Ocean during the period June 2010-June 2011. The $k-\varepsilon$, $k-w$ and $k-kl$ closures are known as two-equation models because the differential equation for turbulent kinetic energy is solved alongside a second differential equation that determines the mixing length scale.

Alternatively, single equation models, like the Turbulent Kinetic Energy (hereafter TKE) model, uses an algebraic expression for the mixing length scale and a differential equation for the turbulent kinetic energy (Reffray et al., 2015). Comparing GLS turbulence scheme with TKE turbulence scheme, Reffray et al. (2015) found that GLS is more accurate in reproducing the mixed layer depth deepening of an initially linear stratified fluid subjected to a stationary surface stress than the

TKE closure. As a consequence, $k-\varepsilon$ closure of GLS turbulence scheme was employed to compute turbulence parameters of vertical eddy viscosity and diffusivity in this study.

The background vertical eddy viscosity and diffusivity are set to ensure a minimum level of mixing (Reffray et al., 2015). Typical values used in process studies are:

$$\begin{aligned} \nu_b &= 1.2 \times 10^{-4} \mathrm{m^2 s^{-1}}, \\ \kappa_b &= 1.2 \times 10^{-5} \mathrm{m^2 s^{-1}}, \end{aligned} \tag{1.2}$$

where ν_b is background vertical eddy viscosity and κ_b is background vertical eddy diffusivity (Madec, 2012). These two values must be greater than those associated with molecular viscosity of $\sim 10^{-6}$ $\mathrm{m^2 s^{-1}}$ and molecular diffusivity of $\sim 10^{-9}$ $\mathrm{m^2 s^{-1}}$ for salinity (Madec, 2012). Actual values are the maximum of values calculated from the $k-\varepsilon$ configuration of GLS turbulence scheme and the corresponding background values that are set.

1.5 Mixing in a River Plume

A river plume impacts shelf circulation and ecosystem health by its salinity dilution and transport processes. Dilution is driven largely by vertical mixing (Horner-Devine et al., 2015). In a single system, the mixing of the plume and the associated plume structure can change with forcing, such as river discharge, tidal range, winds and the Coriolis force (Horner-Devine et al., 2015). Three interacting dynamical regions have been previously identified provided that the width of river mouth is small relative to the Rossby deformation radius: the estuary, near-field and far-field (Hetland, 2005). The Rossby deformation radius is defined as below:

$$R_d = \frac{\sqrt{g^{'}h}}{f}, \qquad g^{'} = g\frac{\Delta\rho}{\rho_0} \tag{1.3}$$

where h is the depth at the river mouth, g is acceleration of gravity, ρ_0 is the reference density, and $\Delta\rho$ is the difference in density between the plume and the layer below and f is the Coriolis parameter.

The estuary and near-field are characterized by intense shear-mixing of freshwater and salt water and the near-field is also referred to as a tidal plume in regions with large tides (Horner-Devine, 2009; Horner-Devine et al., 2015). Far-field refers to the region beyond the near-field where wind induced mixing is dominant in vertical mixing processes. Wind stress generally causes lower turbulence levels than are observed in the near-field (Houghton et al., 2009), but since wind usually acts over the entire plume domain, the net effect due to the spatial area of active mixing makes wind driven mixing important (Horner-Devine et al., 2015).

In this thesis, the terms near-field and far-field are defined according to the importance of tides or winds in mixing, with the near-field characterized as the tide mixing dominated region, while far-field refers to the wind dominated mixing region.

Most past studied river plumes are located on the shelf, for example, the Columbia River, Changjiang River and Merrimack River. Mixing studies on these river plumes are common and the plume is usually divided into those dynamical regions discussed above. However, as for the Fraser River plume, mixing induced by tides and winds for the Fraser River plume which lies within a semi-enclosed ocean basin, can be different. Tides in the SoG are relatively strong, especially in

the Haro Strait region (Thomson, 1981). Therefore, mixing generated by tides is likely to respond differently than on the shelf, where the tides are only significant near the river mouth. The wind driven circulation in the SoG might also behave differently from the Ekman dominated flow driven by winds in shelf systems (Halverson and Pawlowicz, 2008).

Past studies on mixing of the Fraser River plume are numerous. Halverson and Pawlowicz (2008) studied the impact of river discharge and tides on the Fraser River plume based on four-years (2003-2006) of ferry data. The effect of river discharge on plume salinity is that plume salinity is a quasi-linear function of river discharge on time scales of 25 days. However, the fresh water residence time, defined as the total volume of fresh water divided by input of river flow is about 2 days (Halverson and Pawlowicz, 2011), which is roughly independent of river discharge. Tides were found to impact plume salinity over three time scales: semi-diurnal, diurnal and fortnightly (Halverson and Pawlowicz, 2008). The plume is fresher at lower-low water than higher-high water. Plume salinity fluctuates in phase with the daily maximum tidal height, being fresher during neap tides and saltier during spring tides on fortnightly scales (Halverson and Pawlowicz, 2008). Entrainment is a principal physical process that causes the transfer of salt water into the fresh water in the estuary. By examining the entrainment process along a transect in the Fraser River estuary and using nitrate as a tracer to study entrainment, Yin et al. (1995a,b,c) found the entrainment was affected by river discharge, tides and winds. Specifically, more nitrate was entrained during higher river discharge than lower river discharge. This result was partially explained by the seaward fresh water spreading that allows a wider area for nitrate transfer. More entrainment occurs during spring tides than neap tides. Wind is a major factor in increasing nitrate concentration in the upper layer by increasing entrainment. Recent studies quantified the entrainment velocities in the Fraser River plume and estuary. Halverson and Pawlowicz (2011) estimated entrainment velocities

of a few mm s^{-1} from the entrainment flux using a quasi-steady salinity budget. These entrainment velocities were calculated by assuming the mixing primarily occurs along the salt-wedge estuary or in the near-field plume. They are in agreement with MacDonald and Geyer (2004), who estimated vertical velocities on the order of 1-4 mm s^{-1}. Shear instability was investigated in the Fraser River estuary based on echo sounder observations (Geyer and Farmer, 1989; Tedford et al., 2009). Tedford et al. (2009) also pointed out that the majority of the observed mixing in the Fraser estuary was due to shear instabilities at the pycnocline, although mixing due to bottom generated turbulence is observed during late ebb during low discharge periods.

1.6 Transport in a River Plume

Transport in a plume on the shelf away from the river mouth is driven mainly by the plume's buoyancy, wind stress and ambient coastal currents and is strongly modified by Earth's rotation (Horner-Devine et al., 2015). For the Fraser River plume, tides should also be considered as surface tidal currents can reach 0.5 m s^{-1} (Foreman et al., 1995; Halverson and Pawlowicz, 2016), potentially composing a large part of the total surface velocities. Variable tidal rapids occur near and within the narrow and shallow passages leading into the Strait, with maximum flood and ebb flows up to 5 m s^{-1} (LeBlond, 1983).

In the Strait of Georgia, wind stress was found to drive the highest surface currents relative to river forced and tidal forced flows based on HF radar data averaged over the period from August 2012 to May 2013 (Halverson and Pawlowicz, 2016). The wind-driven flow speeds are approximately 3-5% of the wind speeds. The dominance of wind-forcing in the subtidal surface currents over other factors in the SoG was discovered in multiple drifter studies, all of which indicated that the surface flow primarily follows the wind (Thomson, 1981). Drifters go southward in the case of northwesterly

winds, indicating the wind can overcome the tendency for the buoyant outflow to turn northward under the Coriolis force.

An unsteady growing anticyclonic recirculation offshore of the river mouth referred to as the bulge, is commonly reported by studies for plumes on the shelf (Oey and Mellor, 1993; Kourafalou et al., 1996; Garvine, 2001; Fong and Geyer, 2002; Horner-Devine et al., 2015). It forms when the width of river mouth is small relative to the Rossby deformation radius (1.3) and under sufficiently low wind conditions (Horner-Devine et al., 2015). The main role of a bulge on plume transport is to accumulate a fraction of between 25% and 75% of the river discharge and thus reduce in the transport of fresh water away from the river mouth region in the coastal currents (Fong and Geyer, 2002; Horner-Devine et al., 2006). However, in the Fraser River plume, the bulge feature is rarely observed. Halverson and Pawlowicz (2016) reported an anticyclonic turning seen in the mean surface current of HF radar data averaged from August 2012 to May 2013. Although this structure shows some resemblance to the bulge pattern, it is not clear if this pattern fits with classic bulge model described by Horner-Devine (2009) and Horner-Devine et al. (2015). Halverson and Pawlowicz (2016) found the mean HF radar surface flow was inconsistent with the gradient-wind relationship determined by Horner-Devine et al. (2015). Under the gradient-wind relationship, the pressure gradient is balanced by both the centrifugal and the Coriolis forces. A second reason could be that the west boundary of the semi-enclosed Strait of Georgia may not be favourable for bulge formation. Nonetheless, the mean surface flow field averaged over the period from August 2012 to May 2013, forced by the Fraser River observed with HF radar data is characterized as a jet-like outflow near the river mouth, flanked by two counter-rotating eddies, with the bulge-like eddy at the north and a cyclonic eddy at the south (Halverson and Pawlowicz, 2016). The mean flow speed near the river mouth was 0.14 m s^{-1}, while the flow further away from the mouth was no more than

0.05 m s^{-1} (Halverson and Pawlowicz, 2016).

1.7 Research Questions

It is interesting but also challenging to realistically model the Fraser River plume velocity and salinity fields. The reason why it is challenging is that plume motion is sensitive to many forcing factors that can vary significantly in time. In addition, it is necessary to understand mixing and transport processes impacted by various forcing agents in the Fraser River plume.

The objectives of this study are to answer the following research questions:

1. How well do the modeled flows and salinity compare to the observations?

2. What geometry of the Fraser River should be used in the NEMO model and how sensitive are the salinity and surface currents in the plume to the geometry of Fraser River estuary and the region around its mouth?

3. How do vertical eddy viscosity and diffusivity affect the plume properties?

4. What is the importance of tides, winds and the Coriolis force on the mixing of the plume and how does the importance vary with different river flows?

5. What is the importance of tides, winds and the Coriolis force on the transport of the plume and how does the importance vary with different river flows?

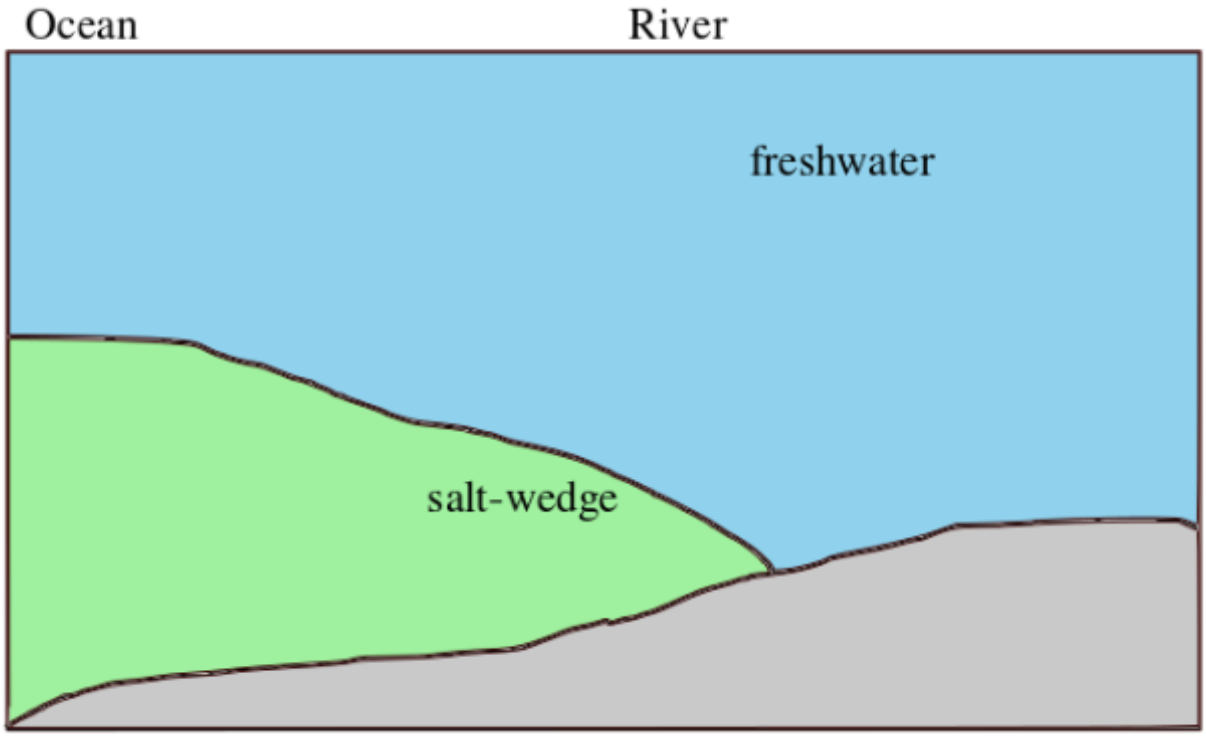

Figure 1.1: Salt-wedge schematic diagram. Diagram shows a vertical cross-section from the mouth of the river (on the left) to upstream. The depth shown is about 10 m and the length shown is about 15 km. Salt water below the freshwater that penetrates into the river is the salt-wedge.

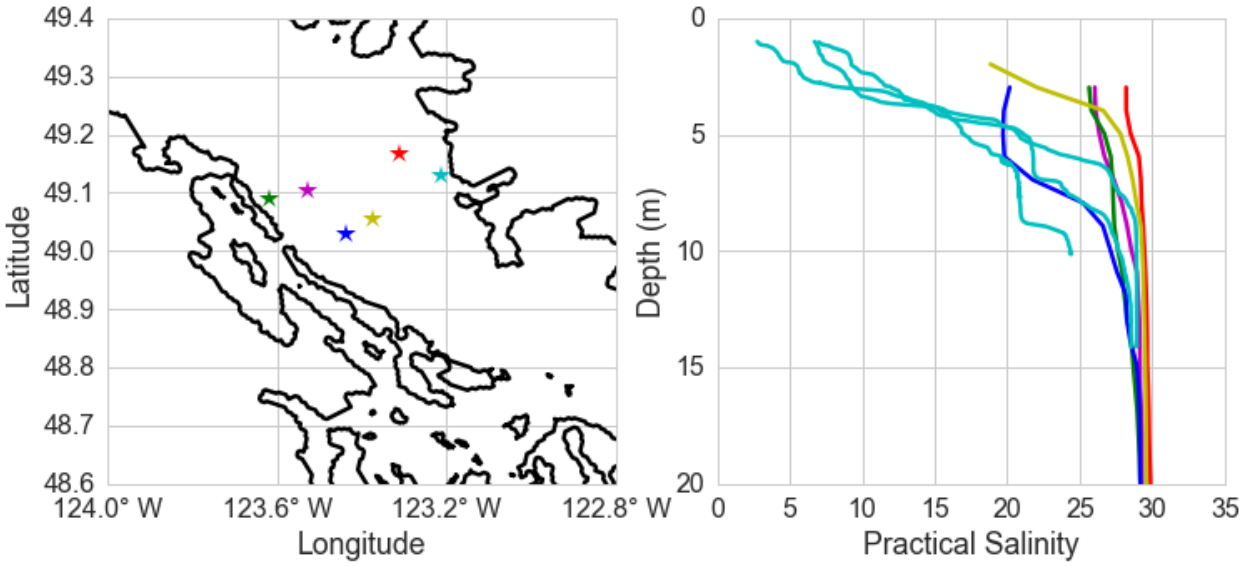

Figure 1.2: Observation sites and salinity profiles in October 2014, from Institute of Ocean Sciences, Joanne Breckenridge and Evgeny Pakhomov at University of British Columbia. Left panel: CTD observations shown (stars). Right panel: salinity profiles at those observation sites. Color of the site and the salinity profile correspond. Three different observations (teal color) are carried out at the same location during October 2014 by Joanne Breckenridge. Salinity stratification occurs mostly in the upper 10 m with salinity values below about 30.

Chapter 2

Plume Sensitivities to Model Parameters and Forcings

2.1 Introduction

The Salish Sea NEMO nowcast system has run daily since October 24, 2014. This operational modeling system employs the NEMO model to run the Salish Sea domain daily and the hourly results of temperature, salinity, sea surface height and currents are published on the web (`https://salishsea.eos.ubc.ca/nemo/results/`). One of the results of this modeling system is storm surge prediction (±10 cm) in the Strait of Georgia, which can be accessed through the web (`https://salishsea.eos.ubc.ca/storm-surge/forecast`). More details of how this nowcast modeling is configured is available in the Introduction 1.3.

Several discrepancies were found in the Fraser River plume salinity and surface currents of the nowcast results compared to different observations. First, by comparing to near-surface observations available from a ferry that crosses the Strait, it was found that the modeled minimum salinity value along the ferry track was higher than the ferry observations. Second, the position of the minimum salinity along the ferry track was found to be far to the east in the model results. This comparison suggests that the cross-strait velocities are too weak in the modeled surface currents. The same

discrepancy was seen comparing to available surface drifter tracks. Third, modeled surface currents generally have too strong southward along-strait flows compared to the drifters. Therefore, this thesis has a goal of improving the modeled Fraser River plume surface currents and salinity by improving these modeled plume properties by adjusting model parameters.

In addition to determining the sensitivity of the plume to model parameters, the sensitivity of the plume (including its mixing and transport) to variation in its forcings, such as the winds, tides, river discharge and the Coriolis force, is also determined. Insights into how plume mixing and transport vary with forcing factors are helpful for plume prediction. Winds and tides are both important in plume mixing, but understanding which region of the plume is dominated by tide-induced mixing or by wind-induced mixing increases our knowledge of river plume dynamics. River discharge generally increases the plume area, however, whether the amount of river discharge changes the plume location or not remains unclear. The Coriolis force is important for river plumes that occur on the shelf, but the impact of the Coriolis force on modeled movement of a plume located in a small scale semi-enclosed basin, such as the Strait of Georgia, has not been well studied before. Hence, a model study of the Fraser River plume and how mixing and transport are influenced by these forcing factors is needed.

Here, two model sensitivity studies are conducted. First, model sensitivities to river bathymetries and turbulence parameters are investigated by evaluating the modeled surface currents and salinity of the plume with available observations. Second, by employing the improved configuration from the evaluation, model sensitivities to forcings: the winds, tides, river flow and the Coriolis force, are studied to understand plume mixing and transport.

In the first part of this chapter, baseline run conditions, various observational data and comparison methods between model results and observations are described. Several bathymetric variations

and sensitivity experiments using varying turbulence parameters are conducted with a goal of improving the plume properties compared to the baseline. Evaluation of the results from the baseline and the variations are analyzed. The improved configuration is determined.

In the second part of this chapter, based on the improved configuration, plume dynamics in the model are studied. In particular, how mixing and transport processes in the plume are affected by river discharge, tides, winds and the Coriolis force are studied. Numerical simulations with and without each of the forcings above are performed. Plume mixing and transport metrics are developed to quantify and analyze mixing extent and freshwater transport.

2.2 Methods

2.2.1 The Model Description

The model employed in this study is the Nucleus for European Modelling of the Ocean (NEMO) version 3.4 in a regional configuration (Madec, 2012) for the Salish Sea region (Figure 2.1). The numerical grid is 398 by 898 by 40 grid cells, with a horizontal grid spacing of around 440 m by 500 m. The vertical z-levels are unequally spaced, with 1 m vertical grid spacing down to about 10 m in depth and a maximum grid spacing of 27 m starting from around 150 m to the bottom. Eight tidal constituents (K_1, O_1, P_1, Q_1, M_2, K_2, N_2, and S_2) are forced at two open boundaries that connect to the Pacific Ocean, the western boundary at the mouth of Juan de Fuca Strait and the northern boundary in Johnstone Strait (Soontiens et al., 2016). All the model results for analysis in this study are hourly averages. In order to limit large changes in depth across grid cells, bathymetry over the entire domain was smoothed so that $\Delta h/\overline{h} \leq 0.8$, where Δh is the difference in depth between two adjacent grid cells, and $\overline{h}$ is their average depth (Soontiens et al., 2016).

Compared with the study of Soontiens et al. (2016), differences for the baseline simulation for this study are:

(1) Lateral eddy viscosity of 15 m^2s^{-1} was used rather than 20 m^2s^{-1}.

(2) The western Canada component of the High Resolution Deterministic Prediction System (HRDPS), a nested 2.5 km resolution atmospheric model provided by Environment Canada (`https://weather.gc.ca/grib/grib2_HRDPS_HR_e.html`), was employed instead of the Canadian Meteorological Centre's 33 km global atmospheric reforecasting model (CGRF) wind products (Smith et al., 2014; Soontiens et al., 2016). The temporal resolution of the operational wind is hourly.

(3) Daily Fraser River runoff at Hope (`https://wateroffice.ec.gc.ca/report/report_e.html?type=realTime&stn=08MF005`) was used rather than climatology data. For all other rivers and contributions to the Fraser River downstream of Hope, climatology was used.

(4) The background vertical eddy viscosity and diffusivity were set to the same values in the baseline run as Soontiens et al. (2016): 1×10^{-4} and 1×10^{-5} m^2s^{-1}, respectively. The NEMO model selects the maximum values of the vertical eddy viscosity and diffusivity between background values and the values that are calculated by the $k-\varepsilon$ configuration of the GLS turbulence scheme. We evaluate variations in background vertical viscosity and diffusivity.

(5) The initial bathymetry we employed here is the same as Soontiens et al. (2016), which contains a short river channel for the Fraser River (left panel, bathymetry #2, Figure 2.2). We evaluate

variations in bathymetry.

The model equation of state implicitly assumes that model salinities are equivalent to observed Practical Salinities on the Practical Salinity Scale 1978 (Unesco, 1981).

2.2.2 Strategies in this Study

For modeled plume properties sensitivities to model parameters, two criteria were considered to choose simulation periods: 1) the availability of observational data and 2) a variety of forcing conditions. Three types of data were available for October 1-31, 2014: drifter data, ferry-based salinity data on a track crossing the plume and CTD observations. June 15-29, 2015 was selected because it is during the Fraser River freshet period and thus quite different than the October period. Also, ferry-based salinity data is available to evaluate against modeled salinity during this simulation period. Finally, October 1-31, 2015 was chosen since measurements of surface current are available for this period.

It is important to evaluate the salinity and surface currents in the modeled Fraser River plume because these two variables reveal plume physical characteristics. Magnitudes of surface cross-strait velocities and along-strait flows near the river mouth directly reflect features of surface currents in the Fraser River plume. Plume position will be used as this variable is also related to surface currents and it reflects the surface currents.

In order to evaluate the modeled plume salinity, the minimum salinity value and fresh water fraction along the ferry track were chosen. These variables will be related to the total plume salinity, and can be directly compared with observations. To evaluate the modeled plume position, the location of the minimum salinity value along the ferry track was adopted since this variable

indicates the plume location along the ferry route in general. In addition to evaluating the modeled plume results against observations, it is useful to determine the sensitivity of the modeled plume results with different configurations. For example, the volume flux and salinity time series at a river mouth transect with different river bathymetries were analyzed because they provide another view of the strength of cross-strait velocities and salinity values, respectively.

In the plume sensitivity to forcing section, the simulations were divided into January 1-31, 2016 (low river flow), October 1-31, 2014 (moderate river flow) and May 1-31, 2015 (high river flow) periods. These three periods were chosen because they allow us to investigate the effects of the amount of river flow on mixing and transport processes within the plume.

To study the mixing processes within the Fraser River plume, the total amount of mixing in the top 10 m of the water column within the plume is used to determine the total mixing a water parcel has experienced. Furthermore, the total mixing induced by different forcing factors will be estimated. A goal of this thesis is to study the relative importance of tide- and wind-induced mixing in the Fraser River plume and how it varies with the river flow. Understanding the relative importance of tides versus winds in mixing in the Fraser River plume is novel as past studies of mixing in river plumes focused on coastal shelf regions instead of a semi-enclosed ocean basin.

To investigate the transport processes within the Fraser River plume, the amount and the direction of freshwater transport under different forcing factors are determined. In addition, it is interesting to investigate how the fresh water plume moves around due to winds and river flows.

2.2.3 Data for Model Evaluation

Ferry-based Observational Salinity Data

Two passenger ferries run by BC Ferries Inc. were instrumented by Ocean Networks Canada (ONC). These ferries travel between Tsawwassen and Duke Point (diagonal route) and Tsawwassen and Swartz (southern route) (Figure 2.1), each crossing the Fraser River plume to different extents. They make four round trips during weekdays and fewer on the weekends. Each trip takes around 2 hours (1 hour and 35 minutes) to cover the complete transects of around 70 (44 km) for the diagonal (southern) route (Figure 2.1). Seawater near-surface salinity was derived by ONC from measurements of temperature and conductivity every 10 seconds using a SeaBird Thermosalinograph SeaKeeper in the FerryBox. The effective water sampling depth is approximately 2 m (Wang, 2015). In the model, grid points are at 1.5 m depth and 2.5 m depth and so 1.5 m depth was selected to compare against the ferry data.

Drifter Data

A total of nine Microstar GPS drifters, with a drogue 1.22 m tall centred at a depth of 1 m (Ohlmann et al., 2005), were released on October 8th, 2014, at three different locations around Sand Heads (Figure 2.1), by Mark Halverson and Rich Pawlowicz, University of British Columbia. All the drifters were released during ebb tides and drifted 7-29 hours before recovery.

CTD Data

Five Conductivity Temperature Depth (CTD) profiles obtained by Peter Chandler from Institute of Ocean Sciences (IOS) in October, 2014, in the central SoG were used (Figure 2.1). Three other CTD casts conducted by Joanne Breckenridge and Evgeny Pakhomov, University of British Columbia,

measured at the same location near the mouth of the Fraser River during different days in October were also used (pink star, Figure 2.1).

Water Level and River Discharge Data

Hourly real-time water level data from June 15-29, 2015, at Steveston, Deas Island Tunnel, New Westminster and Mission were acquired from Environment Canada (`https://wateroffice.ec.gc.ca/search/searchRealTime_e.html`).

2.2.4 Comparison Methods

Comparison with Ferry Salinity Data

All ferry tracks were visually checked to confirm they included the full transect across the Strait and did not include data obtained while the ferry was sitting in port or outside the Strait. The Inverse Distance Weighting Interpolation method is applied to interpolate gridded model values onto the observational points on the ferry routes (Appendix A). Linear interpolation between hourly model results is used to interpolate to the time of the ferry observations.

Comparison with Drifter Data

Model particle trajectories were calculated using Ariane (Blanke and Raynaud, 1997) based on hourly average output from the model. Model particles were forced to remain in the uppermost model grid box, nominally 0.5 m depth. Individual drifter-particle track comparisons were made. Particles are released at the same time and same position for the same duration as the observed drifters. Particles are also released every hour, at the drifter position at the corresponding time, and tracked for one hour. Based on this, statistics of the separation between the drifters and modeled

particles after every hour were derived. Furthermore, particle tracks offset by 0.5 hour and by 500 m relative to the initial released time and position of the drifter were also calculated.

Comparison with CTD Data

For each CTD cast, model results for the grid point closest to the cast were averaged over a UTC day and the minimum and maximum hourly-average salinity values over the day were found. Scatter diagrams of the observed CTD versus model results were made.

Comparison with Water Level Data

A time series from June 15 to 29, 2015, was selected to calculate the maximum, minimum and averaged modeled tidal amplitudes at Steveston, Deas Island Tunnel, New Westminster and Mission (locations on Figure 2.2), and compared to those calculated from observations at the corresponding stations.

2.2.5 Variations Attempted

To test the sensitivity to model parameters, a set of 11 runs are described (Table 2.1). Four different bathymetries were evaluated.

Short River Channel (baseline, bathymetry #2)

In the baseline case (Figure 2.2), the river channel is 10 km long by 2 km wide with a closed boundary at the head of the river. The river channel and banks are uniformly 4 m deep.

Extended River Channel (bathymetry #5)

An extended river channel (Figure 2.2) was based on the measured bathymetry of the Fraser River (Canadian Hydrographic Chart #3492) from Gravesend Reach to New Westminster with depth at New Westminster of 13 m. Beyond this location, the model channel turns to the north and extends for another 40 km (Figure 2.2) and then runs eastward along the model grid to the edge of model domain. The depth after New Westminster is set to 13 m. The total length of the river channel is about 76 km from the river mouth at Steveston, which is over 7 times longer than that of bathymetry #2. Based on the chart, the minimum width of the river channel is only one grid cell, approximately 500 m.

Extended and Deepened River Channel (bathymetry #6)

Bathymetry #5 has weak tides in the lower Fraser River. Bathymetry #6 was created based on bathymetry #5, by deepening the region around the river mouth by 5 m. This region in the Strait is around 10 km along-strait by 4.5 km cross-strait. In addition, the area from the river mouth and into the river until Gravesend Reach (Figure 2.2) was also deepened by 5 m; the length of this region is around 10 km (Figure 2.3). Note that some grid cells in the river mouth region were already modified in bathymetry #5, and they were not further deepened in bathymetry #6. This geometry was generated to correct the tidal amplitudes in the Fraser River estuary.

Vertical Eddy Viscosity and Diffusivity

Model results with lower background vertical eddy viscosity of $1\times\ 10^{-5}$ m^2s^{-1} and both lower background vertical eddy viscosity and lower background eddy diffusivity of 1×10^{-6} m^2s^{-1} were evaluated (Run # 4 and 5, Table 2.1).

Sensitivity Runs for Model Evaluation

Fifteen-day sensitivity experiments, from June 15 to 29, 2015 (Run #1a, 2 and 3a, Table 2.1, Figure 2.4), were performed to examine whether the extended river channel (bathymetry #5) and extended and deepened river channel (bathymetry #6) improve the surface velocity and tidal amplitudes inside the river channel and to further investigate how sensitive the plume properties are to the geometry of the river.

Run #1a is initialized from the operational nowcast, and thus started from non-zero velocities. Run #2 and #3a started with zero velocities and same temperature and salinity values used to start Run #1a, that is operational results from June 14, 2015. In the added river channel grid cells, temperature values are set to $14°C$, salinity values are set to 0 east of Deas Island Tunnel and 1 west of it.

One month sensitivity experiments, from October 1 to 31, 2014 (Runs #1b, 3b, 4 and 5, Table 2.1, Figure 2.5) were made to compare the model results of the three different bathymetries and of lower background vertical eddy viscosity and lower background vertical eddy diffusivity, respectively, with various available observations. Run #6 and 7 (Table 2.1) were designed to investigate the effects of bathymetry without winds. Run #8 was conducted to evaluate the impact of adding a representation of the Steveston Jetty (Appendix C). All these runs were initialized with temperature and salinity from the operational nowcast on September 25, 2014 and run for 5 days to spin up the model before analysis start for October 1, 2014 (Table 2.1).

All these runs (Runs #3b, 4 and 5, Table 2.1) started from zero velocities except Run #1b, which is initialized from the operational nowcast.

Another one month sensitivity experiment, from October 1 to 31, 2015 (Run #9, Table 2.1) was performed with the extended and deepened river channel (bathymetry #6), lower background

vertical eddy viscosity and lower background vertical eddy diffusivity, respectively, to evaluate the mean surface currents with HF radar data (Appendix D). It also started from zero velocities. Initial temperature and salinity were from the operational model results from September 18, 2015.

2.2.6 Sensitivity Studies of Plume Properties Affected by Forcing Factors

Plume Physics Runs

A total of fifteen runs were conducted to study how plume salinity stratification and fresh water transport are influenced by: the river runoff, tides, winds and the Coriolis force. These fifteen simulations are divided into three river flow periods: low, moderate and high (Table 2.2, Figure 2.6, 2.5 and 2.7). All the sensitivity runs were started at least five days prior to the river flow period of interest with zero initial velocities, temperature and salinity from the operational model, climatology sea surface heights, temperature and salinity at the boundaries. The model Fraser River discharge is realistic and daily. Five different runs were done for each river flow category:

1. Combined all forcing case. In this run, river flows, tides, winds and the Coriolis force are all present, which can be considered the most realistic simulation.

2. Only river discharge case. The model is only forced with daily river flow, without any other external forcings and includes the Coriolis force.

3. River + tides case. The model is forced with all the forcing conditions, except the operational winds.

4. River + winds case. The model is forced with all the forcing conditions, except the tides.

5. No Coriolis force case. The model is forced with all the forcing conditions, and the Coriolis force is set to zero.

Weak, Moderate and Strong Wind Period Selection

For each of the simulations during low, moderate and high river flow period, different wind magnitude periods, are chosen in order to study the impact of the wind on plume mixing and transport processes. A weak wind period is that when over 90% of the wind magnitudes during the selected period is weaker than 5 m s^{-1}. A moderate wind period is selected when the wind speed within the range of 5-10 m s^{-1} accounts for more than 40% of the total time. In addition, for the moderate wind period, to make sure the wind magnitude is mainly less than 10 m s^{-1}, wind component with magnitudes larger than 10 m s^{-1} should constitute no more than 5% of the overall wind values during the selected period. A strong wind period occurs when wind speed larger than 10 m s^{-1} occupying over 20% of the selected wind period. In addition to the criteria for each wind period discussed above, for the moderate and strong wind events, wind direction prior to the event is considered. Wind periods are not selected if the winds are strong in the opposite direction to the wind in the event period. This last requirement is to avoid the wind lag effect as much as possible.

Defining the Plume

It is necessary to identify the plume in the model output. The edge of the plume is defined using a threshold surface salinity (Halverson and Pawlowicz, 2011):

$$S_{thresh} = S_{ref} - S_{offset} \tag{2.1}$$

where the S_{ref} is the 2.5 km by 2.5 km spatially averaged surface-level (nominally 0.5 m depth) salinity over the northwest corner of the subdomain (Figure 2.1). This region is close to the area where Halverson and Pawlowicz (2011) selected S_{ref} for their calculation. For each of January, 2016, October, 2014 and May, 2015, the monthly average of the combined all forcing case is used. S_{offset} is selected to be a linear function of the reference salinity:

$$S_{offset} = 4.8 - 0.14 \times S_{ref} \tag{2.2}$$

(Halverson and Pawlowicz, 2011).

Note the subdomain (Figure 2.1) which is used to analyze plume impacted by forcings has some limitations. Halverson and Pawlowicz (2016) and Tabata (1972) observed that plume can go further south than the southern boundary of the selected subdomain. However, due to computational and storage limitations, this subdomain was not extended further south.

Upper Layer Depth, Reference Salinity and Reference Density Selection

The upper layer depth h is selected to be 10 m as we expect that the plume is mostly trapped within the top 10 m (Stronach, 1981) and indeed we find that no more than 1% of the time does the plume reach 10 m depth during three months based on salinity criteria (2.1) at NS station (Figure 2.1, 2.8). The reference salinity value is chosen to be 30 since this is a typical mean salinity value in the range of 50 to 100 m depth in STRATOGEM observations [Figure 3.1, (Riche, 2011)], and we found this value corresponds with the mean salinity at 50 m depth in October 2014 over the northwest corner of the subdomain (Figure 2.1). The reference density of 1023 kg m^{-3} selection is based on temperature of $10°C$ and salinity of 30. Similarly, this value of reference salinity represents the mean density at 50 m depth in October 2014 over the northwest corner of the subdomain (Figure 2.1).

2.3 Results

2.3.1 Fraser River Plume Sensitivity to Model Parameters

Evaluation of Operational Results – Runs #1a and #1b

In addition to the methods introduced in Methods (2.2.4) to compare model results with ferry-based data, three other metrics are used for quantitative comparisons: the minimum salinity value, the location of the minimum salinity value and fresh water fraction along a complete diagonal ferry transect. Location of the minimum salinity value here is the longitude of the minimum salinity value along a single ferry track. This metric indicates how far the plume has moved offshore from the river mouth. Freshwater fraction, F_a, for every available ferry track is calculated through the

formula below:

$$F_a = \frac{1}{L}\int_0^L \frac{S_0 - S(x)}{S_0} dx \tag{2.3}$$

where the reference salinity S_0 is taken to be 30, $S(x)$ is the salinity value at position x at 1.5 m depth on the ferry route, and x is the distance along the ferry track.

Eighty-six ferry crossings were used to compare to the model (e.g., Figure 2.9). A typical comparison from October 8, 2014, shows modeled salinity values for Run #1b in a similar range as the ferry-based salinity for both routes, ranging between 14 and 28 for the diagonal route and from 20 to 30 for the south route during this moderate river flow period (Figure 2.9). Lower values are seen on the diagonal route as it cuts the plume closer to its centre. However, the locations of the modeled minimum salinity value along the ferry track are closer to the mainland coast, indicating too weak cross-strait velocities (Figure 2.10). Furthermore, the modeled minimum salinity along the diagonal track is always higher. The integrated fresh water fraction (2.3) is generally too small although there are some examples when the model has a higher fresh water fraction compared to that observed (Figure 2.11). For example, on June 21, 26 and 27, the baseline has a higher freshwater fraction than the ferry observations.

The drifter-particle comparison (e.g., Figure 2.12) confirms the problem of too weak cross-strait flows in Run #1b. The modeled particle does not go far enough offshore. Averaged modeled particle velocity during ebb tide is about 0.4 m s^{-1} while drifter's velocity is 0.6 m s^{-1}.

All of these features are robust as revealed from the statistics based on ferry data (Figure 2.10). In addition, the model has too strong along-strait surface flows (e.g., Figure 2.12).

Evaluation of Bathymetric Changes

With a longer and deeper river channel (Run #3a and #3b, bathymetry #6), the location of the minimum salinity value along the diagonal and south track moves further offshore compared to the baseline (Run #1a and #1b, bathymetry #2) (Figure 2.10 and example on Figure 2.9). The position of the plume is improved about 50% from the statistics of 86 ferry crossings in June and 23 ferry crossings in October (Figure 2.10). The drifter trajectories show slightly stronger cross-strait flow, although the along strait flow remains too strong (e.g., Figure 2.12).

Overall, the extended river channel (Run #2, bathymetry #5) reduces the values of the plume salinity, making it closer to the observations (Figure 2.10). However, this channel does not generate stronger cross-strait velocities (Figure 2.10).

Compared to most ferry tracks, the model has too little integrated freshwater along the diagonal route (Figure 2.11). This result is consistent with the minimum salinity value being too high in the model (Figure 2.10) as well as a saltier near-surface plume in general compared to observed CTD casts (Figure 2.13). The bathymetry variations caused little change in the fresh water fraction.

Generally, both the observed and modeled tidal amplitudes decay in the river channel with distance from the river mouth (Table B.1, Appendix B). Tidal amplitude at Steveston agrees with observations for both the extended river channel (Bathymetry #5) and the extended and deepened river channel (Bathymetry #6) (Table B.1, Appendix B). However, tidal amplitudes at Deas Island Tunnel and New Westminster are too small in bathymetry #5, whereas they are slightly overestimated in bathymetry #6. Tidal amplitude at Mission is too high in bathymetry #6, but this is unlikely to impact the plume itself.

The volume flux V, through a cross-section is defined as:

$$V = \iint u dy dz \tag{2.4}$$

where u is the velocity perpendicular to the transect, and y is along-transect distance and the integral is over the whole transect to the bottom or just the top 4 m. An integral over the just top 4 m depth is selected because it is the original depth (bathymetry #2) of this transect.

The salinity integral S_I, is defined as:

$$S_I = \iint S dy dz \tag{2.5}$$

where S is the salinity, and the integral is evaluated across the river channel and over the top 4 m or the full water column.

The volume flux (2.4) across and salinity integral (2.5) along transects at the river mouth and inside the river channel between longer and deeper river channel (Run #7, bathymetry #6) and short channel (Run #6, bathymetry #2) were calculated (Figure 2.14). Large differences of the instantaneous volume fluxes occur at the river mouth transect (Figure 2.14 b) between these two river channels, and the magnitude of peak instantaneous volume flux at peak ebbs with the longer and deeper river channel is nearly three times larger than the short shallow channel. Indeed, the volume flux over only the upper 4 m exceeds that of short river channel by a factor of two. Across the transect inside the river channel, the variation of volume flux with the tides is very weak with the original bathymetry (Figure 2.14 f), reflecting the closeness of this transect to the original river

head in the model. The net daily volume flux over the full depth is weaker than that integrated only over the top 4 m at the river mouth transect (Figure 2.14 c) whereas the net daily outflow volume flux over full depth is stronger than that integrated over only the top 4 m at the transect inside the river channel (Figure 2.14 g). Generally, the total volume flux is not affected by the bathymetry changes (Figure 2.14 c and g).

The salinity integral (2.5) at both transects is much higher with the extended and deepened river channel (bathymetry #6) (Figure 2.14 d and h), which is consistent with a saltier signal from the ferry comparisons (Figure 2.10) presumably caused by stronger mixing effect. This saltier signal with the extended and deepened river channel (bathymetry #6) arises because a salt-wedge intrusion usually occurs in this deeper river.

Evaluation of the Reduced Viscosity and Diffusivity Cases

Reducing the background viscosity and reducing both the background viscosity and diffusivity improved the model salinity compared to observations along the ferry routes (Figure 2.10 and example in Figure 2.9) by reducing the near-surface salinity.

Variation of the viscosity and diffusivity has little impact on salinity profiles (Figure 2.13). In the top 10 m, most of the modeled results are saltier than observations by up to 5 practical salinity units; the difference is less significant at deeper depths and the model is too fresh in the bottom layer.

For the example shown, modeled particle tracks show substantial improvements with lowered viscosity, especially in the along-strait movements (Figure 2.12). Changes in diffusivity make only small changes to the drifter track (Figure 2.12). Although improvements were seen in this drifter-particle trajectory comparison (Figure 2.12), the general ability of the model to track surface drifters

was not improved from the statistics of averaged distance between the drifters and modeled particles after one hour (Figure 2.15). The cause can be two-fold. One could be that the tidal currents in the model are not accurate enough, leading to inaccurate tidal variability in the surface flows. The other reason might be the randomness of the drifters, which could suggest chaotic features in the real SoG.

To illustrate the spatial and temporal variation of particle trajectories, particles offset by 500 m and by half an hour relative to the initial released position and time of the corresponding drifter were done (Figure 2.16). There are large variations of the modeled surface flows in both time and space. Maximum spread among the nine particles in each case occurs at the final hour. The maximum separation distances between the modeled trajectories are 3.7 km, 6.2 km, 17.1 km and 16.4 km for run #1b, #3b, #4 and #5, respectively. Although the general patterns of the particle tracks in each run case does not vary much, modeled trajectories of the particles released half an hour late give the best qualitative results.

2.3.2 Fraser River Plume Sensitivity to Forcing

Mixing

To investigate the extent of mixing within the plume, a ratio was employed (Masunaga et al., 2016):

$$Rmix = \frac{S_{Surf}}{< S >} \tag{2.6}$$

where S_{Surf} is the surface salinity and $< S >$ is the mean salinity over the top 10 m of the water column ($< S >$ never has a zero value in this study). The larger the value of $Rmix$, the more

intense the mixing that has occured in the water column. Specifically, $Rmix = 1$ indicates that the water column is fully mixed vertically while $Rmix = 0$ occurs when pure fresh water exists at the surface.

Recall the near- and far-field plume region in Introduction 1.5. The major difference between these two regions is the relative importance between tides and winds in inducing mixing. Therefore, we can operationally define the near- and far-field plume region based on the $Rmix$ ratio from different scenarios:

$$P_r = \frac{Rmix(river + winds) - Rmix(river + tides)}{Rmix(river + winds + tides)} \tag{2.7}$$

If the value of P_r is greater than 0.1, it shows mixing induced by winds is much greater than the tides. This region is defined as the far-field, where winds dominate mixing. Otherwise, this region belongs to near-field plume. We select 0.1 as the threshold rather than 0 because greater than 0.1 shows the dominance of wind in mixing although 0.1 is somewhat arbitary.

Potential energy, employed to measure shear-induced mixing relative to the fully mixed state, is defined as:

$$\begin{aligned} PE\_FullMixed &= \int_0^{10\mathrm{m}} (\rho - \overline{\rho}) g z dz, \\ \overline{\rho} &= \frac{\int_0^{10\mathrm{m}} \rho dz}{10 \quad \mathrm{m}} \end{aligned} \tag{2.8}$$

One can also define an unmixed system (two-layer). To conserve mass:

$$\begin{aligned} \overline{\rho}D &= \rho_{min}l + \rho_{max}(D-l), \\ D &= 10 \quad \text{m}, \\ \rho_{min} &= 999.7 \quad \text{kgm}^{-3}, \\ \rho_{max} &= 1023.0 \quad \text{kgm}^{-3} \end{aligned} \tag{2.9}$$

where ρ_{min} is the density of a surface layer of depth l calculated with salinity 0 and temperature $10°C$, and ρ_{max} is the density of the lower layer of depth $D-l$ calculated with salinity 30 and temperature $10°C$. D is the total depth. Equation (2.9) can be solved for l. Then the potential energy of this unmixed system is:

$$Unmixed = \frac{-g(\rho_{min}-\overline{\rho})l^2}{2} - (\rho_{max}-\overline{\rho})(D-l)g \times (l + \frac{D-l}{2}) \tag{2.10}$$

By subtracting (2.10) from (2.8), the potential energy relative to a completely unmixed state, $PE\_UnMixed$, can be calculated.

$$PE\_Unmixed = PE\_FullMixed - Unmixed \tag{2.11}$$

NS station is always within the plume region (Figure 2.17, 2.18) according to the salinity criteria (2.1). The fresh water, mainly from the Fraser River, enters into the SoG and at NS station, the water body with salinity below the salinity criteria threshold (2.2), is mostly trapped in the top 5 m for the river only case (Figure 2.17 a, e and i, Figure 2.18 a, e and i). For river only case,

strong stratification due to river outflow restricts the mixing processes (a, e and i of Figure 2.17 and 2.18). However, potential energy generated by shear-induced mixing by the river is about 600 J m^{-2} in these three months (Figure 2.19), which illustrates the non-negligible role of the river itself in creating shear mixing.

The stratification varies with different discharge rates of the Fraser River. In general, strongly stratified water with salinity values below 12 can reach around 4 m depth in early May (Figure 2.17 i and Figure 2.18 i), when the Fraser River discharge is around 4000 m^3 s^{-1}, while water with the same salinity is confined in the upper 1 m when Fraser River discharge is around 900 $m^3 s^{-1}$ in January (Figure 2.17 a and Figure 2.18 a).

Periodic, tidally modulated vertical mixing structures are simulated by the model (Figure 2.17 b, f and j, Figure 2.18 b, f and j). Without winds, the upper 6 m of the water column is stratified during low and moderate river flow periods (Figure 2.17 b and f), which is similar to the river only forcing case. However, without winds in May, the mixing pattern induced by the tides is comparable to the all forcing case (Figure 2.17 j). Under weak wind conditions, the salinity mixing and restratification driven by the tides (Figure 2.18 b, f, and j) is similar to that with all forcing factors (Figure 2.18 d, i and l). During moderate and strong wind events in low and moderate river flow periods, the tide-induced mixing region is tightly constrained near the mouth (Figure 2.20 d, g, e and h) while the near-field region expands substantially during the high river flow period (Figure 2.20 f and i), to include NS station. In all flow periods, at the river channel near the mouth, salinity is around 4-8 fresher at 4 m depth by adding tides and adding tides restricts the salt-wedge position to within 15 km from the mouth (Figure 2.21 b, e and h).

At NS station, wind-induced vertical mixing is relatively strong compared to that induced by tide under moderate wind conditions during low and moderate river flow periods, where the surface

salinity can reach 24 (Figure 2.17 g) and the mixing patterns are comparable between the river and winds and the all forcing case. On average, shear-mixing induced by winds at NS station is stronger than that due to the tides (Figure 2.19). The wind-dominated mixing region grows considerably within the plume area during low and moderate river flow periods when the magnitude of wind is greater than 5 m s^{-1} (Figure 2.20 d, e, g and h). Under weak wind conditions, wind-induced mixing region is limited during low and moderate river flow periods (Figure 2.20 a and b) while it grows in high river flow period (Figure 2.20 c). The effects of wind-driven mixing are generally weaker than tides at NS station for all river discharges under weak wind conditions. Inside the river channel, the salt-wedge (10 salinity contour) can propagate up to New Westminster with river and winds forcing and low discharge (Figure 2.21 a). The intrusion distance decreases under moderate and high discharge (Figure 2.21 d and g). Compared to that with river and tides or with all forcing, mixing is less intense in the river channel with river and winds.

For all three river flow conditions, with the Coriolis force, we see fresher water northward of the Fraser River mouth along the mainland BC coast (g, h and i of Figure 2.22); the freshwater continues into English Bay near the city of Vancouver. Without the Coriolis force, the plume is generally wider (d, e and f of Figure 2.22).

For the all forcings case, the effects of river discharge, tides, winds and the Coriolis force are superimposed. However, the relative strengths of mixing are distinctive across three different river flow periods. During high river discharge in May (Figure 2.17 l and Figure 2.18 l), mixing is weaker according to $Rmix$ (2.6) than under low and medium river discharge.

The relative size of the instantaneous momentum compared to the internal wave speed is the

upper layer Froude number, defined operationally here as:

$$Fr = \frac{\Delta U}{\sqrt{g^{'} h}} \tag{2.12}$$

where

$$\begin{aligned}
\Delta U &= \sqrt{(u_s - u_b)^2 + (v_s - v_b)^2} \\
u_s &= \frac{\int_0^h u dz}{h}, u_b = \frac{\int_h^H u dz}{H-h}, \\
v_s &= \frac{\int_0^h v dz}{h}, v_b = \frac{\int_h^H v dz}{H-h}, \\
g^{'} &= \frac{g(\rho_b - \rho_s)}{\rho_0}, \\
\rho_s &= \frac{\int_0^h \rho dz}{h}, \rho_b = \frac{\int_h^H \rho dz}{H-h}, \\
\rho_0 &= 1023.0 \quad \mathrm{kgm}^{-3}, \\
g &= 9.8 \quad \mathrm{ms}^{-2}
\end{aligned} \tag{2.13}$$

u and v are cross-strait and along-strait velocities, respectively. u_s and v_s represent the averaged upper layer cross-strait and along-strait velocities while the upper layer depth h is determined as the location where $\partial\rho/\partial z$ is maximum. In the other words, the depth of the pycnocline. u_b and v_b are the averaged lower layer (from upper layer depth h to the bottom depth H) cross-strait and along-strait velocities. Averaged upper layer density ρ_s and lower layer density ρ_b are found similarly; Density ρ is calculated from temperature and salinity based on Pond and Pickard (1983). If the value of Froude number is greater than a critical number of approximately 1, this indicates the

flow is internally supercritical. Conversely, when internal wave speed is larger than the speed of the outflow, Froude number is smaller than a critical number of approximately 1, which is subcritical flow.

At peak ebb in a given day, the active high momentum region with maximum speed in excess of 1 m s^{-1} is mainly concentrated toward the southern boundary of the subdomain where the barotropic tides are strong, as well as in the river mouth, where the jet-like plume discharges into the Strait (Figure 2.23 d,e and f). The strong barotropic tides at the southern boundary of the subdomain are due to relatively shallow water and not related to the plume. Therefore, the internally supercritical flow when Froude number is larger than order of 1 occurs predominately at where tides are strong in the Strait rather than the region of near-field plume. The internal wave speed is generally greater in May than in January and October because of the fresher upper layer (Figure 2.23 g, h and i). The Froude number at peak floods shows similar results with these at peak ebbs, except that the momentum is slightly weaker at peak floods for all three river flow periods (Appendix H).

Transport

The freshwater transport through an across-strait transect of 10 m thickness is defined as:

$$Q_{fcc} = \iint_0^{10\mathrm{m}} v \frac{\Delta S}{S_0} dz dx, \tag{2.14}$$

where S_0 denotes the ambient water salinity, here defined to be 30. $\Delta S = S_0 - S$ is the difference between the ambient salinity and salinity within the plume, and v is the along-strait velocity.

It is clear to see that with only river forcing, the integrated freshwater transport is southward and has the maximum southward flux (Figure 2.24). With river and tides, the direction of cumulative

freshwater flux is south by the end of the month (Figure 2.24), but the amount is only 20-30% of that with only river forcing. The Coriolis force has a non-negligible impact on the freshwater transport, with much more freshwater transported to the south without the Coriolis force (Figure 2.24), indicating the importance of the northward velocity that the Coriolis force generates. Larger fluctuations of freshwater flux with time are found without the Coriolis force compared to scenarios with the Coriolis force. Northward freshwater transport occurs under the combine all forcings case only (Figure 2.24).

The location of the plume centre is defined as the "centre of mass" of the freshwater thickness:

$$\begin{aligned} x_0 &= \frac{\iint x f(x,y) dxdy}{\iint f(x,y) dxdy}, \\ y_0 &= \frac{\iint y f(x,y) dxdy}{\iint f(x,y) dxdy}, \\ f(x,y) &= \int_0^{10\mathrm{m}} \frac{\Delta S}{S_0} dz \end{aligned} \tag{2.15}$$

where x and y are the along-strait and cross-strait directions, respectively, and $f(x,y)$ is the vertically integrated freshwater amount at each grid cell, representing the freshwater thickness of the upper 10 m. Note that the valid domain for this calculation excludes the Fraser River channel, English Bay, as well as Howe Sound (Figure 2.1), so that the impact of other river plumes is minimized. Effects of winds and river discharge on the plume centre location will be investigated.

The plume centre (2.15) moves northward up to 3 km by increasing discharge from low to high river flows (Figure 2.26). Under moderate and strong southeasterlies, the position of plume is advected northward while under weak wind forcing, the plume centre does not move significantly.

The maximum plume centre displacement can reach 12 km (Figure 2.27, Table 2.3).

2.4 Discussion

2.4.1 Plume and Estuary Response to Different River Geometries

A longer river channel (bathymetry #5) does not seem to generate more cross-strait flow at the river mouth of the Fraser River. It is likely due to the tidal amplitudes inside the river channel not being produced realistically, indicating an unrealistic dissipation of tidal energy. The problem is shown by the weak tidal amplitudes at Deas Island Tunnel and New Westminster stations compared to the observations from EC (Table B.1). By deepening the river mouth region (bathymetry #6), tidal amplitudes at these two stations are corrected and meanwhile, cross-strait flows (Figure 2.10) are improved compared to the longer river channel (bathymetry #5), which demonstrates the influence of tidal energy on total cross-strait currents at the river mouth.

In bathymetry #6 we see that net daily outflow volume flux integral over top 4 m is stronger than that integrated over full depth (Figure 2.14 c). This is due to the reversal in the direction of the currents with depth caused by the salt-wedge intrusion, where below 4 m depth the inflow that occurs during floods is much stronger than the outflow that occurs during ebb tides.

Bathymetric changes do not affect net daily outflow volume flux integrated over full depth (Figure 2.14 c and g) because the volume of freshwater input to the South Arm in the model is the same between different bathymetries. As a result, changing to a longer and deeper river channel (bathymetry #6) only changes instantaneous volume flux, rather than daily integral volume flux.

The saltier plume produced by a longer and deeper river channel (bathymetry #6) at the river mouth transect (Figure 2.14 d) is mainly caused by the deepened bathymetry, which allows salt-

wedge propagation into the river channel and with vertical mixing, results in a relatively saltier vertical water column. This also explains the higher minimum salinity value with bathymetry #6 compared to the baseline case (Figure 2.10).

Overall, cross-strait velocities are improved with this longer and deeper river channel (bathymetry #6). However, large discrepancies still remain, such as too strong along-strait flows compared to observed drifter tracks (e.g., Figure 2.12), and a saltier plume compared to the ferry observations (Figure 2.10).

2.4.2 Effects of Vertical Eddy Viscosity and Diffusivity

With reduced background eddy viscosities and diffusivities, the time-averaged values of vertical eddy viscosities and diffusivities at most depth levels are larger than the background values (e.g., Figure 2.28); thus NEMO selects the values calculated from the GLS turbulence scheme. Reduced viscosity enables more shear between the upper layer and layers below and this is reflected in the modeled particle trajectories (e.g., lower right panel, Figure 2.12), mainly by reducing the near-surface along-strait flows, which are driven by the barotropic tides. However, reduced viscosity has little impact on the near-surface salinity value of the Fraser River plume (Figure 2.10) as this parameter only directly controls the vertical momentum transfer. Reducing the background vertical eddy diffusivity reduces vertical mixing, resulting in a fresher near-surface waters (Figure 2.10). However, this does not necessarily mean that the plume is fresher everywhere with lowered background vertical eddy diffusivity because plume advection is also changed by changing background vertical eddy diffusivity. As a result, the difference in salinity at some places is saltier and others fresher (e.g., Figure 2.13). However, if one looks at the averaged surface salinity in the plume region (2.1) and (2.2) over October 1-31, 2014, a 0.5 practical salinity unit fresher plume is generated with reduced background vertical

eddy diffusivity.

Our values for vertical viscosity and diffusivity are typical. For example, 1×10^{-5} m^2s^{-1} was used as background value of vertical eddy viscosity to simulate the Rhine River plume using the Delft3D-Flow model with a vertical grid resolution of 2 m. It was considered to generate the most realistic salinity profiles compared to vertical viscosity values of 1×10^{-2}, 1×10^{-3}, 1×10^{-4} and 1×10^{-6} m^2s^{-1} (Jacobs, 2004). Background vertical eddy viscosity and diffusivity of 5×10^{-6} m^2s^{-1} was selected to model the Columbia River plume using Regional Ocean Modeling System with a terrain-following coordinate. Vertical resolution in the model varies and an average resolution is 1.0 m in the upper 4 m in a depth of 100 m (MacCready et al., 2009; Liu et al., 2009).

Although model results are in a better agreement with the observations by adding a longer and deeper river channel as well as reducing background vertical eddy viscosity and diffusivity, substantial discrepancies still exist. For example, the cross-strait velocities are still weak compared to ferry-based observations (e.g., Figure 2.9); the near-surface plume is still saltier compared against CTD and ferry observations (Figure 2.9, 2.10 and 2.13), which could be partially caused by incorrect plume position. In addition, relatively strong northward mean surface flows from June 22 to August 25, 2016 are found north of the river mouth off the banks compared to HF radar data (Figure D.2), which might be related to the absence of the Steveston jetty in the model.

2.4.3 Four Important Forcing Mechanisms Reproduced by Numerical Simulations

Effects of river flows

The increase in amount of fresh water stratifies the water column (a, e and i of Figure 2.17, 2.18), increases the size of plume and expands the near-field region. These features are significant in May

with wind greater than 5 m s^{-1} (e and h of Figure 2.20) compared to October and January when wind magnitude is greater than 5 m s^{-1}. A larger near-field region when the wind is stronger than 5 m s^{-1} in May compared to October and January is probably an artifact of a non-local tide impact. Without tides, more freshwater was transported to the south to fulfill the stronger estuarine circulation due to the lack of tidal mixing in Haro Strait. This southward advection, particularly of the May plume result could also be due to advection caused by winds from north-west. Winds from northwest advect the plume more to the southeast compared to October, when prevailing winds from south-east advect the plume against the mainland coast. In either of these two cases, the size of modeled near-field region is not directly related to mixing, but a result of advection.

During weak wind periods, the near-field region dominates the plume region in October and January. However, the near-field region is smaller in May compared to October and January for weak winds (c of Figure 2.20).

Halverson and Pawlowicz (2008) investigated Fraser River plume salinity affected by river discharge and tides based on four-years (2003-2006) of ferry observations. They suggested that the ferry only samples the near-field plume during high river flow but not during low flow in winter when the near-field plume remains much closer to the river mouth. With a threshold of 0.1 for our $Rmix$ based near-field criteria, our results show that the near-field is constrained near the river mouth in January and October, which agrees with their interpretation of the ferry data. Furthermore, they interpreted the result using a conceptual model for the combined effects of tides and river flow on plume salinity. For example, in summer, the position of salt-wedge is more downstream than in winter (Kostaschuk and Atwood, 1990; Halverson and Pawlowicz, 2008), suggesting mixing at the river mouth would be stronger since intense mixing occurs around the salt-wedge. As a result, the near-field plume area is larger in summer than in winter (Halverson and Pawlowicz, 2008). A

major difference between the study of Halverson and Pawlowicz (2011) and my study is that they estimated local intense mixing. On the other hand, my study measures the total mixing based on the water column stratification.

Overall, the impact of river discharge on the location of the plume centre is small, with no more than 3 km northward movement between low river flow (January, 2016) to high river flow (May, 2015). This small displacement that is observed is possibly caused by more northward spreading with increasing river discharge.

Effects of winds

Wind is the major factor causing mixing in the Fraser River plume under moderate and low river flows, provided the wind is greater than 5 m s^{-1} (Figure 2.20). Thus the far-field plume, defined as the region dominated by wind mixing, is the largest part of the plume. Wind typically mixes the surface plume (Horner-Devine et al., 2015), which can be seen by the smaller area enclosed by the 25.3 practical salinity isohaline plume boundary (Figure 2.27). In general, both the amount of the freshwater transport across the northern transect and plume centre location correlate with the wind. The 3-day time-averaged plume centre location can move 12 km when pushed by a strong wind (Figure 2.27 i) and the averaged rate of freshwater transport across the northern transect (Figure 2.24) caused by wind can exceed the river discharge rate during the same period (Table 2.3, Figure 2.25), indicating the importance of winds in freshwater transport.

Wind impacts the spatial freshwater thickness pattern of the plume. Even without wind forcing, the freshwater thickness distribution and plume centre location vary about 2-3 km (Figure 2.27), which could be caused by the combined effects of river discharge and spring/neap variations due to the tides.

A plume bulge is an unsteady anticyclonic eddy circulation that forms offshore of the river mouth in the absence of external forcing, such as winds [Section 1.5, Horner-Devine et al. (2015)]. It is very unlikely that a bulge forms in the Fraser River plume. According to the bulge circulation theory, momentum of the bulge flow in a steady state satisfies the gradient-wind balance (Horner-Devine et al., 2015; Horner-Devine, 2009), where the pressure gradient is balanced by both the centrifugal force and the Coriolis force. Modeled 3-day mean surface currents, in October in the without wind forcing case, have a bulge-like pattern with velocities of about 0.01 m s^{-1}. These are much smaller than an inertial flow, $v = fr$, velocity of nearly 0.8 m s^{-1} given that the radius r of the eddy-like feature is about 7 km (Figure 2.27 e). The modeled mean surface flow is also smaller than the geostrophic buoyant flow estimated by thermal wind relationship:

$$\frac{\partial v}{\partial z} = \frac{g}{f\rho_0}\frac{\partial \rho}{\partial x} \tag{2.16}$$

Scaling analysis is performed to estimate V velocity:

$$V \approx \frac{g}{f}\frac{\Delta z}{\rho_0}\frac{\Delta \rho}{\Delta x} \approx 0.4 \mathrm{ms}^{-1} \tag{2.17}$$

where Δz is about 10 m for plume depth, f is approximately 1×10^{-4} s^{-1}, Δx is the length scale over the bulge-like pattern (Figure 2.27 e), around 7 km, $\Delta \rho$ of this region is about 3 kg m^{-3} given the salinity change of 4. This 0.4 m s^{-1} velocity is much larger than modeled mean along-strait V velocity in the bulge-like area, which is only around 0.01 m s^{-1}.

Using the gradient-wind relationship, the expected flow should exceed flow under geostrophy alone because the centrifugal and pressure gradient terms are in the same direction. Then the difference between the modeled speed and the expected speed further increases. Therefore, the mean flow is not explained by the gradient-wind balance.

On the other hand, the tidal excursion at the centre location of bulge is 7 km, which is comparable to the Rossby deformation radius in this region (R_d ~7 km). The fluctuation caused by strong tides may inhibit the bulge formation in the SoG.

Weak amplitude wind (0-5 m s^{-1}) has little effect on the centre plume location and the amount of freshwater transport compared to moderate or strong wind conditions (Table 2.3). The wind directions during weak wind periods are usually variable. As a result, the net influence of weak winds on the plume location is small.

Effects of tides

The region dominated by tide-induced mixing (near-field) is tightly constrained near the Fraser River mouth during low and moderate river flow (Figure 2.20). Tides cause more mixing than the winds inside the river channel and the salt-wedge propagation is more limited with just tides than with just winds (Figure 2.21). Mixing in the river channel is less intense in May, which is likely due to the strong river outflow that causes stronger stratification. However, even under strong river flow, the tides are still important in vertical mixing inside the river channel compared to the winds (Figure 2.21).

The distance of salt-wedge propagation S' (unit: m) is calculated from the empirical equation

(Kostaschuk and Atwood, 1990):

$$S' = 82419\text{m} - 9835\text{m} \times \log_{\text{e}} \text{Q} + 22458\text{m} \times \log_{10} \text{T} \tag{2.18}$$

where Q is the river discharge (unit: m^3s^{-1}) at Hope, T is the tidal height (unit: m) at Point Atkinson. The distance of salt-wedge (S') is measured relative to Sand Heads in study of Kostaschuk and Atwood (1990). It is converted to refer to Steveston by:

$$S'_s = S' - 8300\text{m} \tag{2.19}$$

Modeled position of salt-wedge propagation is defined as the point of intersection of the 10 practical salinity isohaline with the estuary bed (Kostaschuk and Atwood, 1990).

The model results for the position of the tip of the salt-wedge when it is high tide at Point Atkinson are compared to the predictive regression model results based on observations using 2.18 from Kostaschuk and Atwood (1990) (Figure 2.29). Model results with only river and winds show very small variations in the salt-wedge position since there is no fortnightly tidal cycle. The salt-wedge location is similar between the tides only case and the combine all case and the position is subject to fortnightly tidal modulation. The striking feature of this set of comparisons is that the modeled salt-wedge intrusion is closer to the river mouth at Steveston by about 5 km compared to the predictions, indicating too much mixing in the model. However, Kostaschuk and Atwood (1990) pointed out a couple of sources of errors in predicting this salt-wedge position, such as the time lag in discharge between Hope and the estuary, which results in potential errors in the salinity-discharge relationship since variation in discharge at Hope may not be felt in the estuary for one or two days.

More importantly, this prediction is based on a limited dataset (19 observations), which may have limitations due to the quantity.

Freshwater flux in the upper 10 m with tides shows large differences compared to that with river only (Figure 2.24). The amount of freshwater carried southward in the river only case, without tides is 3-5 times greater than that with the tides. This large difference of freshwater amount is most likely due to the role of tidal mixing in Haro Strait (Figure 2.1). Tidal mixing significantly reduces estuarine exchange (Nagai and Hibiya, 2011). However, the reduced freshwater transport due to the lack of tides cannot last forever, as the freshwater input is the same for all the different forcing runs. Nonetheless, this result for a short period simulation is completely different compared to results of Li and Rong (2012) for the Changjiang River plume located on the shelf, where they argued that by adding tides, freshwater transport was enhanced. They interpreted this phenomenon as tidal currents forcing the plume water to move in the direction of the tidal currents, thus freshwater transport downstream increased. Without tides, most of the Changjiang River plume was trapped near the river mouth and formed a bulge, which accumulated a large portion of freshwater, and therefore led to less freshwater transported downstream. Comparison of Changjiang River plume and Fraser River plume undoubtedly illustrates different roles of tides on plume transport between on the shelf and in a semi-enclosed ocean basin. On the shelf, tidal currents mainly advect the plume in the direction of the tidal currents, which impacts freshwater transport. However, the freshwater transport is insensitive to the strength of turbulent mixing (Li and Rong, 2012). On the other hand, in a semi-enclosed ocean basin, such as in the SoG, tides contribute to mixing that decreases the freshwater transport by estuarine circulation and this reduction of freshwater flux is not caused by advection due to the tides.

Effects of Coriolis force

The Coriolis force is important in weakening the mixing of the plume, due to its role in producing a thicker plume because of the northward deflection of the plume along the mainland coast, and this thicker plume is not as easily mixed by the winds. The Coriolis force results in fresher water in English Bay. This phenomenon is robust and independent of river flow conditions (Figure 2.22). My study shows the Coriolis force generally reduces the Fraser River plume mixing in the far-field plume, which is in agreement with previous studies (Garvine, 1999).

Generally, much more freshwater is carried northward across the northern transect (Figure 2.24) with the Coriolis force (Table 2.3), except during strong winds. Winds appear to impact the plume more without the Coriolis force (Figure 2.25). Specifically, a moderate wind to the north results in more northward flux. This is because the Coriolis force constrains the plume along the mainland coast and the depth of plume is thicker to conserve the plume buoyancy. A deeper plume is more difficult to move by the winds.

2.4.4 Conclusions

Surface flows and salinity in the Fraser River plume in a three-dimensional baroclinic model were evaluated against various types of observations. The major problems in the model are too weak cross-strait flows, too strong along-strait flows and too salty a plume. By employing a longer and deeper river channel (bathymetry #6) for the Fraser River, cross-strait flows improve substantially compared to both ferry-based salinity data and drifter data.

Plume movements and properties are sensitive to values of vertical eddy viscosity and diffusivity. By reducing the background vertical eddy viscosity and diffusivity to $1\times\ 10^{-5}$ and 1×10^{-6} m^2s^{-1}, respectively, both surface flows and salinity in the plume improved. From a single drifter-particle

comparison, the along-strait flows were reduced in magnitude by reducing the background vertical eddy viscosity. However, of the nine drifters, only two showed reduced along-strait velocities, two showed increased along-strait velocities and five showed no significant change. The near-surface salinity values were generally reduced by reducing the background vertical eddy diffusivity.

Using the longer and deeper river channel (bathymetry #6), lowered background vertical eddy viscosity and diffusivity, mixing and transport processes within the Fraser River plume were studied. The relative strength of momentum and internal wave speed was investigated. Instantaneous momentum is generally weaker during peak floods than during peak ebbs. Internal wave speed is overall higher during high river flow period than low and moderate river flow periods.

The impact of river discharge, tides, winds and the Coriolis force on mixing and freshwater flux were investigated and the principle findings are:

1. The amount of runoff impacts mixing by stratifying the water column. The size of the plume and tide-induced mixing region expands with increasing river discharge. However, the plume centre location does not change much.

2. The region dominated by tide-induced mixing is tightly constrained near the river mouth during low and moderate river flow conditions. The tide-induced mixing in the river itself is stronger than that due to the wind. The amount of freshwater flux across the northern transect in runs with tides decrease to 20-33% compared to runs without tides due to tidal mixing in Haro Strait that significantly reduces the freshwater transport.

3. Wind is the dominant factor in mixing in the Fraser River plume during low and moderate river flow periods, provided the magnitude of wind is greater than 5 m s^{-1}. For most of the plume, wind mixing controls the total mixing. Wind contributes to considerable change in both the freshwater flux (2.14) and plume centre location.

4. The Coriolis force constrains the plume along the mainland coast and the plume freshens English Bay. The Coriolis force contributes to much more northward freshwater transport along the mainland coast when the wind is not strong. The plume is deeper and less easily affected by winds.

Table 2.1: List of simulations for evaluation. ν_b and κ_b are background vertical eddy viscosity and diffusivity, respectively.

Run	Scenario	Bathymetry version	ν_b (m^2s^{-1})	κ_b (m^2s^{-1})	Wind	Time period
1 a	Baseline	2	1×10^{-4}	1×10^{-5}	Yes	June [1]
1 b	Baseline	2	1×10^{-4}	1×10^{-5}	Yes	October [2]
2	Extended river channel	5	1×10^{-4}	1×10^{-5}	Yes	June [1]
3 a	Extended and deepened river channel	6	1×10^{-4}	1×10^{-5}	Yes	June [1]
3 b	Extended and deepened river channel	6	1×10^{-4}	1×10^{-5}	Yes	October [2]
4	Lower viscosity	6	1×10^{-5}	1×10^{-5}	Yes	October [2]
5	Lower viscosity and diffusivity	6	1×10^{-5}	1×10^{-6}	Yes	October [2]
6	Baseline bathymetry without wind	2	1×10^{-5}	1×10^{-6}	No	October [2]
7	Extended and deepened river channel without wind	6	1×10^{-5}	1×10^{-6}	No	October [2]
8	Extended and deepened river channel with jetty	10	1×10^{-5}	1×10^{-6}	Yes	October [2]
9	Extended and deepened river channel	6	1×10^{-5}	1×10^{-6}	Yes	October [3]

[1] June 15-29, 2015, Initialized June 14, no spin-up
[2] October 1-31, 2014, Initialized September 25, 5 days spin-up
[3] October 1-31, 2015, Initialized September 18, 12 days spin-up

Table 2.2: List of plume physics simulations

Scenario	Averaged river discharge (m^3 s^{-1})	Initialization	Time period
Low river flow	1316	Dec 19, 2015	Jan 1-31, 2016
Moderate river flow	2051	Sep 25, 2014	Oct 1-31, 2014
High river flow	4970	Apr 18, 2015	May 1-31, 2015

Table 2.3: Mixing and transport parameters impacted by winds and the Coriolis force for various wind event periods during three river flow periods. Flux is across the northern transect (Figure 2.24). Change of plume centre location is calculated with (2.15). Along-strait and cross-strait distance in the near-field region starts from the river mouth.

River flow	Dates	Wind condition		Near-field (km)		Coriolis impact on flux (with - without) (m^3 s^{-1})	Wind impact (with - without)	
		Magnitude	Direction (to)	along-strait	cross-strait		Flux (m^3 s^{-1})	Change of plume centre (km)
[1] Low	Jan 27-28	Strong	Northwest	8	2.2	-2034	534	9.3
	Jan 17-19	Moderate	Northwest	8	2.4	-926	969	8.4
	Jan 8-10	Weak	–	–	–	2066	374	3.1
[2] Moderate	Oct 21-23	Strong	Northwest	2.6	2	278	3855	12.5
	Oct 18-20	Moderate	Northwest	6.5	2.2	-580	2687	12.1
	Oct 3-6	Weak	–	–	–	1089	439	1.7
[3] High	May 2-3	Strong	Southeast	30	16	7957	8814	11.8
	May 19-21	Moderate	Southeast	41	23	4829	6564	2.5
	May 9-11	Weak	–	–	–	4573	4856	2.6

[1] January 1-31, 2016
[2] October 1-31, 2014
[3] May 1-31, 2015

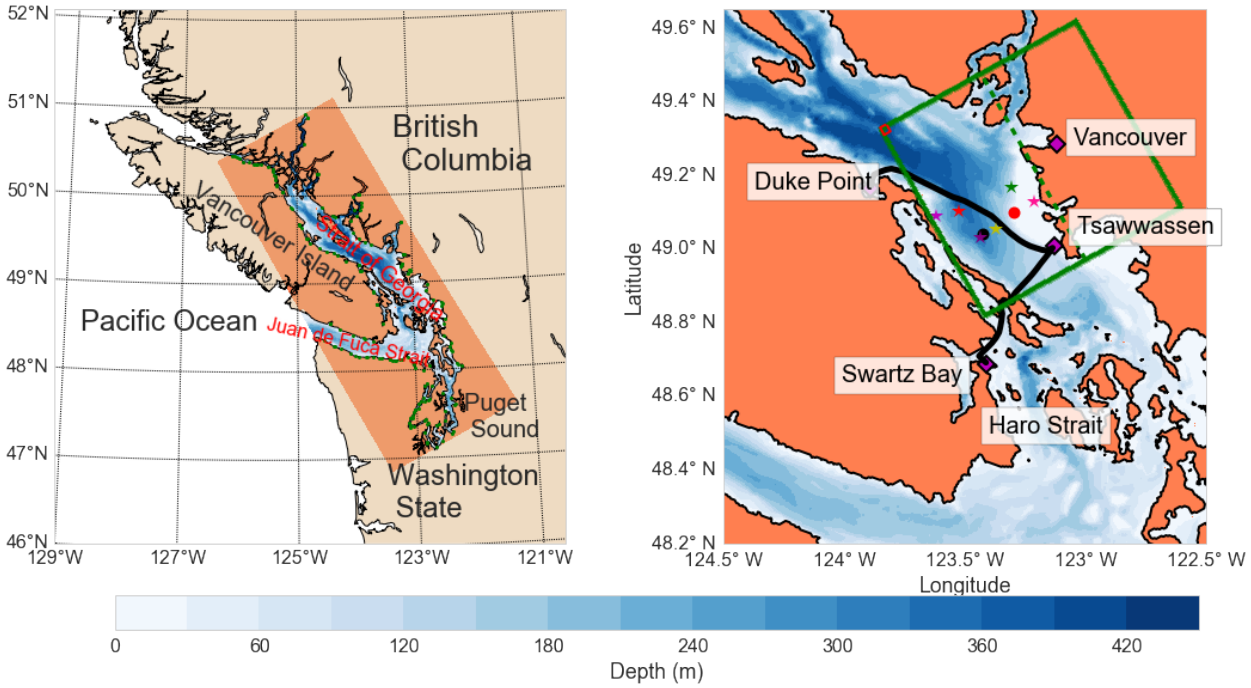

Figure 2.1: Domain and observation sites. Left panel is model domain (colored rectangular area) including bathymetry and rivers (green circles). Right panel displays the locations of observations. Two ferry routes (black lines) with terminal locations. Location of the CTD casts (stars) in the Fraser River plume region and NS station (green star). Location of Sand Heads station (red circle), VENUS Central station (black circle). Subdomain that will be used to analyze the plume (box bounded by four green solid lines). The northwest corner of this subdomain (box bounded by four red lines), used to calculate a reference salinity. Half the subdomain is used to calculate plume centre location (west half of green box as split by the green dashed line).

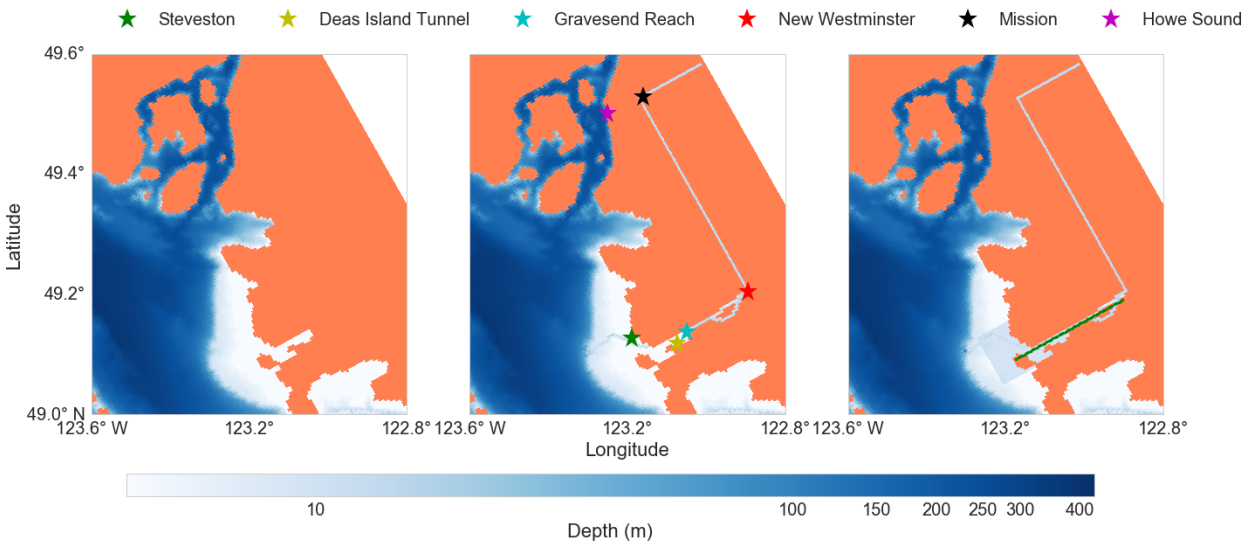

Figure 2.2: From left to right are bathymetry #2, #5 and #6, respectively. Centre panel shows station locations. Right panel shows the along river transect (in green).

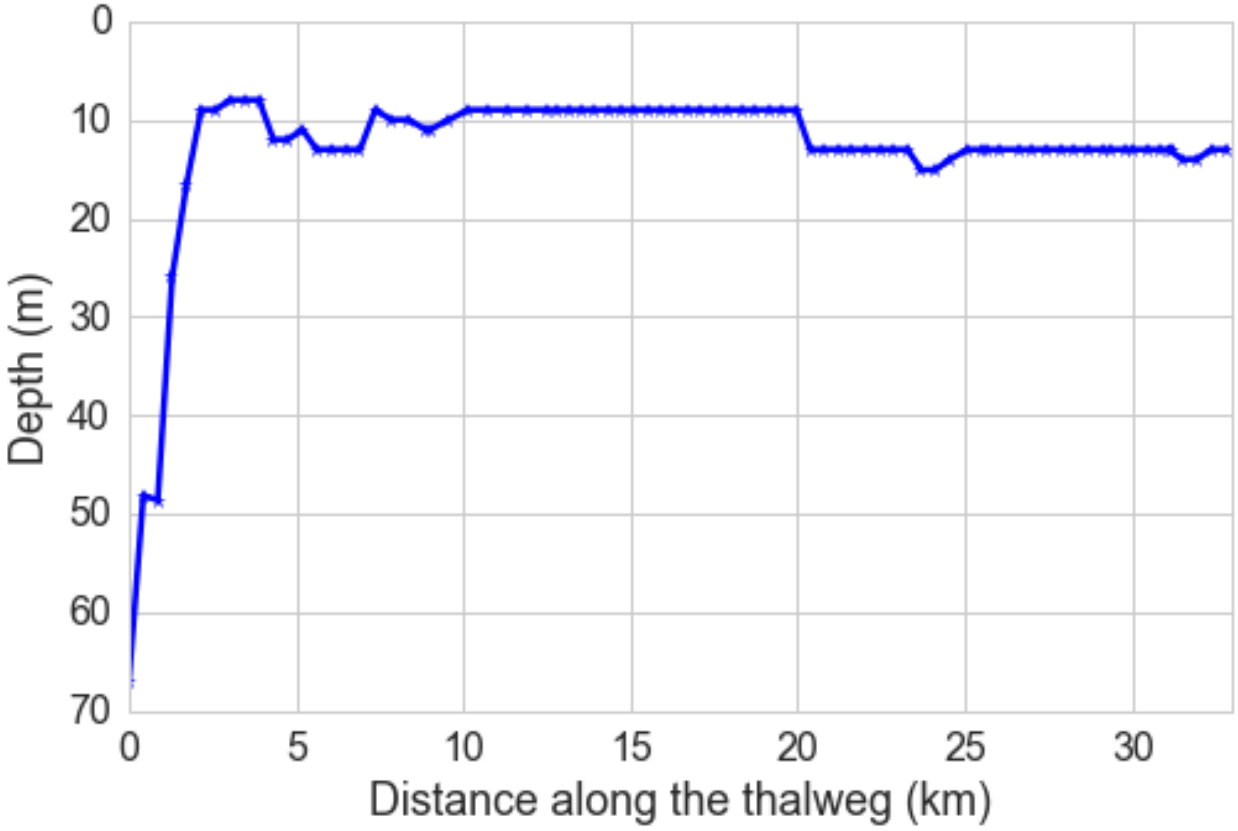

Figure 2.3: Thalweg of bathymetry#6 in the model. Distance starts from the 67 m isobath, and increases upriver. 35 km is at New Westminster.

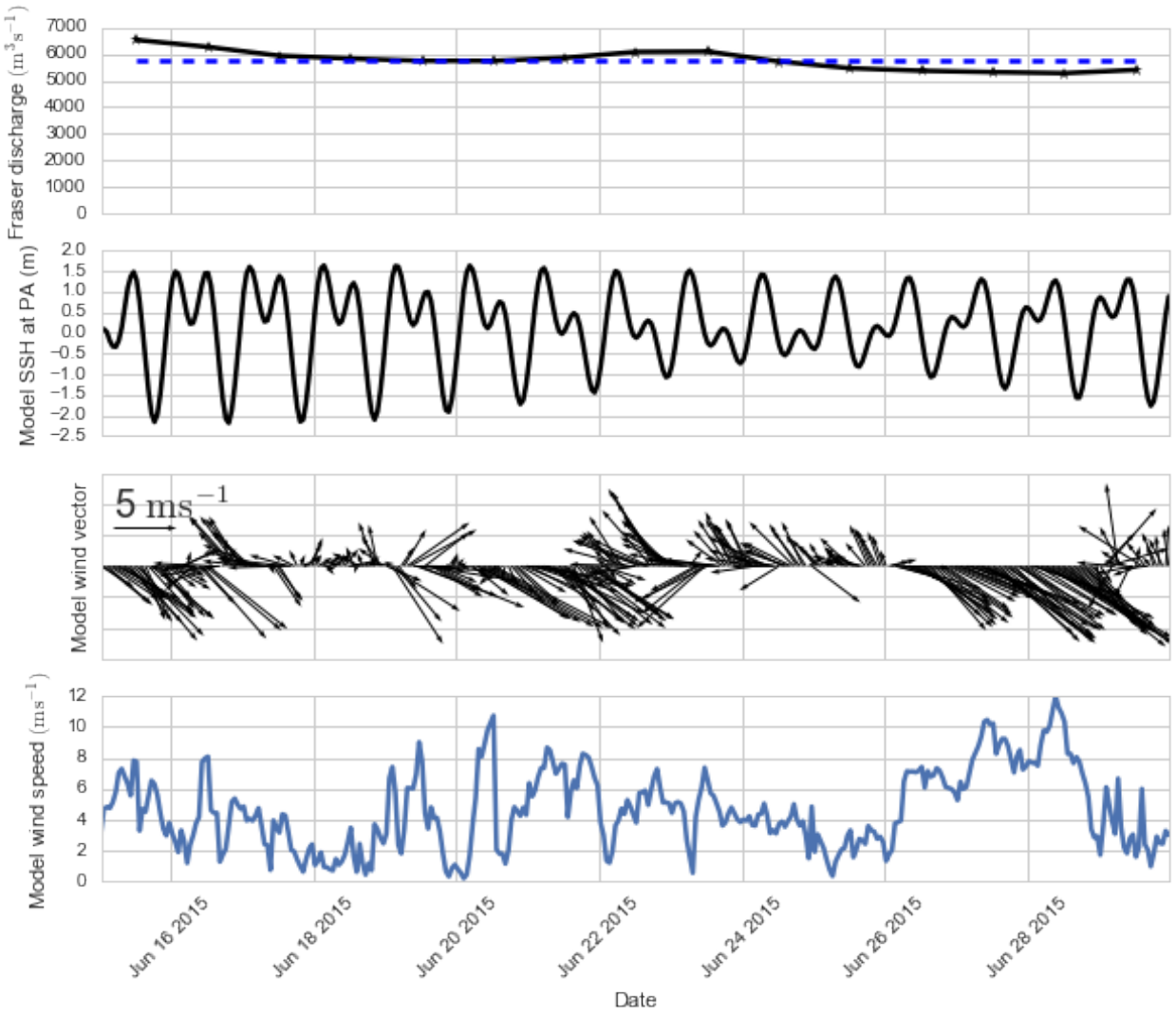

Figure 2.4: Model forcing for June 15-29, 2015. Top panel shows daily Fraser River discharge (black) at Hope and averaged river discharge during this time period (blue). Second panel from top is hourly modeled sea surface height at Point Atkinson. Third panel from top shows wind vectors with north upward at Sand Heads. Arrows represent the to direction of wind. Bottom panel shows the hourly model wind speed at Sand Heads.

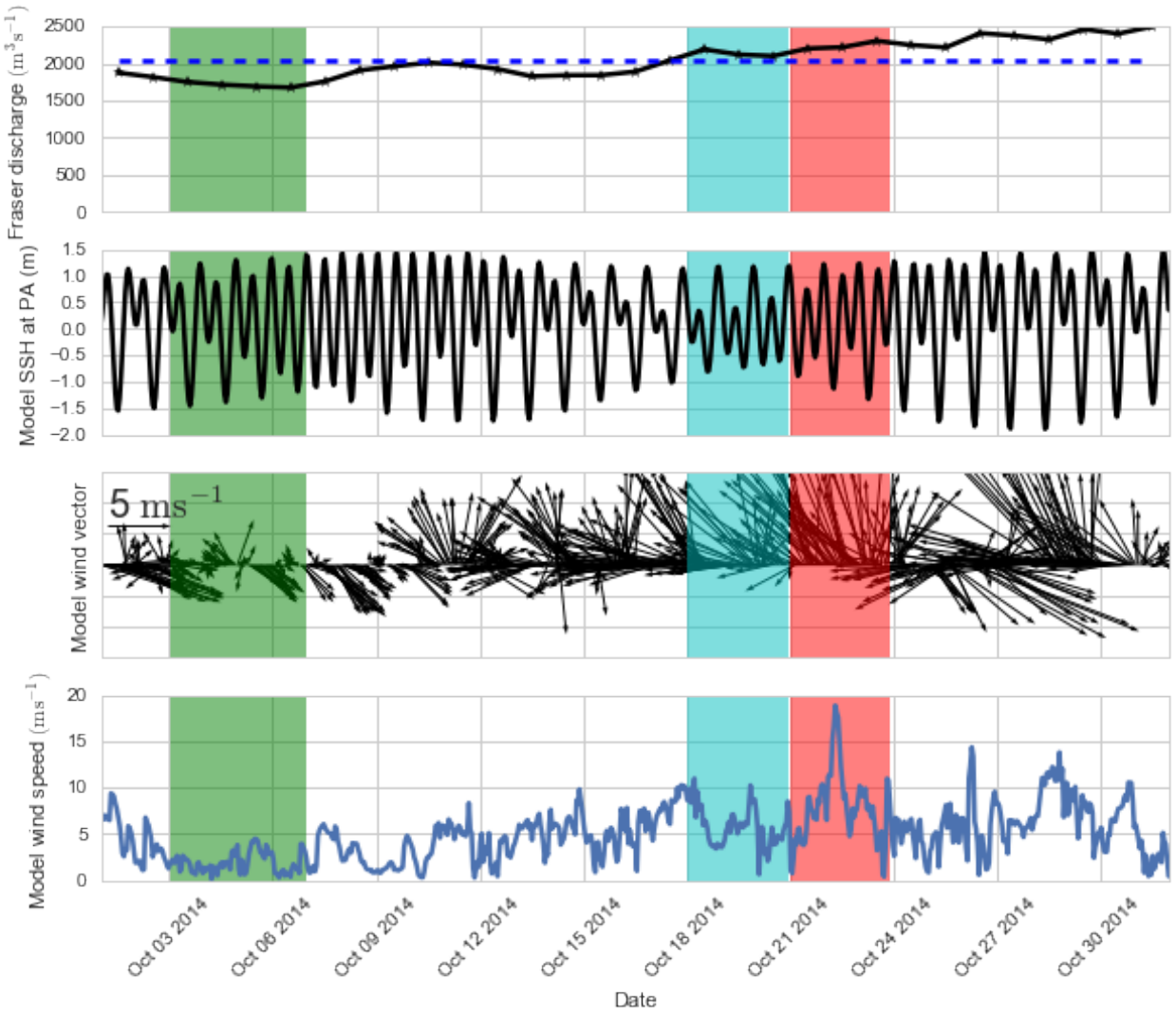

Figure 2.5: Model forcing for October 1-31, 2014. Top panel shows daily Fraser River discharge (black) at Hope and averaged river discharge during this time period (blue). Second panel from top is hourly modeled sea surface height at Point Atkinson. Third panel from top shows wind vectors with north upward at Sand Heads. Arrows represent the to direction of wind. Bottom panel shows the hourly model wind speed at Sand Heads. Green, blue and red columns in each panel represent the weak, moderate and strong wind event periods, respectively.

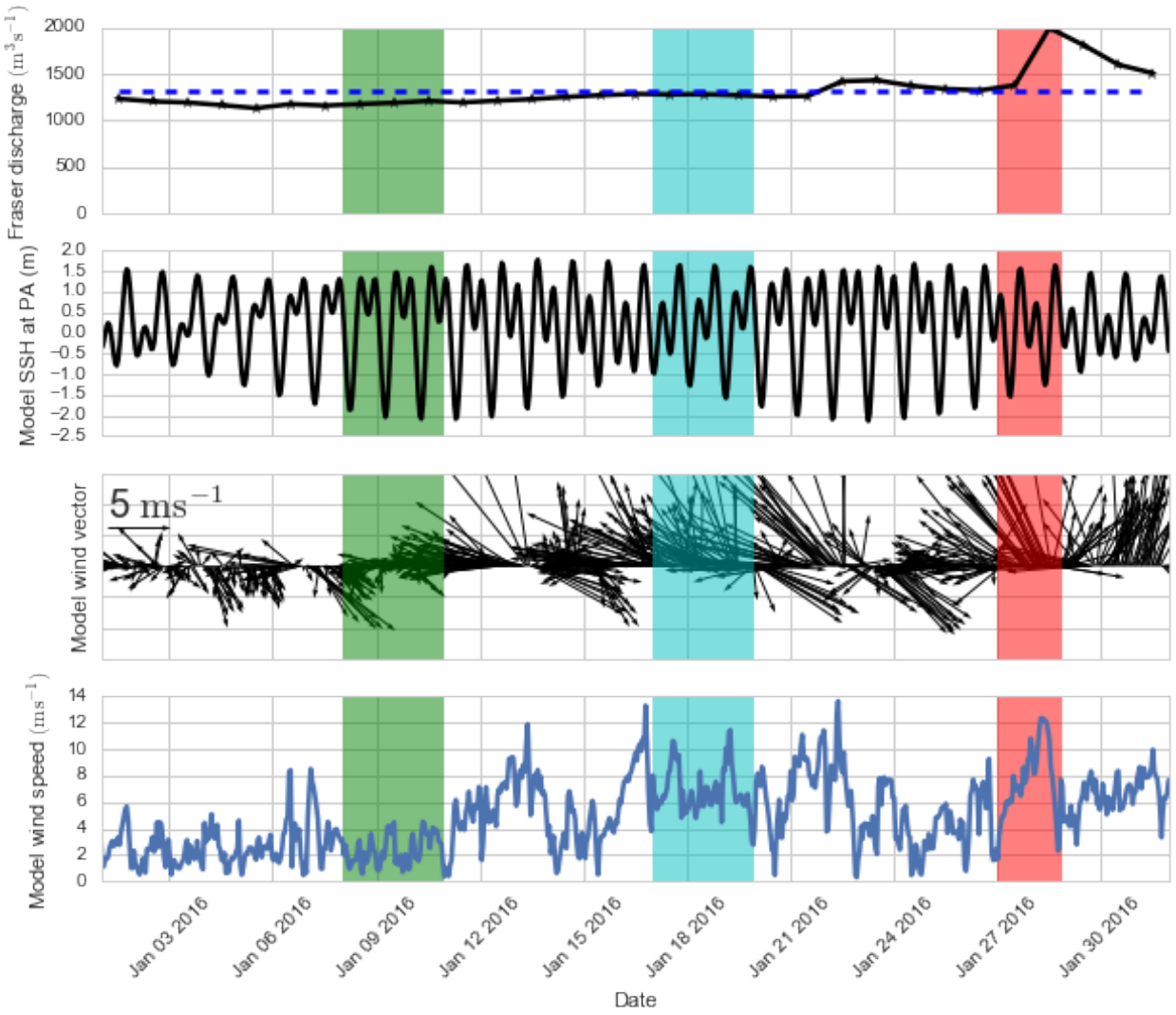

Figure 2.6: Model forcing for January 1-31, 2016. Top panel shows daily Fraser River discharge (black) at Hope and averaged river discharge during this time period (blue). Second panel from top is hourly modeled sea surface height at Point Atkinson. Third panel from top shows wind vectors with north upward at Sand Heads. Arrows represent the to direction of wind. Bottom panel shows the hourly model wind speed at Sand Heads. Green, blue and red columns in each panel represent the weak, moderate and strong wind event periods, respectively.

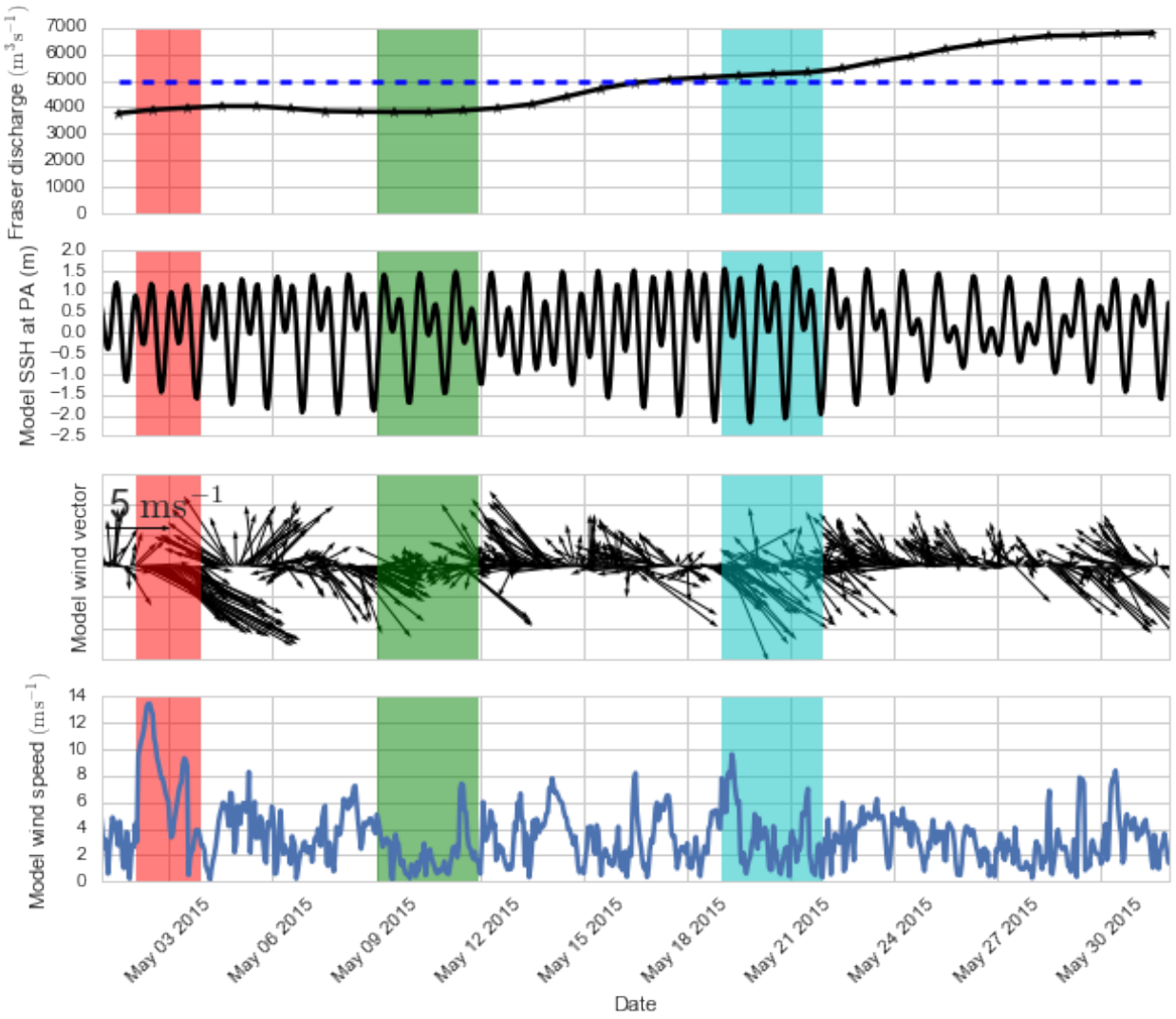

Figure 2.7: Model forcing for May 1-31, 2015. Top panel shows daily Fraser River discharge (black) at Hope and averaged river discharge during this time period (blue). Second panel from top is hourly modeled sea surface height at Point Atkinson. hird panel from top shows wind vectors with north upward at Sand Heads. Arrows represent the to direction of wind. Bottom panel shows the hourly model wind speed at Sand Heads. Green, blue and red columns in each panel represent the weak, moderate and strong wind event periods, respectively.

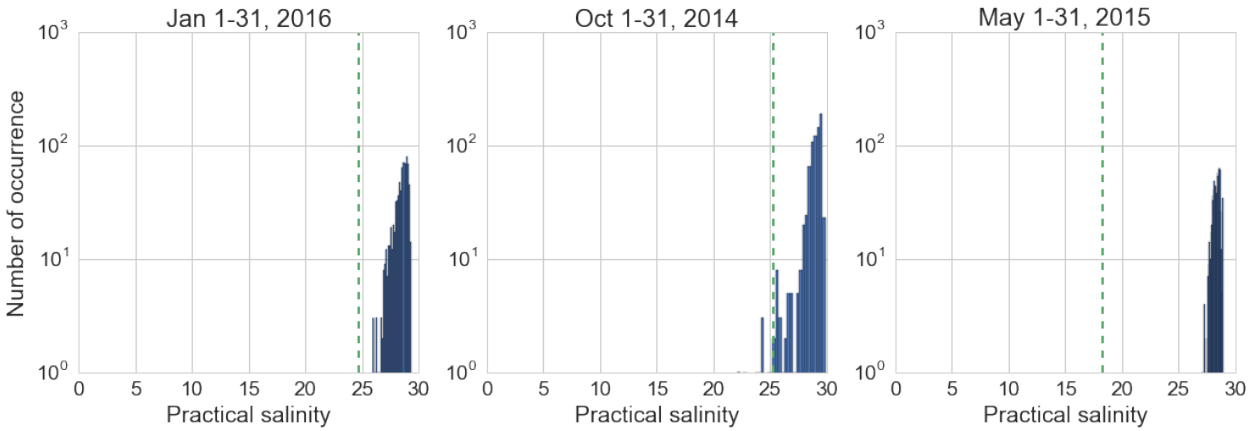

Figure 2.8: Number of occurrence of salinity of 10.5 m depth at NS station (Figure 2.1) in January 2016, October 2014 and May 2015 from left to right, respectively. Dashed green line labels the salinity threshold (2.1). Overall, no more than 1% of the time does the plume reach beyond 10 m depth during these three months according to the salinity criteria.

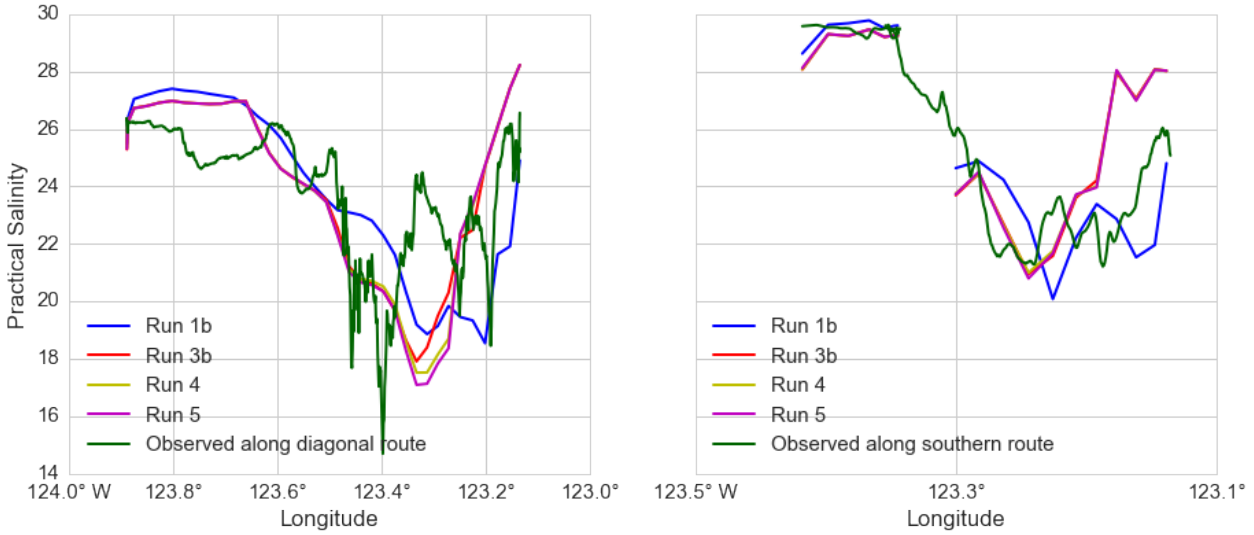

Figure 2.9: Comparison of the 1.5 m depth model results for Runs 1b, 3b, 4 and 5, and the ferry-based salinity along diagonal ferry route (left panel) and south ferry route (right panel) on October 8, 2014, from 3:15 to 5:15 (UTC), and 2:15 to 3:40 (UTC), respectively. On the right panel, results of Run 4 and Run 5 are underneath that of Run 3b. Run 5 (Lower both viscosity and diffusivity) produces the closest minimum salinity value compared to observations on the diagonal route. Location of minimum salinity value moves more than half way towards the observed minimum in Run 3b, 4 and 5 for diagonal route. Run 3b, 4 and 5 show improvement in reducing discrepancy of minimum salinity location compared to Run 1b on the south route.

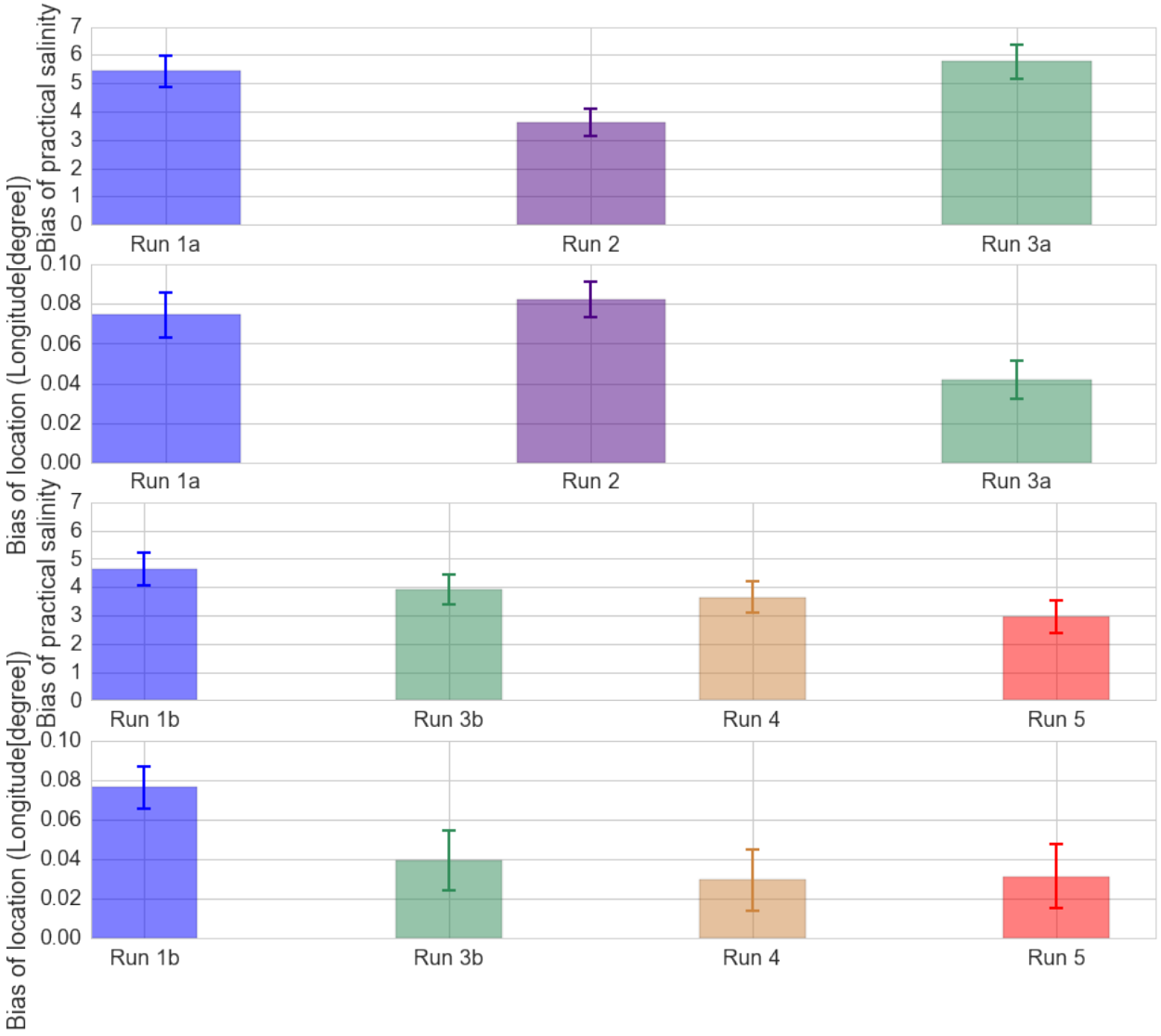

Figure 2.10: Statistics of bias (model - data) of eighty-six (upper two panels) and twenty-three (lower two panels) ferry crossing comparisons of minimum salinity value and location between modeled results of run 1a, run 2, run 3a (upper two panels) and and ferry-based salinity along the diagonal track, and between modeled results of run 1b, run 3b, run 4, run 5 (lower two panels) and ferry-based data along the diagonal track. Errorbars show the standard error of the bias for each run, respectively. Run 3a improves plume location by generating stronger cross-strait velocities, but does not reduce the salinity value (upper two panels). Run 5 decreases the salinity values.

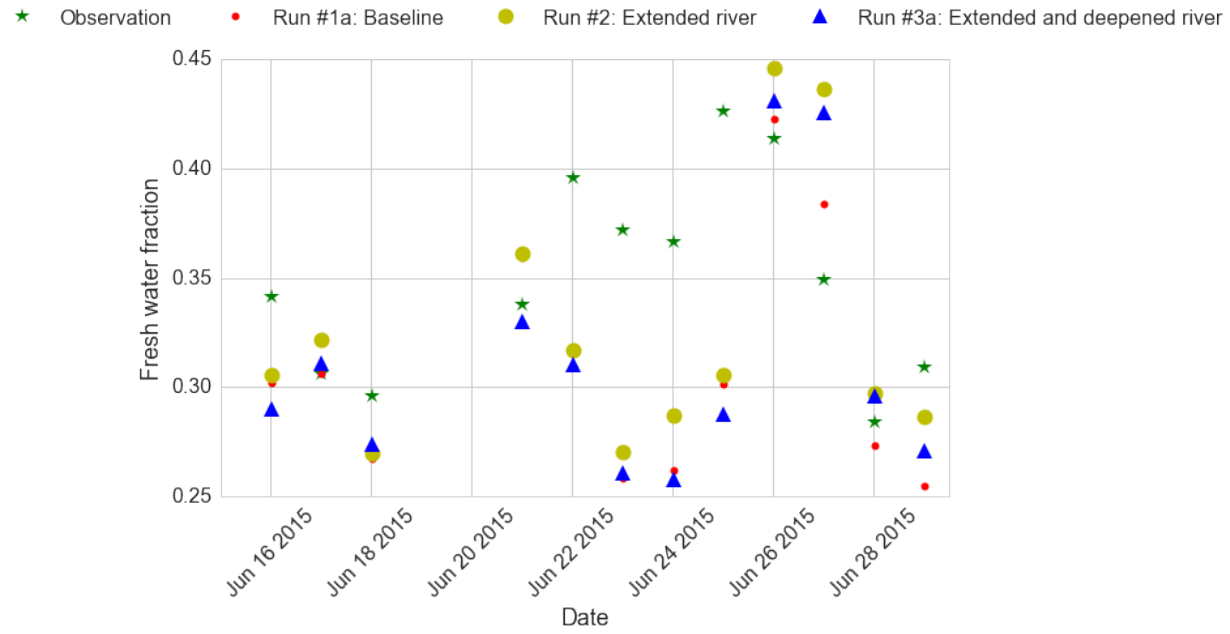

Figure 2.11: Daily averaged fresh water fraction along the diagonal ferry route of June 16-29, 2015. Even after extending and deepening the river channel (Run #3a), the fresh water fraction is still too low compared to the observations.

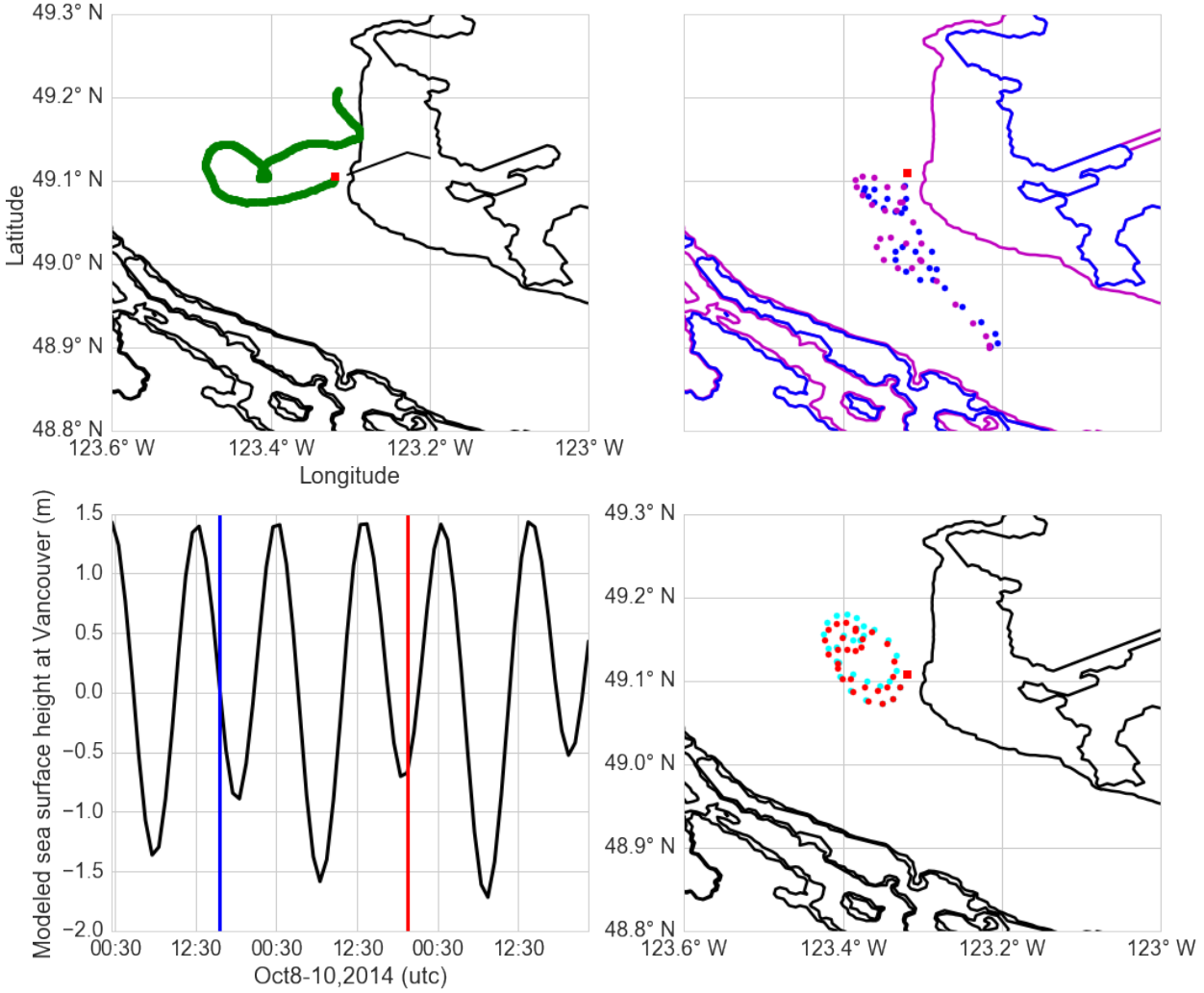

Figure 2.12: A drifter comparison with modeled surface particles. Upper left panel: observed drifter. Upper right panel: Run 1b (blue dots) and run 3b (magenta dots). Lower right panel: run 4 (teal dots) and run 5 (red dots). Lower left panel shows the sea surface height at Vancouver, BC, Canada, with the blue and red vertical lines representing the release and recovery time for this drifter at 16:10 (UTC) on October 8, 2014 and at 20:55 (UTC) on October 9, 2014, respectively. Model cross-strait velocities are slightly stronger with run 3b than run 1b. Along-strait flows are reduced substantially with run 4 and 5.

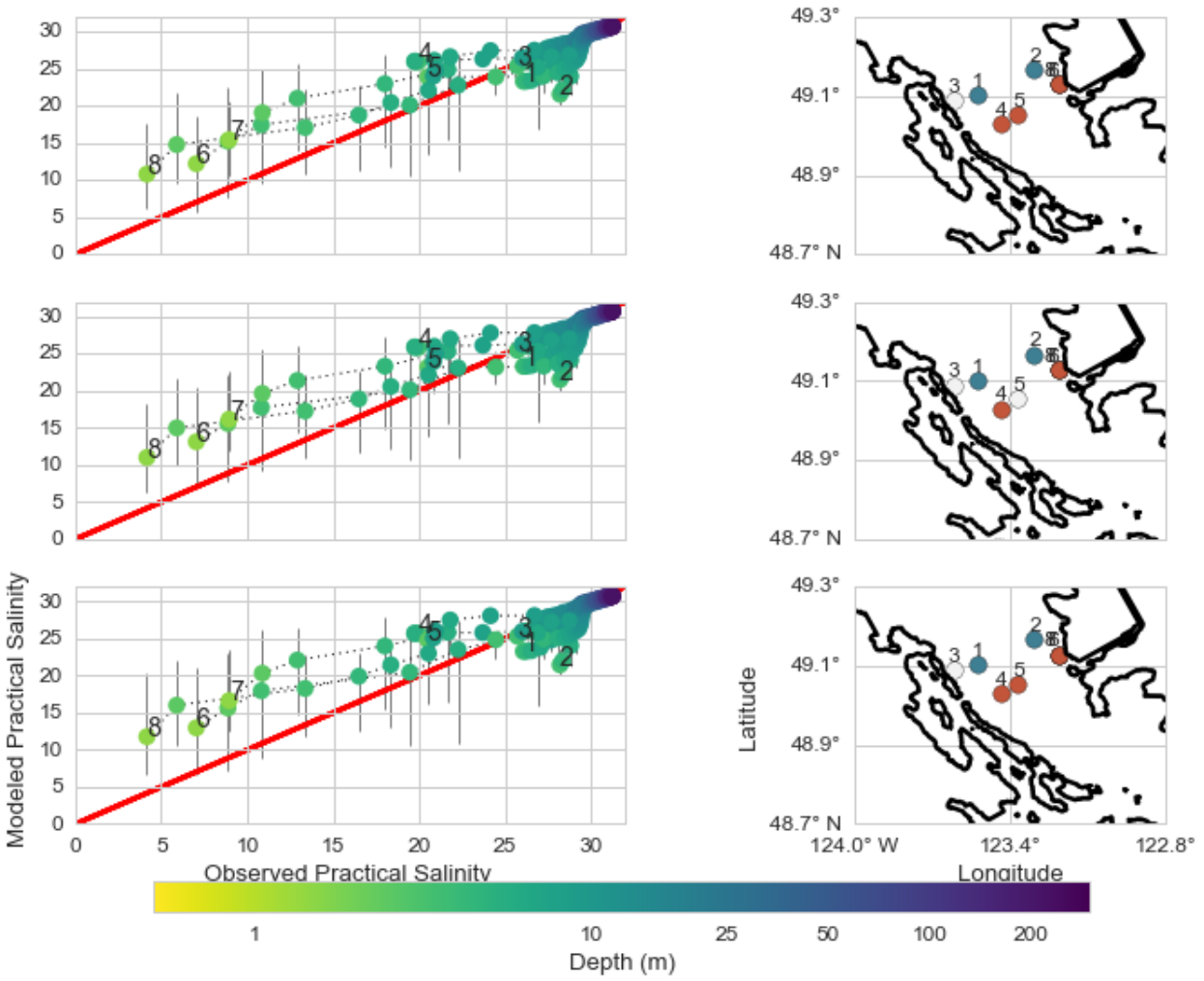

Figure 2.13: Scatter diagram of the observed CTD versus modeled results and cast locations on the map. Errorbars show the minimum and maximum hourly-average salinity values and symbols show the model daily averaged salinity. Cast numbers are labeled. In the panels on the right, the red color indicates modeled salinity is saltier than the observation at the shallowest available depth of the observed cast, blue indicates the modeled salinity is fresher and white shows the modeled salinity value is within 1 compared to observations. This depth ranges between 1.5 and 3.5 m. Upper panel: observation versus results of run #3b. Middle panel: observation versus results of run #4. Lower panel: observation versus results of run #5. Variation of viscosity and diffusivity has little impact on the salinity profiles.

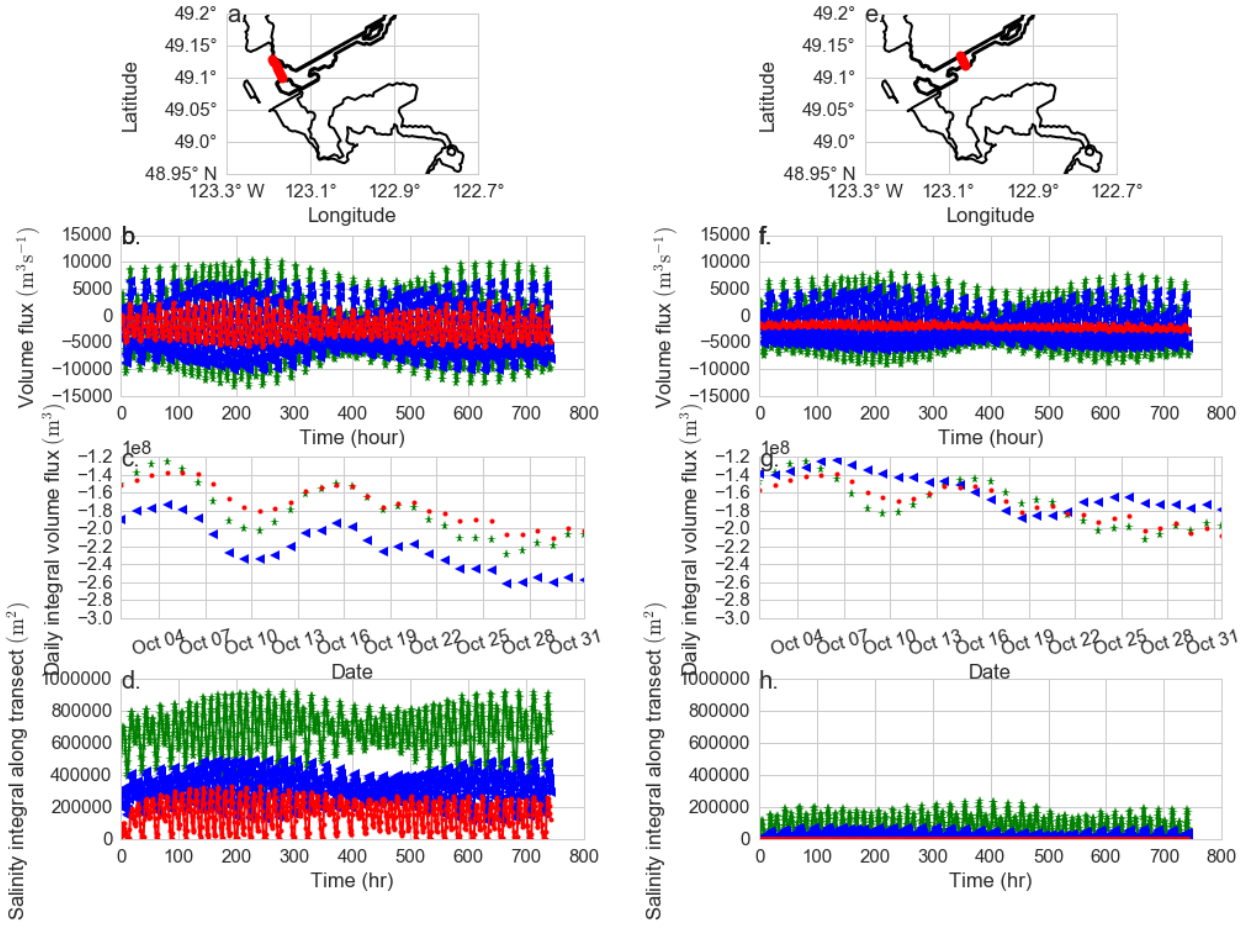

Figure 2.14: Transect locations, instantaneous volume flux, daily integrated volume flux and salt flux. Locations of transects (Upper panel). Panel b and f: hourly volume flux integrated (2.4) over full depth for run #6 (red), integrated over full depth for run #7 (green) and integrated over only the top 4 m for run #7 (blue) across the transect shown in Panel a and e. Hours since 00:30 (utc) on October 1, 2014. Panel c and g: as Panel b and f but for daily volume flux. Panel d and h: as Panel b and f but for the salinity integral (2.5). With a longer and deeper river channel (bathymetry #6) (green), larger amplitude fluctuations in the hourly volume flux and much saltier water are obtained.

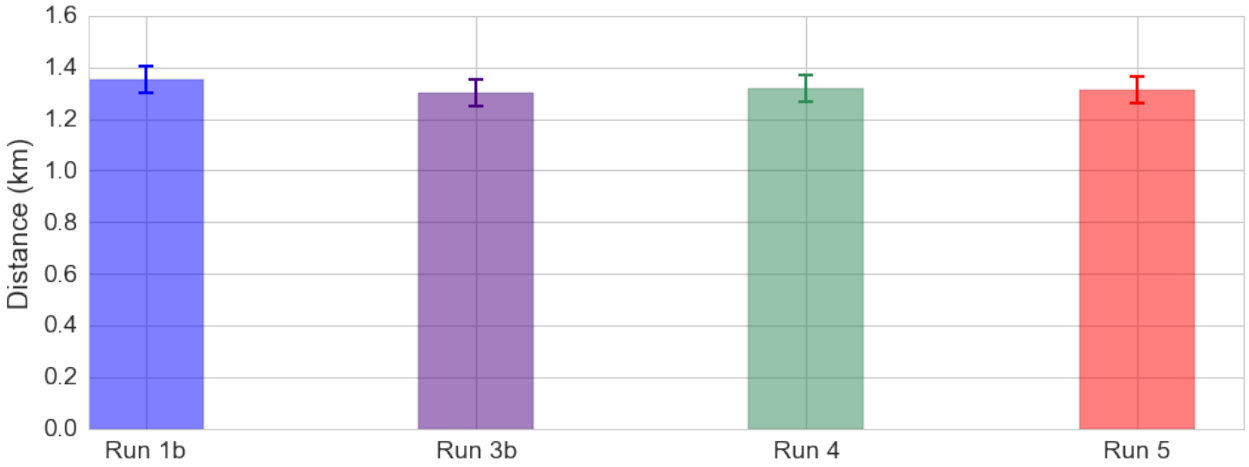

Figure 2.15: Statistics of averaged distance between the observed drifters and various modeled particles after one hour. Errorbars show the standard error of the averaged distance of each model run (Run #1b, 3b, 4 and 5), respectively. There is no statistically significant improvement with the longer and deeper river channel (Run #3b), lower viscosity (Run #4) and lower both viscosity and diffusivity cases (Run #5).

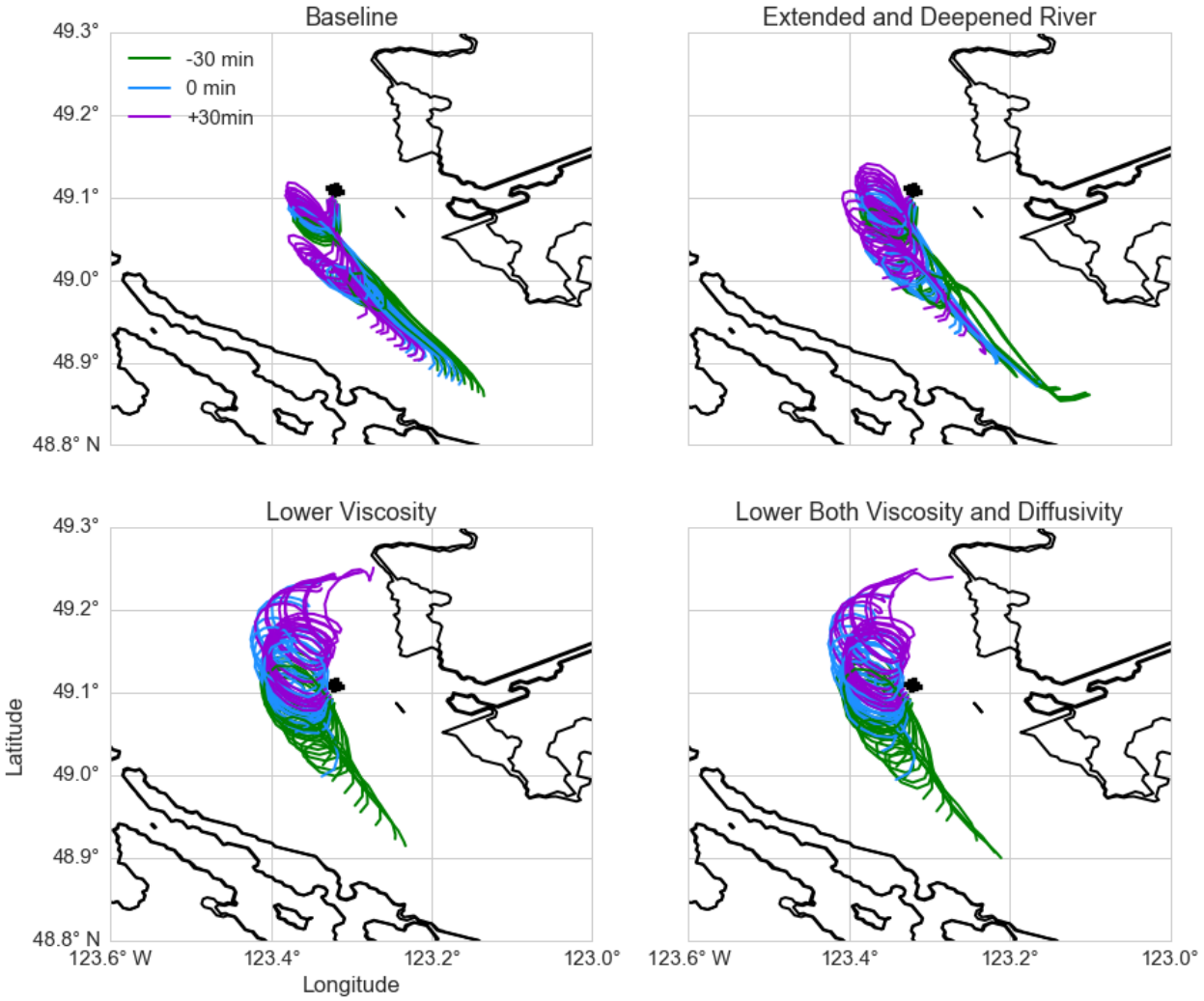

Figure 2.16: Comparison of modeled particle tracks. Upper left panel: run #1b baseline case. Upper right panel: run #3b extended and deepened river channel. Lower left panel: run #4 lower viscosity. Lower right panel: run #5 lower both viscosity and diffusivity case. In each case, in addition to particles released at the drifter release time, tracks of particles released half an hour earlier and later are shown. For each released time, in each run case, particles are released at eight other grid points that surround the grid point closest to the drifter. The blob of black diamonds show the released particle points. The observed drifter track is shown in Figure 2.12. Particles released half an hour late overall give the best results.

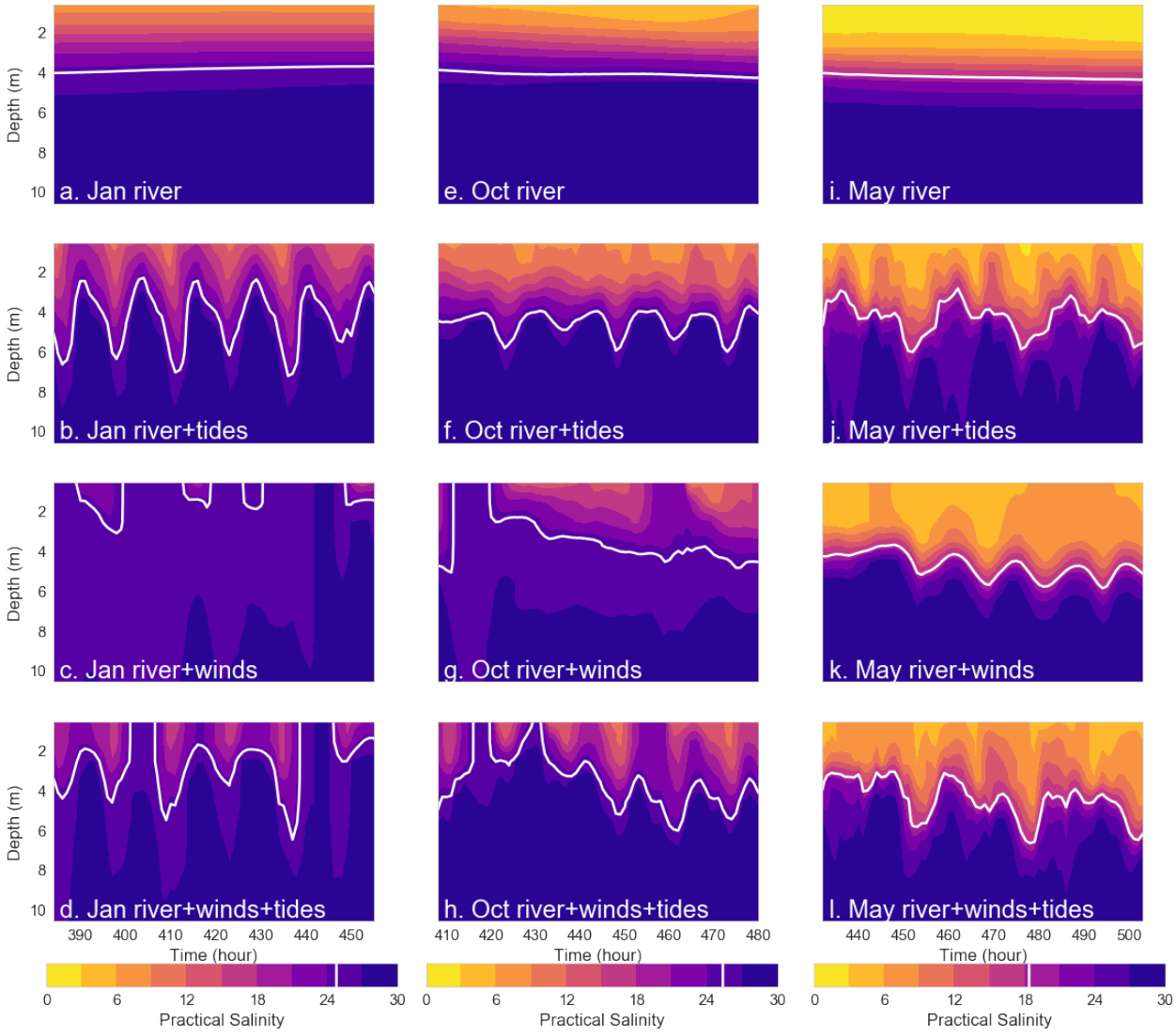

Figure 2.17: Salinity time series at NS station (Figure 2.1) under moderate wind conditions (5-10 m s^{-1}) during low, moderate and high river discharge periods from left to right, respectively, and for only river forcing, river and tides, river and winds, and combine all forcings from top to bottom, respectively. White color contour indicates the plume boundary for each period (2.1). Mixing patterns with winds show more similarity to all forcings case during low and moderate river flow periods while tide-generated mixing controls the mixing structure in the high river flow period in May.

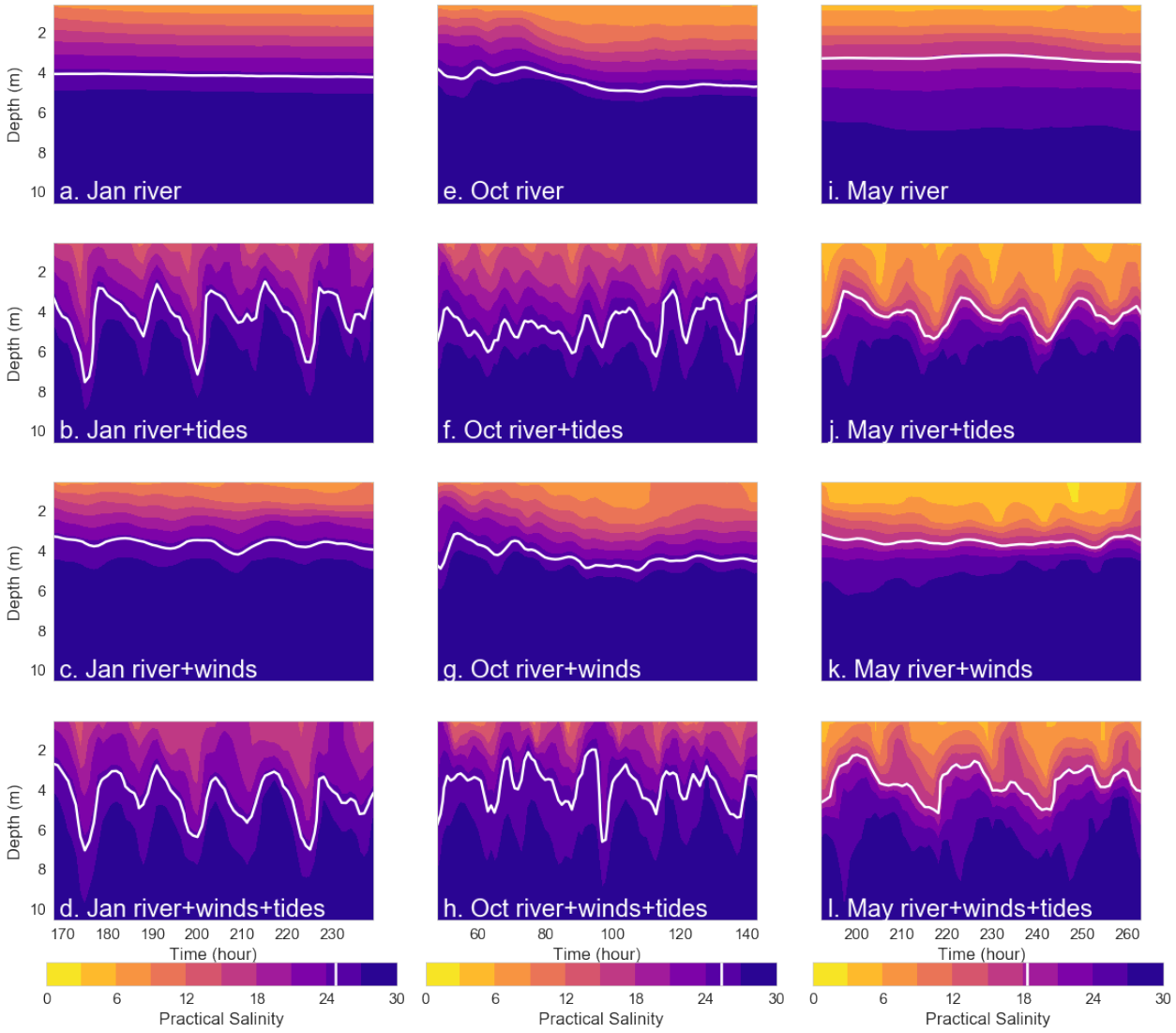

Figure 2.18: Salinity time series at NS station (Figure 2.1) as for Figure 2.17 but under weak wind conditions (0-5 m s^{-1}). White color contour indicates the plume boundary for each period (2.1). River and tides case shows similar mixing as the combine all forcings case during all three time periods.

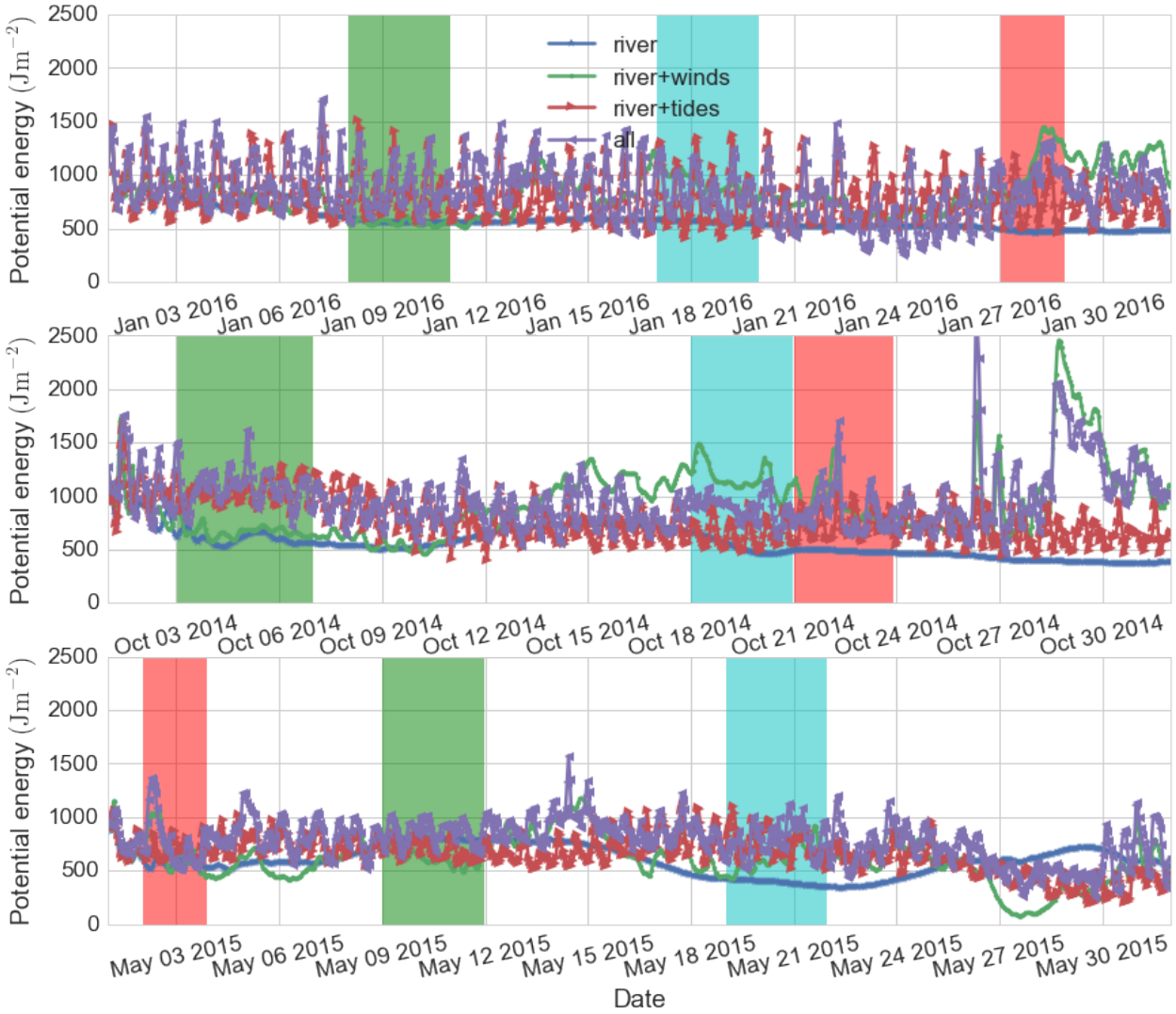

Figure 2.19: Potential energy relative to completely unmixed state (2.11) at NS station (Figure 2.1) for river only (blue), river and tides (red), river and winds (green), and combine all forcings case (purple) in low, moderate and high river flow periods, from top to bottom, respectively. Green, blue and red columns represent the weak, moderate and strong wind event periods, respectively. Potential energy generated by river flow only is non-negligible and on average winds create considerable potential energy.

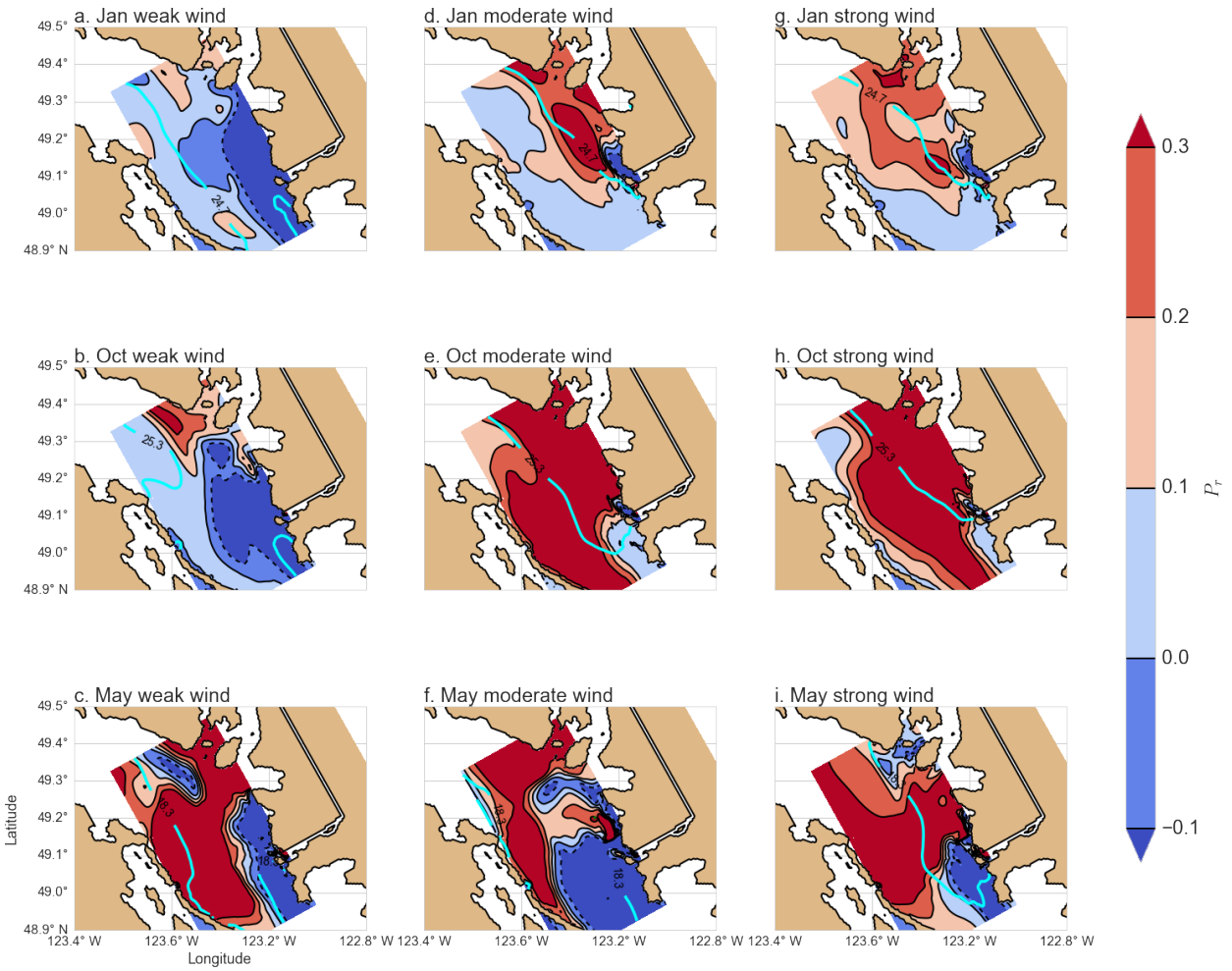

Figure 2.20: Spatial distribution of P_r (2.7) for low, moderate and high river flow periods from top to bottom during weak, moderate and strong wind events from left to right, respectively. Teal color contour indicates the plume boundary for each period (2.1). Moderate and strong wind dominates mixing in the plume region during low and moderate river flow periods. High river flow expands both the plume region and the near-field region defined as where the P_r is less than 0.1.

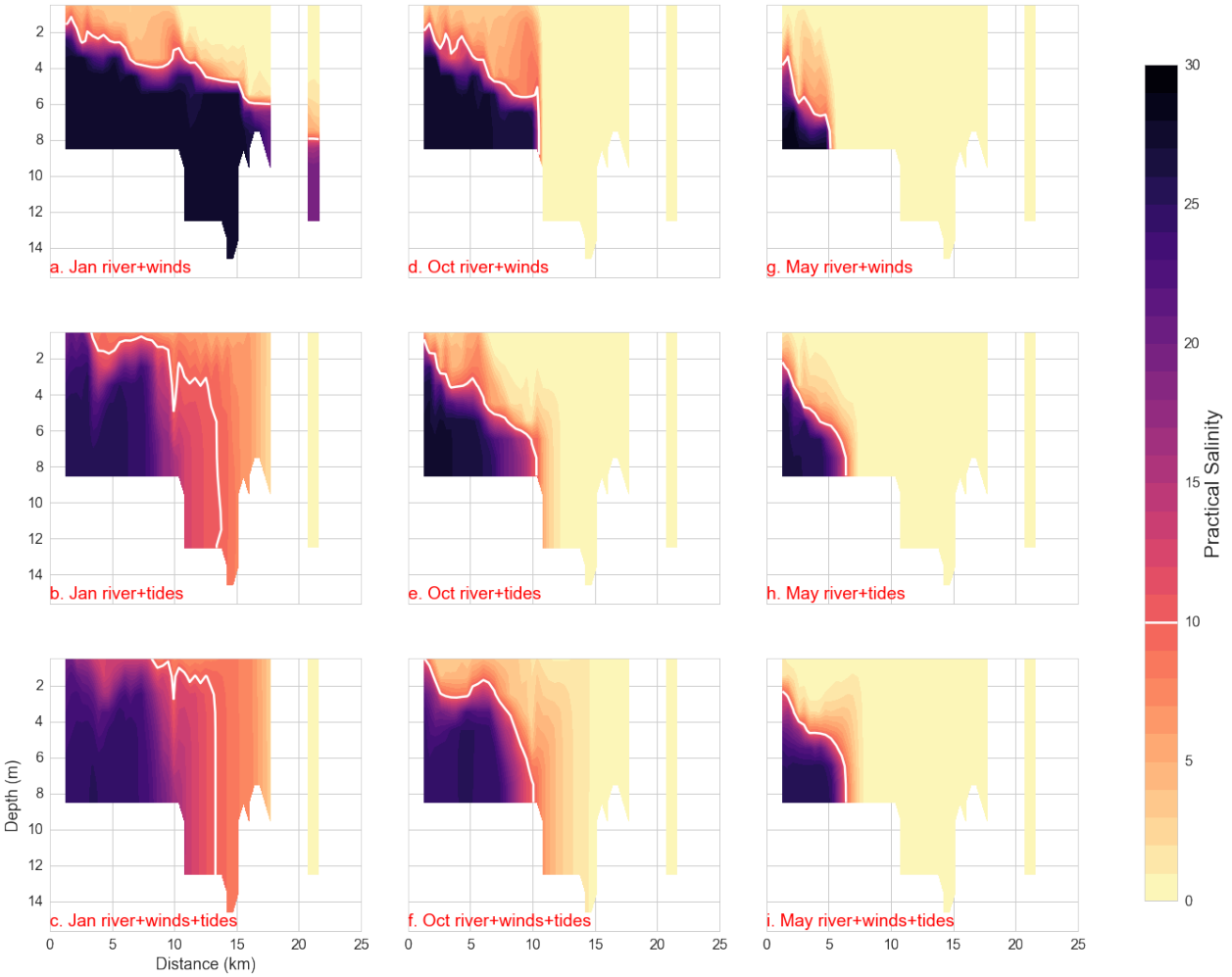

Figure 2.21: Instantaneous salinity along the river transect (Figure 2.2) when it is high tide at Point Atkinson in January, October and May for combine all forcing case from left to right, and for river and winds forcing, river and tides forcing, and combine all forcing from top to bottom, respectively. Distance reference is the start point of this transect at the river mouth. Highlighted white contour line labels the 10 salinity value. Much more mixing is induced by tides in the river channel compared to winds during all three river flow periods.

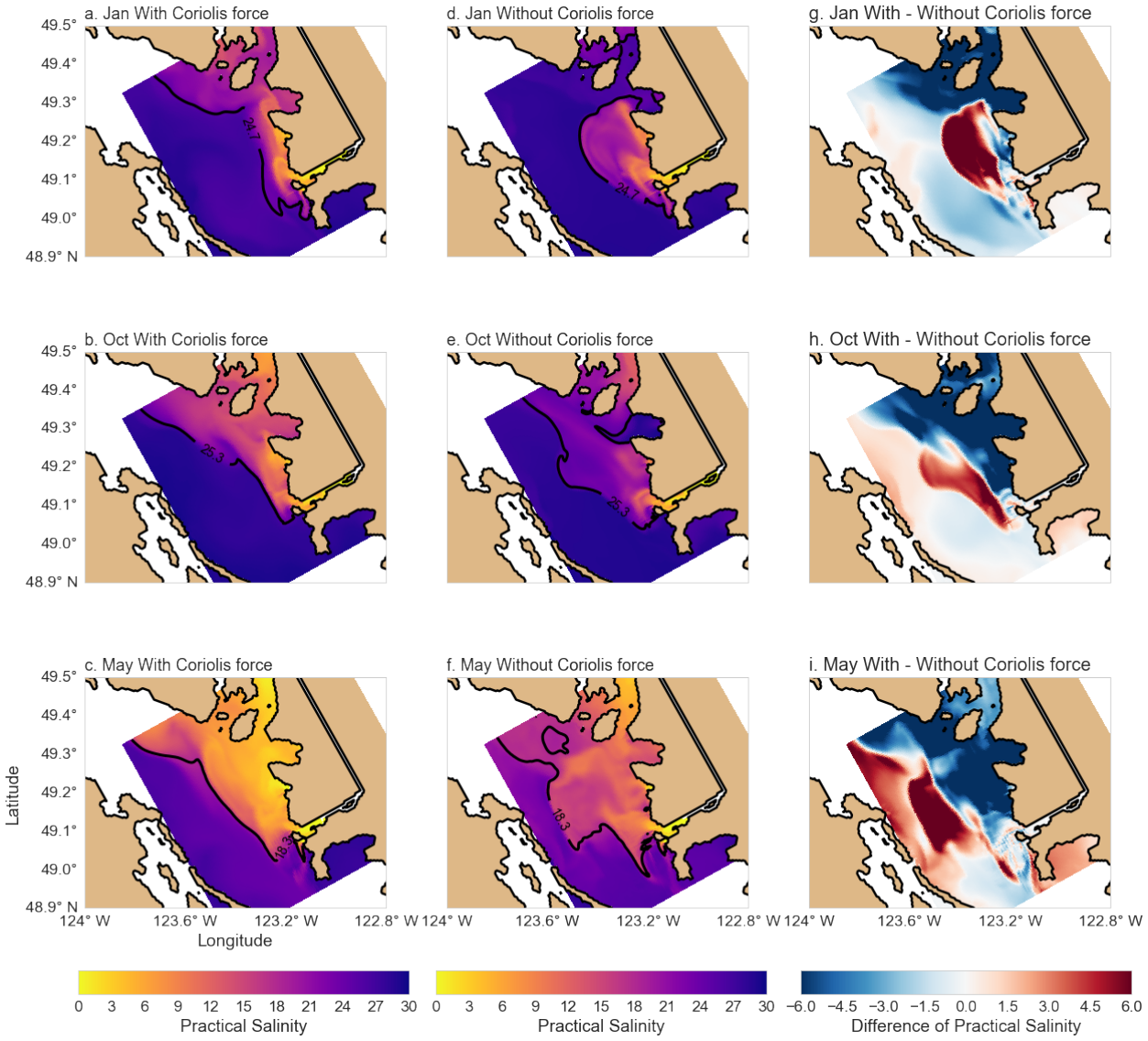

Figure 2.22: The surface salinity with the Coriolis force, without the Coriolis force and their difference (With Coriolis - without Coriolis) at instantaneous peak ebbs when velocity at the river mouth reaches a maximum. From left to right are with the Coriolis force, without the Coriolis force and their difference. Black color contour indicates the plume boundary for each period (2.1). From top to bottom are January 29, 2016, October 19, 2015 and May 15, 2015, respectively. The effect of the Coriolis force is to constrain the plume along the mainland coast, resulting in fresher water in English Bay.

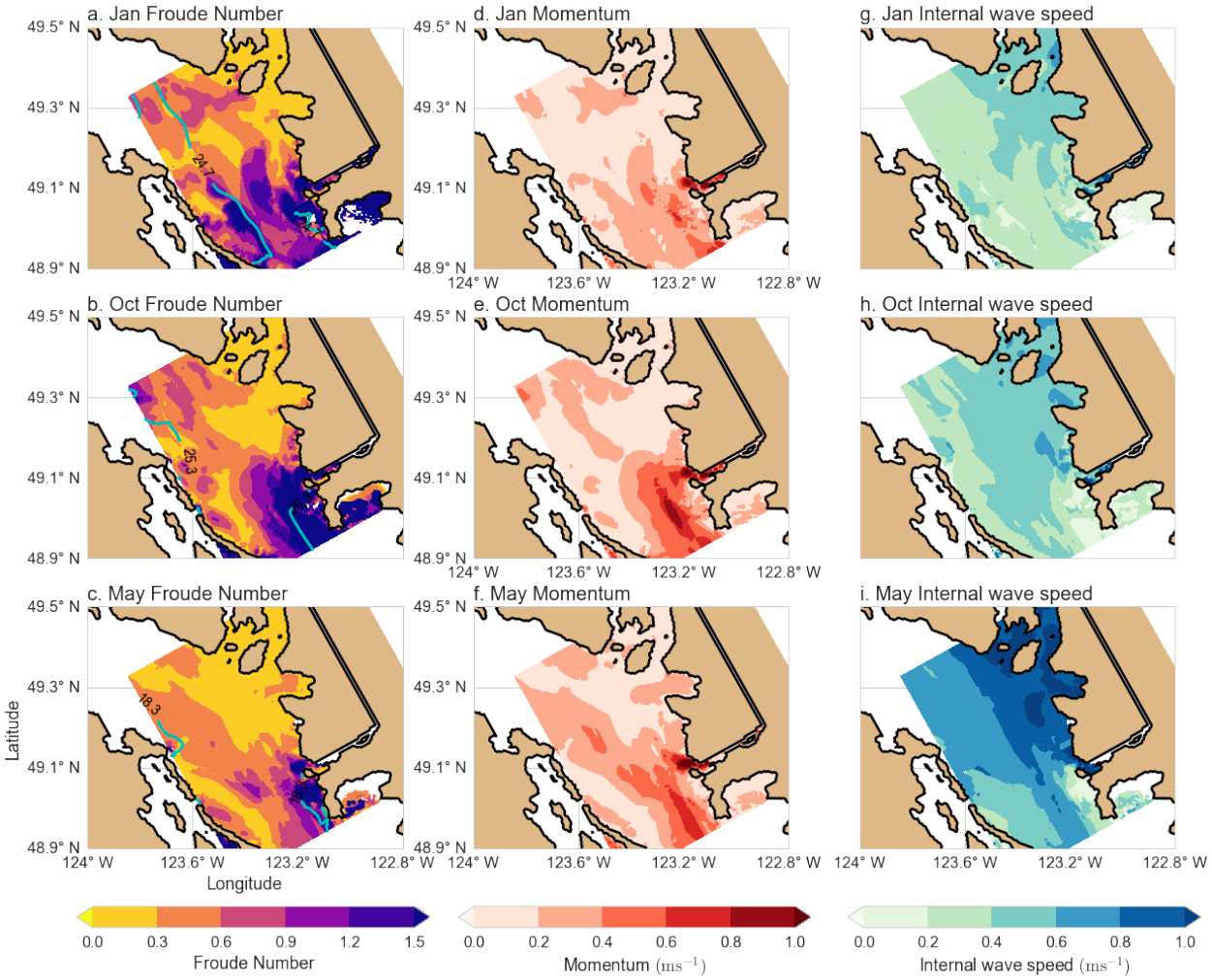

Figure 2.23: Froude Number, momentum and internal wave speed at instantaneous peak ebb in three river flow periods. From left to right are Froude Number, momentum and internal wave speed (2.12) spatial distribution at instantaneous peak ebb. Teal color contour indicates the plume boundary for each period (2.1). From top to bottom are January 9, 2016, October 9, 2014 and May 31, 2015, respectively. Momentum peaks toward the southern boundary of the subdomain due to stronger tides in this region. Internal wave speed is generally higher in May, a high river discharge period.

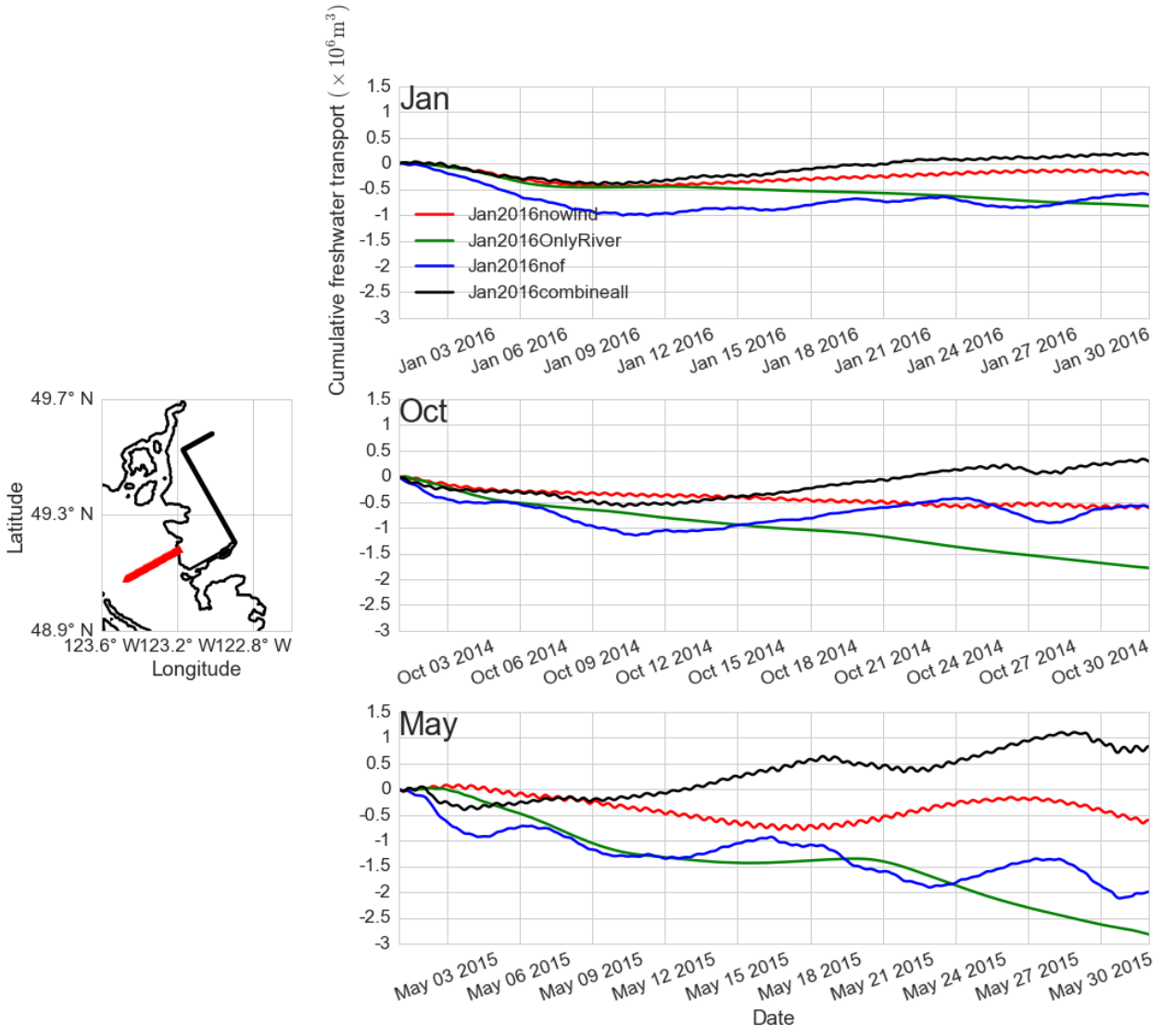

Figure 2.24: Timeseries of cumulative freshwater transport over the upper 10 m across the transect shown in the inset map. The runs are river only (OnlyRiver), river and tides (nowind), without the Coriolis force but with other forcings (nof) and combine all forcings (combineall) cases. Upper panel: each run case in January 2016. Middle panel: each run case in October 2014. Lower panel: each run case in May 2015. Positive values represent northward flux. The southward freshwater flux is the largest in the river only (OnlyRiver) case, followed by the case without the Coriolis force (nof).

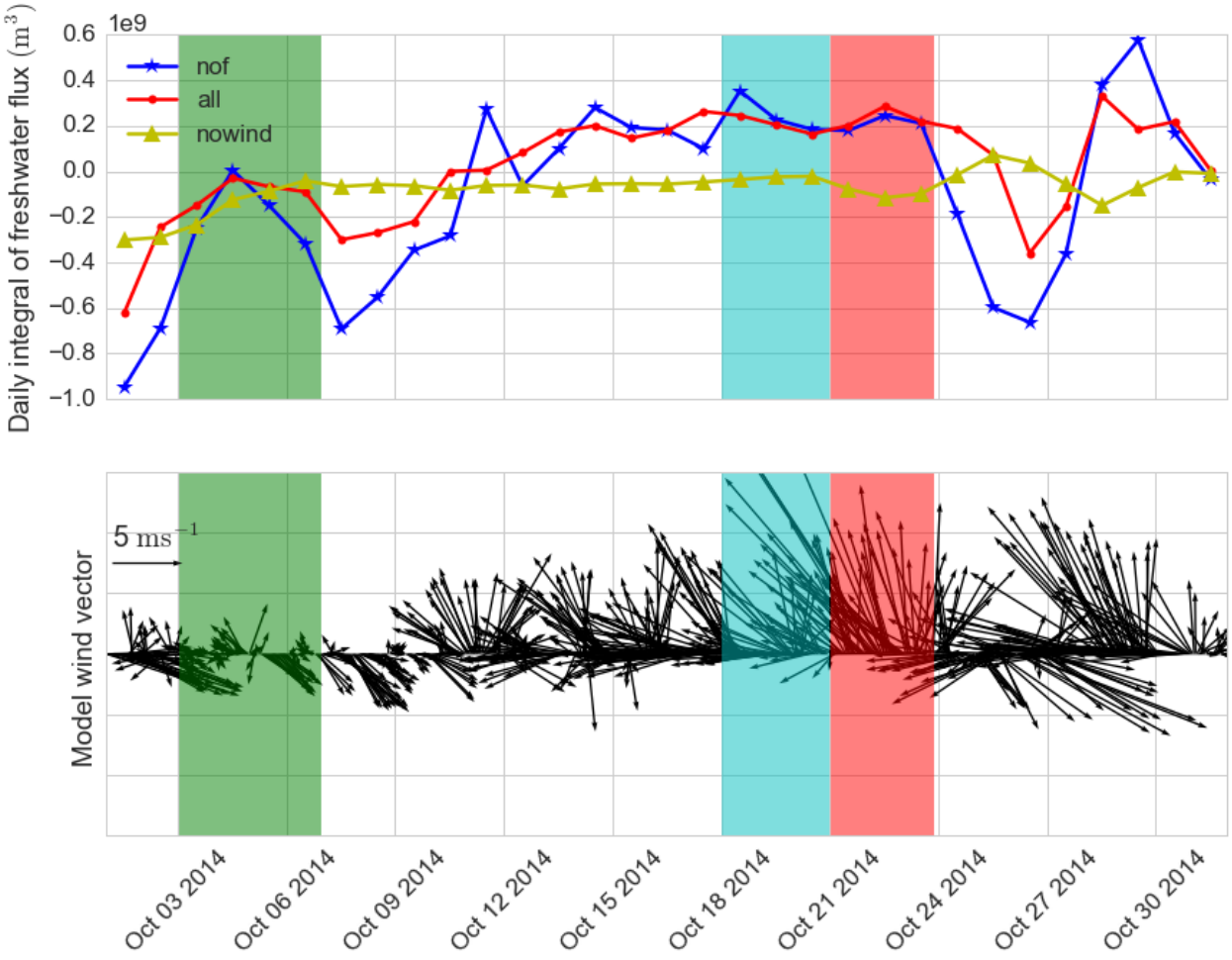

Figure 2.25: Daily integral of freshwater flux for without the Coriolis force (nof), combine all forcings (all) and river and tide (nowind) in October, 2014. Corresponding model wind information at Sand Heads station (Figure 2.1) with arrows represent direction of wind going to (lower panel). Green, blue and red columns represent the weak, moderate and strong wind event periods, respectively. For combine all forcings and without the Coriolis force cases, the flux generally matches the winds, with the flux more sensitive to winds in the without the Coriolis force case.

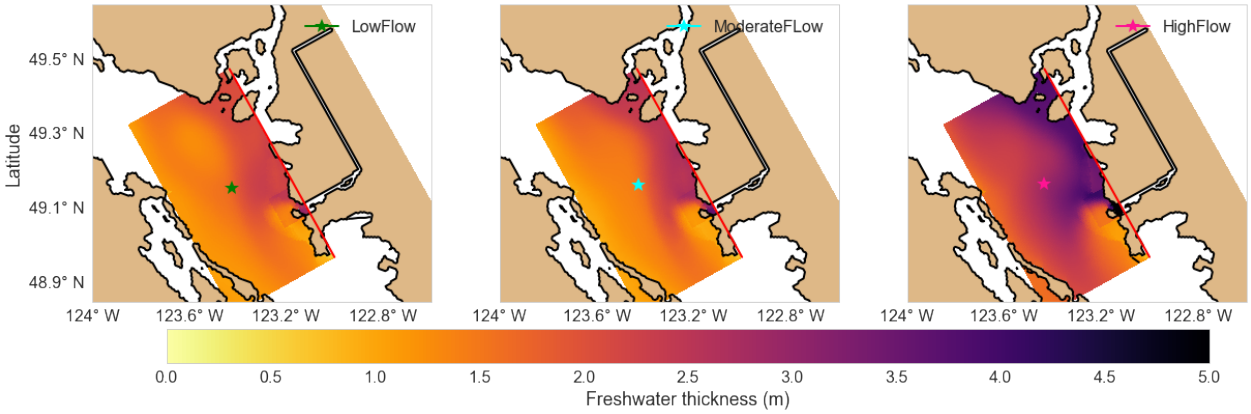

Figure 2.26: Freshwater thickness (2.15) spatial distribution and plume centre location (2.15, star) for January, October and May period from left to right, respectively for river only case. Red line cuts off the Fraser River channel and Squamish river source. Change of plume centre location is small due to variations in river discharge.

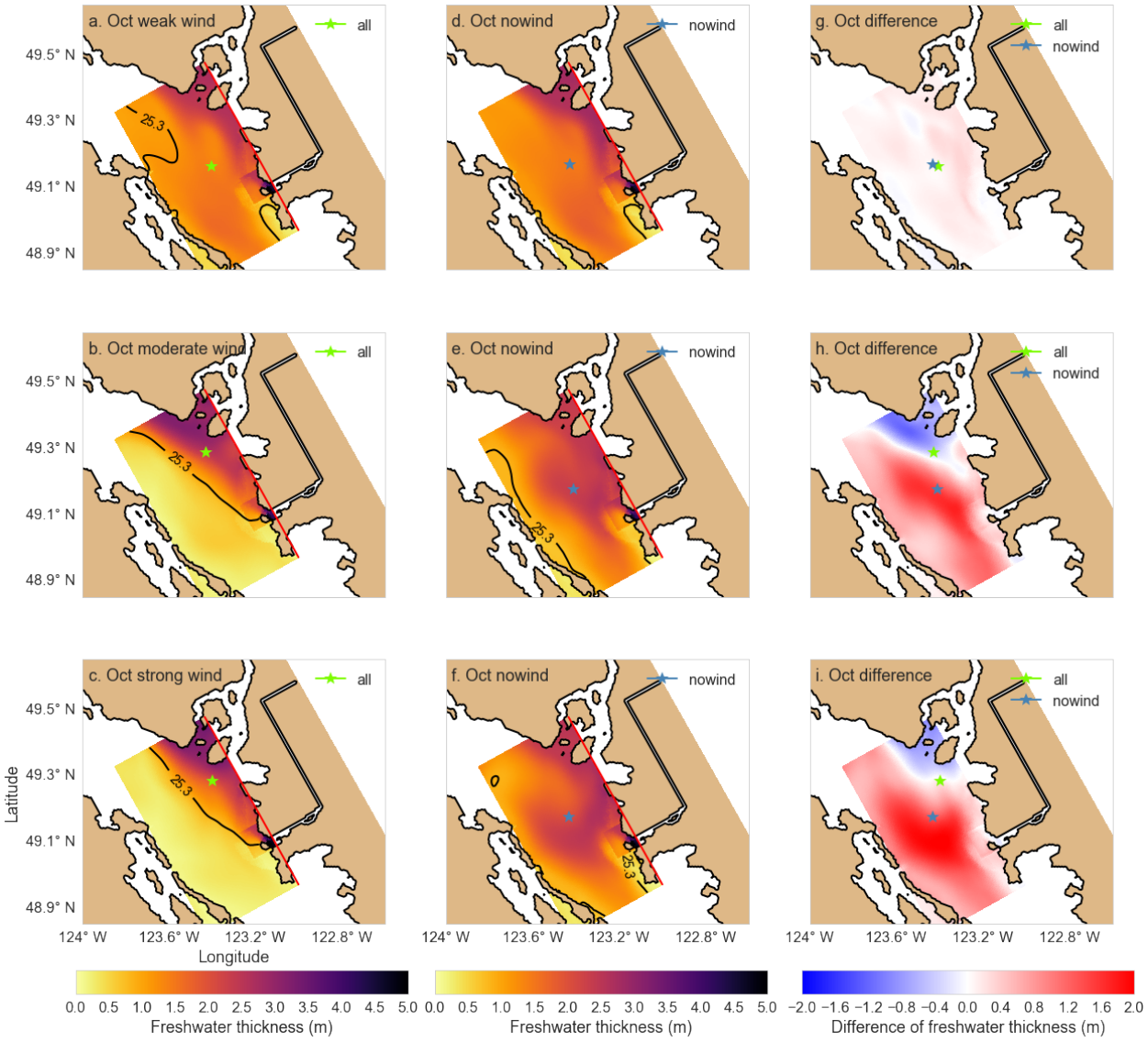

Figure 2.27: Plume centre location (2.15, star) as well as freshwater thickness (2.15) spatial distribution for weak, moderate and strong wind events in October, 2014 from top to bottom, respectively and with wind forcing, without wind forcing, and their difference (With wind - without wind) from left to right, respectively. Change of plume centre location under weak wind conditions is small. Large changes of location occur during moderate and strong wind events.

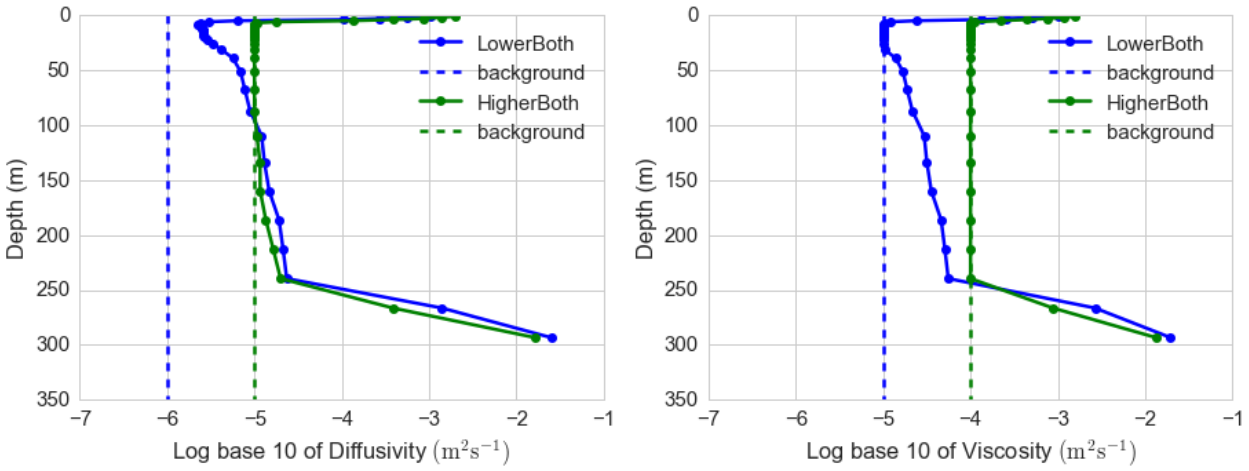

Figure 2.28: Background values and modeled values of vertical eddy diffusivity and viscosity averaged over October 8 to 10, 2014 (Run # 3 and 5, Table 2.1) at VENUS Central station (Figure 2.1). Vertical dash lines represent background values of vertical eddy viscosity and diffusivity, dot curves are values calculated by the NEMO model as the maximum between the GLS turbulence scheme and the background values. LowerBoth refers to run #5 (Table 2.1) and Higherboth denotes run #3 (Table 2.1). Background value for LowerBoth (blue) and the HighBoth (green). With lower background values, more depths use the values that GLS turbulence closure predicts.

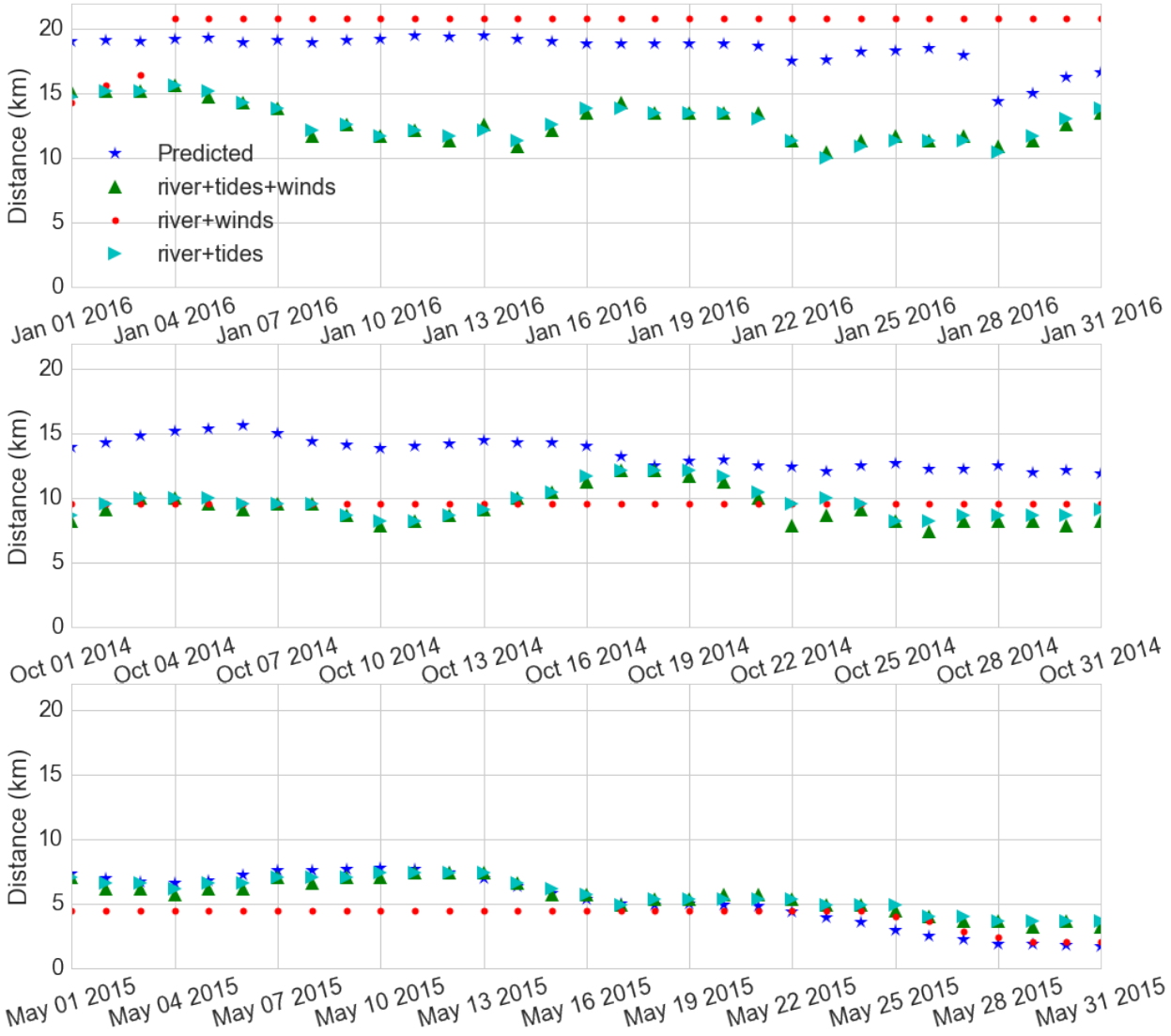

Figure 2.29: Comparison of the position of the salt-wedge tip in the estuary between predictive results based on 19 observations and model results of river plus winds, river plus tides and all forcing, for low, moderate and high river flow from top to bottom. The salt-wedge position is similar between the river plus tides and river plus tides plus winds case, although most of the modeled salt-wedge intrusions are closer to the river mouth than the predictions.

Chapter 3

Conclusions

3.1 Research Questions

The conclusions here are summarized to answer each of the research questions that are proposed in Chapter 1.

1. *How well do the modeled flows and salinity compare to the observations?*

Ferry-based salinity data, drifter data, CTD profiles and water level data are used to evaluate the model plume results. Ferry salinity data is available throughout the study period with small gaps and can provide near-surface salinity comparisons along the ferry tracks. The drifter data I am using is concentrated in October, 2014. CTD casts provide salinity profile comparisons, which I mostly focused in the central SoG where the Strait is directly influenced by the Fraser River outflow. Water level data are used to evaluate the tidal heights in the river channel produced by the model by different sensitivity experiments. Overall, near-surface salinity values of the baseline run are in a similar range compared with ferry salinity data. The problems discovered in drifter, ferry-based salinity and CTD comparisons are a saltier plume and the plume position being too close to the mainland BC coast. In addition, the model predicts much stronger along-strait flows relative to the

drifter data.

2. *What geometry of the Fraser River should be used in the NEMO model and how sensitive are salinity and surface currents in the plume to the geometry of the Fraser River estuary and the region around its mouth?*

By referring to the Canadian Hydrographic chart, a longer river channel (bathymetry #5) was created. Salinity values are reduced by employing this longer river channel, but the modeled plume still lacks strong enough cross-strait flows. By further deepening the river mouth region (bathymetry #6), cross-strait velocities are improved considerably and tidal amplitudes inside the river channel correspond with observed water level data.

3. *How do vertical eddy viscosity and diffusivity affect the plume properties?*

Hindcast comparisons are made to compare with drifter data as well as ferry-based salinity. Although lowered background vertical eddy viscosity significantly reduced the along-strait flows in two out of nine drifter-particle comparisons, the overall capability of the model to track the surface currents was not improved statistically. Lowered background vertical diffusivity reduces model salinity, which decreases the discrepancy between ferry observations and the model results.

4. *What is the importance of the tides, winds and the Coriolis force on the mixing of the plume and how does the importance vary with different river flows?*

By conducting fifteen simulations in total, which covered three river flow levels (low, moderate and high), for river only, river plus tide, river plus winds, all forcing, all forcing except the Coriolis force for each of the flow periods, the relative importance of tides, winds, the Coriolis force and river discharge on mixing has been investigated. Tides are found to control mixing in the river channel during all river flow periods compared to the winds. The near-field region is tightly constrained near the mouth during low and moderate river flows. During high river flow periods, the tide-dominated mixing region expands. Winds are the major forcing of mixing over a large area of plume during low and moderate river flow periods when the wind magnitude is greater than 5 m s^{-1}. The Coriolis force results in fresher water being constrained along the mainland coast and freshening English Bay, mainly due to the more northward flow that Coriolis force generates. With increasing of river discharge, both the plume size and the tide-induced mixing region increases.

5. *What is the importance of the tides, winds and the Coriolis force on the transport of the plume and how does the importance vary with different river flows?*

Freshwater flux across the northern transect in simulations with tides decreases considerably compared to that with only the river. This decrease is likely caused by the tidal mixing in Haro Strait that greatly reduces the freshwater transport. In general, the amount of freshwater flux and plume centre location correspond with the winds. Under strong winds from north-west, the plume centre can move 11 km to the south-east. The Coriolis force causes much more northward freshwater transport compared with no Coriolis force when the wind is not strong. I found that without the Coriolis force, winds appear to impact the flux more than with the Coriolis force because winds will affect a thinner plume layer more easily and the plume is more spread out and thinner without

the Coriolis force. Although increasing river discharge expands the plume region, the plume centre location changes little.

3.2 Implications and Future Work

The NEMO model has shown promising skill in predicting the Fraser River plume properties and position with a longer and deeper river channel (bathymetry #6), reduced background vertical eddy viscosity and diffusivity. These results and predictions have great practical implications for oil spill events, search and rescue, biological productivity and marine pollutant transport.

Investigation of mixing and transport processes within the plume strengthens the understanding of the transformation of river discharge and its evolution into the ambient ocean water. A detailed understanding of different forcing mechanisms responsible for plume mixing and transport is especially useful. This study is the first comprehensive investigation of the impact of river discharge, tides, winds and the Coriolis force on the Fraser River plume. It also provides a realistic wind and tide dominant example for comparison to future plume theories that include both these processes.

A number of problems still exist in the model. In addition to what was mentioned in the Discussion 2.4.2, more recent drifter trajectories imply there might be a bulge-like recirculation pattern further away from the river mouth (Figure H.1). However, it is unclear if the model results capture this feature with the improved configuration. Surface mean currents are generally weaker than those are observed by HF radar (Figure D.1). The surface currents are influenced by internal tides as well (Thomson, 1975). Allen (2016) identified that one of the potential origins of internal tides is at the shelf-break at the tidal banks. Interaction of internal tides and the Fraser River plume would provide be another interesting topic to investigate the surface currents in the Fraser River plume.

As mentioned in the Discussion 2.4.3, the freshwater thickness pattern in the absence of winds is associated with increasing river discharge and residual currents induced by tides. Further investigation of the evolution of plume spatial distribution without wind forcing or under weak wind condition would be helpful to understand plume advection.

In addition, separation of Fraser River and other rivers and inlets (e.g., Squamish river, Burrard Inlet) in the simulations will provide a comprehensive way to measure the mixing and transport in the Fraser River plume although this current study generally shows that many forcing mechanisms contribute to plume dynamics.

Bibliography

Allen, S. (2016). Accurate modelling of surface currents and internal tides in a semi-enclosed coastal sea. `https://agu.confex.com/agu/os16/preliminaryview.cgi/Paper89180.html`. presented at 2016 Ocean Sciences Meeting, AGU/ASLO/TOS, New Orleans, LA, 21-27 Feb. Accessed: 2016-12-28.

Blanke, B. and Raynaud, S. (1997). Kinematics of the Pacific Equatorial Undercurrent: an Eulerian and Lagrangian approach from GCM results. *Journal of Physical Oceanography*, 27(6):1038–1053.

Chang, K. T. (2006). *Introduction to Geographic Information Systems*. pp. 117–122. McGraw-Hill Higher Education Boston.

Crean, P., Murty, T. S., and Stronach, J. (1988). *Mathematical Modelling of Tides and Estuarine Circulation: The Coastal Seas of Southern British Columbia and Washington, Lect. Notes on Coastal and Estuarine Stud., vol. 30*. Springer, New York.

Fong, D. A. and Geyer, W. R. (2002). The alongshore transport of freshwater in a surface-trapped river plume. *Journal of Physical Oceanography*, 32(3):957–972.

Foreman, M., Walters, R., Henry, R., Keller, C., and Dolling, A. (1995). A tidal model for Juan-de-Fuca Strait and the Southern Strait of Georgia. *Journal of Geophysical Research*, 100(C1):721–740.

Garvine, R. W. (1999). Penetration of buoyant coastal discharge onto the continental shelf: A numerical model experiment. *Journal of Physical Oceanography*, 29(8):1892–1909.

Garvine, R. W. (2001). The impact of model configuration in studies of buoyant coastal discharge. *Journal of Marine Research*, 59(2):193–225.

Geyer, W. R. and Farmer, D. M. (1989). Tide-induced variation of the dynamics of a salt wedge estuary. *Journal of Physical Oceanography*, 19(8):1060–1072.

Halverson, M. and Pawlowicz, R. (2011). Entrainment and flushing time in the Fraser River estuary and plume from a steady salt balance analysis. *Journal of Geophysical Research: Oceans*, 116:C08023.

Halverson, M. and Pawlowicz, R. (2016). Tide, wind, and river forcing of the surface currents in the Fraser River plume. *Atmosphere-Ocean*, 54(2):131–152.

Halverson, M. J. (2009). *Multi-timescale analysis of the salinity and algal biomass of the Fraser River plume from repeated ferry transects*. PhD thesis, The University Of British Columbia (Vancouver). `https://open.library.ubc.ca/cIRcle/collections/ubctheses/24/items/1.0053481`. Accessed: 2016-12-28.

Halverson, M. J. and Pawlowicz, R. (2008). Estuarine forcing of a river plume by river flow and tides. *Journal of Geophysical Research: Oceans*, 113:C09033.

Hetland, R. D. (2005). Relating river plume structure to vertical mixing. *Journal of Physical Oceanography*, 35(9):1667–1688.

Horner-Devine, A. R. (2009). The bulge circulation in the Columbia River plume. *Continental Shelf Research*, 29(1):234–251.

Horner-Devine, A. R., Fong, D. A., Monismith, S. G., and Maxworthy, T. (2006). Laboratory experiments simulating a coastal river inflow. *Journal of Fluid Mechanics*, 555:203–232.

Horner-Devine, A. R., Hetland, R. D., and MacDonald, D. G. (2015). Mixing and transport in coastal river plumes. *Annual Review of Fluid Mechanics*, 47:569–594.

Houghton, R., Chant, R., Rice, A., and Tilburg, C. (2009). Salt flux into coastal river plumes: Dye studies in the Delaware and Hudson River outflows. *Journal of Marine Research*, 67(6):731–756.

Jacobs, W. (2004). *Modelling the Rhine River plume.* PhD thesis, TU Delft, Delft University of Technology. `http://repository.tudelft.nl/islandora/object/uuid:cf8e752d-7ba7-4394-9a94-2b73e14f9949?collection=education`. Accessed: 2016-12-28.

Kostaschuk, R. and Atwood, L. (1990). River discharge and tidal controls on salt-wedge position and implications for channel shoaling: Fraser River, British Columbia. *Canadian Journal of Civil Engineering*, 17(3):452–459.

Kourafalou, V. H., Oey, L.-Y., Wang, J. D., and Lee, T. N. (1996). The fate of river discharge on the continental shelf: 1. Modeling the river plume and the inner shelf coastal current. *Journal of Geophysical Research: Oceans*, 101(C2):3415–3434.

LeBlond, P. H. (1983). The Strait of Georgia: Functional anatomy of a coastal sea. *Canadian Journal of Fisheries and Aquatic Sciences*, 40(7):1033–1063.

Li, M. and Rong, Z. (2012). Effects of tides on freshwater and volume transports in the Changjiang River plume. *Journal of Geophysical Research: Oceans*, 117:C06027.

Liu, Y., MacCready, P., Hickey, B. M., Dever, E. P., Kosro, P. M., and Banas, N. S. (2009).

Evaluation of a coastal ocean circulation model for the Columbia River plume in summer 2004. *Journal of Geophysical Research: Oceans*, 114:C00B04.

MacCready, P., Banas, N. S., Hickey, B. M., Dever, E. P., and Liu, Y. (2009). A model study of tide-and wind-induced mixing in the Columbia River estuary and plume. *Continental Shelf Research*, 29(1):278–291.

MacDonald, D. G. and Geyer, W. R. (2004). Turbulent energy production and entrainment at a highly stratified estuarine front. *Journal of Geophysical Research: Oceans*, 109:C05004.

Madec, G. (2012). Coauthors, 2012: NEMO ocean engine, version 3.4. *Institut Pierre-Simon Laplace Note du Pole de Modelisation*, 27:357. `www.nemo-ocean.eu/content/download/21612/97924/file/NEMO_book_3_4.pdf`. Accessed: 2016-12-28.

Marinone, S., Pond, S., and Fyfe, J. (1996). A three-dimensional model of tide and wind-induced residual currents in the central Strait of Georgia, Canada. *Estuarine, Coastal and Shelf Science*, 43(2):157–182.

Masson, D. and Cummins, P. F. (2004). Observations and modeling of seasonal variability in the Straits of Georgia and Juan de Fuca. *Journal of Marine Research*, 62(4):491–516.

Masunaga, E., Fringer, O. B., and Yamazaki, H. (2016). An observational and numerical study of river plume dynamics in Otsuchi Bay, Japan. *Journal of Oceanography*, 72(1):3–21.

Mikelbank, B. A. (2001). Quantitative Geography: perspectives on spatial data analysis. *Geographical Analysis*, 33(4):370–370.

Nagai, T. and Hibiya, T. (2011). The processes of semi-enclosed basin–ocean water exchange across a tidal mixing zone. *Journal of Oceanography*, 67(4):533–539.

Oey, L.-Y. and Mellor, G. (1993). Subtidal variability of estuarine outflow, plume, and coastal current: A model study. *Journal of Physical Oceanography*, 23(1):164–171.

Ohlmann, J. C., White, P. F., Sybrandy, A. L., and Niiler, P. P. (2005). GPS-cellular drifter technology for coastal ocean observing systems. *Journal of Atmospheric and Oceanic Technology*, 22(9):1381–1388.

Pawlowicz, R., Riche, O., and Halverson, M. (2007). The circulation and residence time of the Strait of Georgia using a simple mixing-box approach. *Atmosphere-Ocean*, 45(4):173–193.

Pond, S. and Pickard, G. (1983). *Introductory dynamical oceanography 2nd Edition*. 327pp. Pergamon Press Oxford.

Reffray, G., Bourdalle-Badie, R., and Calone, C. (2015). Modelling turbulent vertical mixing sensitivity using a 1-d version of NEMO. *Geoscientific Model Development*, 8(1):69–86.

Riche, O. (2011). *Time-dependent inverse box-model for the estuarine circulation and primary productivity in the Strait of Georgia*. PhD thesis, University of British Columbia. `https://open.library.ubc.ca/cIRcle/collections/ubctheses/24/items/1.0053142`. Accessed: 2016-12-28.

Royer, L. and Emery, W. (1982). Variations of the Fraser River plume and their relationship to forcing by tide, wind and discharge. *Atmosphere-Ocean*, 20(4):357–372.

Royer, L. and Emery, W. (1985). Computer simulations of the Fraser River plume. *Journal of Marine Research*, 43(2):289–306.

Smith, G. C., Roy, F., Mann, P., Dupont, F., Brasnett, B., Lemieux, J.-F., Laroche, S., and Bélair, S. (2014). A new atmospheric dataset for forcing ice–ocean models: Evaluation of reforecasts

using the Canadian global deterministic prediction system. *Quarterly Journal of the Royal Meteorological Society*, 140(680):881–894.

Soontiens, N., Allen, S. E., Latornell, D., Le Souëf, K., Machuca, I., Paquin, J.-P., Lu, Y., Thompson, K., and Korabel, V. (2016). Storm surges in the Strait of Georgia simulated with a regional model. *Atmosphere-Ocean*, 54(1):1–21.

Stronach, J. (1981). The Fraser River plume, Strait of Georgia. *Ocean Management*, 6(2):201–221.

Tabata, S. (1972). The movement of Fraser River-influenced surface water in the Strait of Georgia as deduced from a series of aerial photographs, Pacific Marine Sci. Technical report, Report.

Tedford, E., Carpenter, J., Pawlowicz, R., Pieters, R., and Lawrence, G. A. (2009). Observation and analysis of shear instability in the Fraser River estuary. *Journal of Geophysical Research: Oceans*, 114:C11006.

Thomson, R. E. (1975). Longshore current generation by internal waves in the Strait of Georgia. *Canadian Journal of Earth Sciences*, 12(3):472–488.

Thomson, R. E. (1981). *Oceanography of the British Columbia coast*, volume 56. Canadian Special Publications of Fisheries and Aquatic Sciences. `http://publications.gc.ca/site/eng/9.816310/publication.html`. Accessed: 2016-12-28.

Umlauf, L. and Burchard, H. (2003). A generic length-scale equation for geophysical turbulence models. *Journal of Marine Research*, 61(2):235–265.

Unesco (1981). *Background Papers and Supporting Data on the Practical Salinity Scale 1978*. Technical Report 37, UNESCO, Paris, France.

Wang, C. (2015). *Oxygen budgets and productivity estimates in the Strait of Georgia from a continuous ferry-based monitoring system.* PhD thesis, The University of British Columbia (Vancouver). https://open.library.ubc.ca/cIRcle/collections/ubctheses/24/items/1.0167147. Accessed: 2016-12-28.

Wu, H., Zhu, J., Shen, J., and Wang, H. (2011). Tidal modulation on the Changjiang River plume in summer. *Journal of Geophysical Research: Oceans*, 116:C08017.

Yin, K., Harrison, P. J., Pond, S., and Beamish, R. J. (1995a). Entrainment of nitrate in the Fraser River estuary and its biological implications. i. Effects of the salt wedge. *Estuarine, Coastal and Shelf Science*, 40(5):505–528.

Yin, K., Harrison, P. J., Pond, S., and Beamish, R. J. (1995b). Entrainment of nitrate in the Fraser River estuary and its biological implications. ii. Effects of spring vs. neap tides and river discharge. *Estuarine, Coastal and Shelf Science*, 40(5):529–544.

Yin, K., Harrison, P. J., Pond, S., and Beamish, R. J. (1995c). Entrainment of nitrate in the Fraser River estuary and its biological implications. iii. Effects of winds. *Estuarine, Coastal and Shelf Science*, 40(5):545–558.

Appendix A

Inverse Distance Weighting Interpolation Method for Ferry-based Salinity comparison

The Inverse Distance Weighting Interpolation method (Chang, 2006) is applied to interpolate model grid points onto the ferry routes and acquire model near-surface salinity values along the track (S_mod_track) by using the following equation.

$$S\_mod\_track(x) = \frac{\sum_{i=1}^{9} k_i(x) S\_mod(i)}{\sum_{i=1}^{9} k_i(x)} \tag{A.1}$$

where $k_i(x) = d(x, x_i)^{-1}$, x refers to the interpolated point on the ferry track, x_i denotes an interpolating point of model grid point, d is the distance from NEMO model grid point to the interpolated point on the ferry and is calculated on a sphere based on their longitudes and latitudes (Mikelbank, 2001), i ranges from 1 to 9 as I first find the nearest model grid point from interpolated point, and further select the other eight model grid points, which surround it. S_mod(i) denotes modeled salinity value for each model grid point based on a total nine model points. If there are

more than two model grid points out of these nine model points on land, this position is considered as a land point. If there are fewer than two grid points out of these nine model points are on land, then this position is still used by averaging the available water grid points.

Appendix B

Tidal Amplitude Comparison Inside the Fraser River Channel

Table B.1: Tidal amplitude comparisons inside Fraser River between extended river (bathymetry #5), extended and deepened river (bathymetry #6) and observations

Station names	Distance from mouth (km)	Observations			Bathymetry #5			Bathymetry #6		
		Max (m)	Min (m)	Mean (m)	Max (m)	Min (m)	Mean (m)	Max (m)	Min (m)	Mean (m)
Steveston	0	3.49	2.10	2.88	3.67	2.04	2.89	3.71	2.03	2.90
Deas Island Tunnel	18	3.05	1.85	2.58	1.46	1.01	1.27	3.55	2.04	2.80
New Westminster	36	2.28	1.43	1.91	0.84	0.57	0.71	3.02	1.78	2.42
Mission	52	0.37	0.24	0.31	0.84	0.57	0.70	3.00	1.71	2.37

Appendix C

Extended, Deepened River Channel With Jetty

The real jetty is about 8.8 km long and 10-20 m wide. Bathymetry #10 was created by adding the Steveston Jetty based on bathymetry #6 (Figure C.1). About 5% of the model grid points in the deepened river mouth region are removed by adding the jetty. Compared to bathymetry #6, bathymetry #10 might impact tidal propagation around the river mouth. In the model, the width of this jetty is about 500 m and length is 7 km in total. This jetty geometry does not seem to improve the surface flows (Figure C.1, run #8, Table 2.1) compared to the longer and deeper river channel cases (Run #3b, Table 2.1). The reason could be the unrealistic width of this jetty in the model rather than a few metres in the real world. The wide jetty blocks too much plume water going to the north.

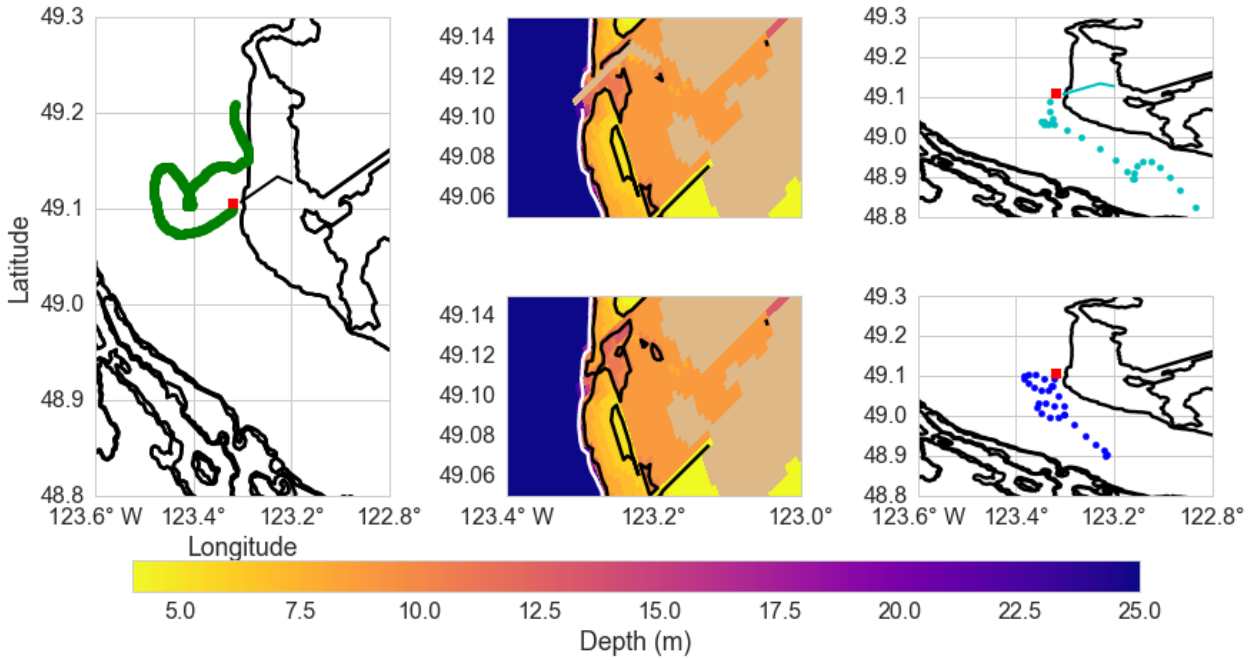

Figure C.1: Bathymetry #10 with the Steveston jetty, longer and deeper bathymetry #6 as well as comparison between the observed drifter and modeled particles with these bathymetries. Left panel: the same drifter track as Figure 2.12 shows. Middle two panels: bathymetry #10 with the Steveston Jetty based on bathymetry #6 in the upper panel and bathymetry #6 in the lower panel. Right two panel: modeled particles for run #3b (blue dots) in the upper panel and for run #8 (teal dots) in the lower panel, respectively. The black contours are bathymetry of 5 m and 10 m and the white contour is bathymetry of 20 m. Much more southward along-strait flow is generated by the jetty bathymetry.

Appendix D

Mean Surface Currents

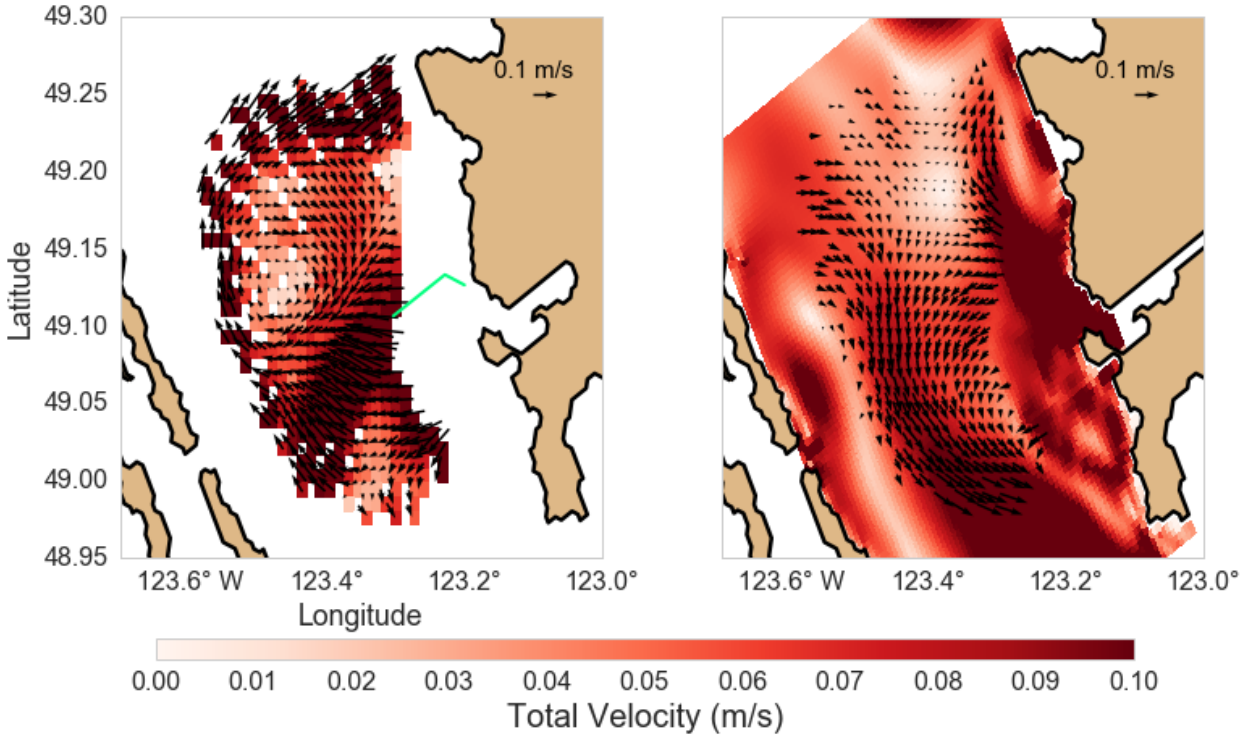

Figure D.1: Mean surface flows of HF radar data (left) and model mean surface currents (right, run #9, Table 2.1) during the same time period in October 1-31, 2015. Mesh color indicates the strength of mean surface currents. Tendency of flows from the data is northward beween 49°N and 49.10°N whereas model results show southward flows. Model flows are much weaker.

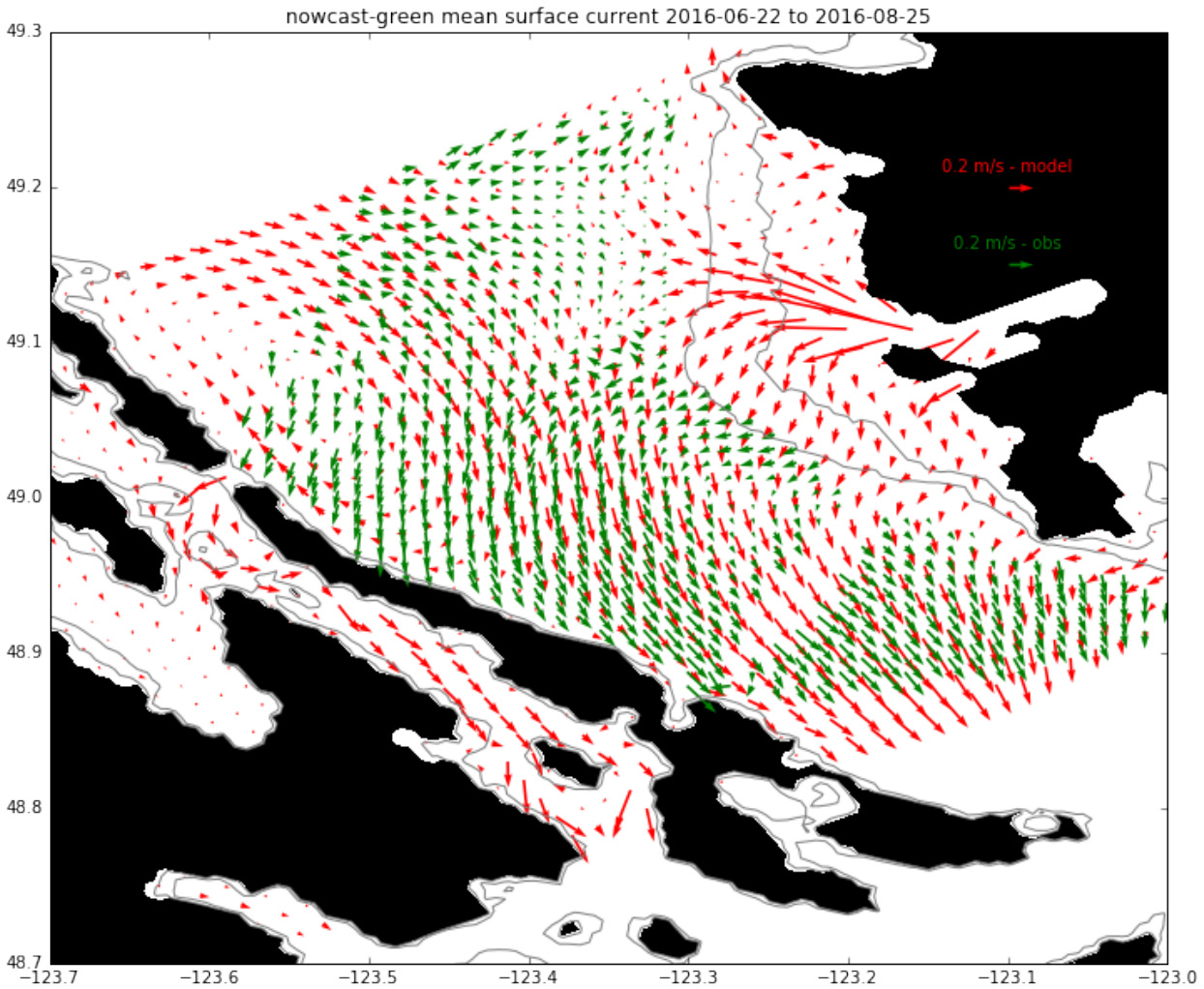

Figure D.2: Mean surface currents of HF radar data (green) and model results with improved configurations (red) from June 22-August 25, 2016. Direction of mean flows between observation and model in the area of 48.9-49.1°N and -123.5-123.2°E is basically the same. Strong modeled mean currents in the region north of 49.1°N and west of the banks are seen. Figure credit: Nancy Soontiens and Mark Halverson.

Mean surface flows in the SoG are assumed to be caused by the mean outflow of fresh water, assuming tides and winds contribute very little response over periods of weeks and longer (Halverson and Pawlowicz, 2016). To isolate the mean surface currents, an average over a long analysis period is employed (Halverson and Pawlowicz, 2016). The modeled mean surface flow of October 1-31, 2015 is evaluated against HF radar data during the same time period. The results show almost opposite flow direction between the modeled and observed currents where modeled mean surface currents go southward from 49.10°N south but the observational mean currents indicate an anti-cyclonic eddy motion at around 49.10-49.15°N (Figure D.1). Southward flow in the model is most likely due to the estuarine circulation in the SoG with freshwater flowing out of the Strait towards Haro Strait. It is more difficult to understand the flow pattern of the observations although Halverson and Pawlowicz (2016) reluctantly attribute this pattern to bulge behaviour.

Mean modeled surface currents with an improved configuration in summer shows more consistency in direction with HF radar data (Figure D.2), especially in the Fraser River plume outflow region within 48.9-49.1°N and -123.5-123.2°E. The magnitude of modeled mean currents is similar with HF radar data in the region within 48.9-49.1°N and -123.5-123.2°E although strong modeled mean currents in the region northern than 49.1°N west of the banks are found.

Appendix E

Froude Number at Peak Floods

The internal wave speed (2.12) does not change much between peak flood and ebb in a given day (g, h and i of Figure 2.23 and Figure E.1). Internal wave speed is higher to the north of the river mouth during high river flow periods (Figure 2.23 i, Figure E.1 i), decreasing down to 0.2-0.6 m s^{-1} during the low and moderate river flow periods (Figure 2.23 g and h, Figure E.1 g and h). Overall, flow speed is weaker over the entire subdomain at peak flood compared to peak ebb.

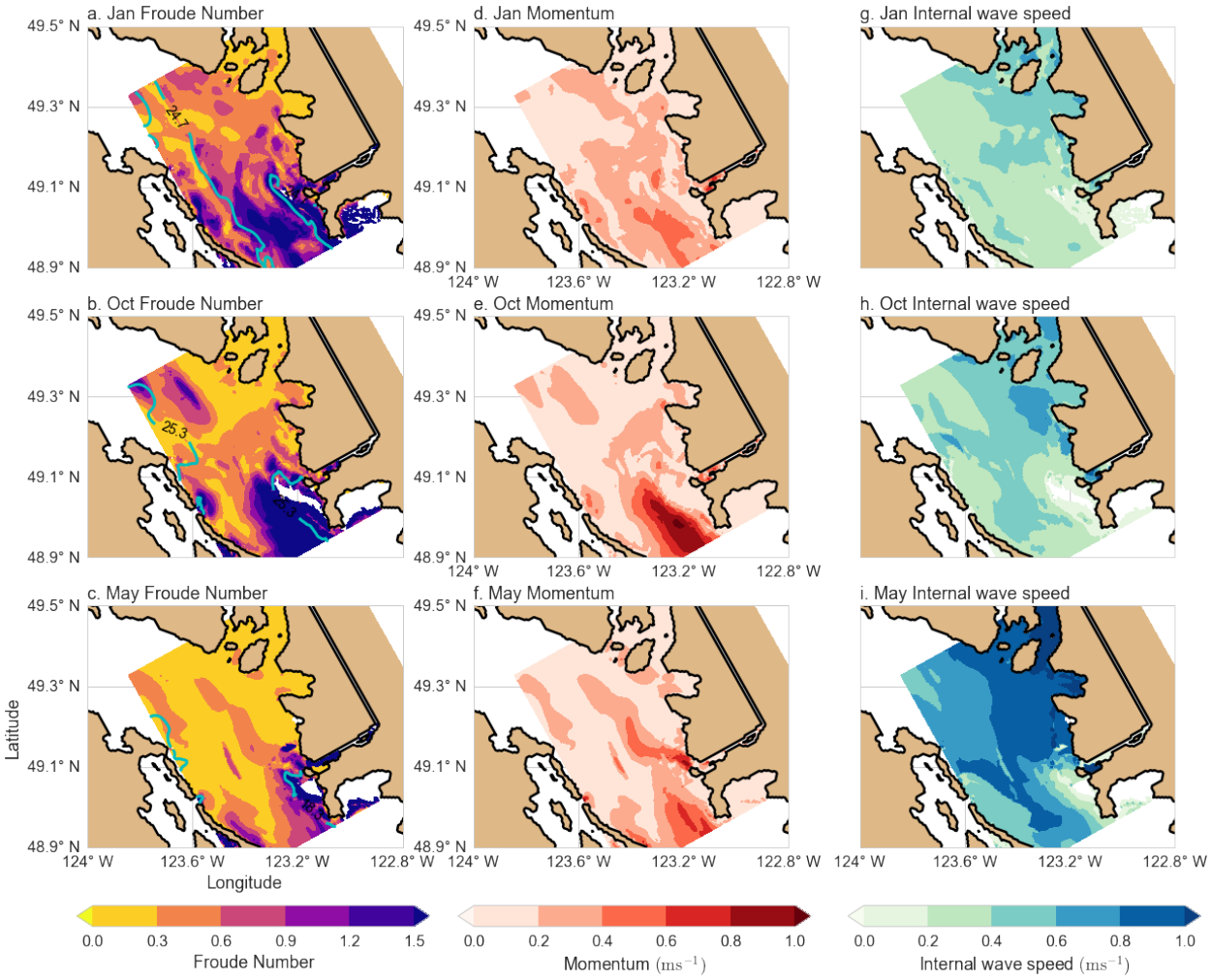

Figure E.1: Froude Number, momentum and internal wave speed at instantaneous peak flood in three river flow periods. From left to right are Froude Number, momentum and internal wave speed spatial distribution at instantaneous peak flood. Teal color contour indicates the plume boundary for each period (2.1). From top to bottom are January 9, 2016, October 9, 2014 and May 31, 2015, respectively. Momentum is less significant at peak floods compared to peak ebbs. Internal wave speed does not change much compared to peak ebb.

Appendix F

Coriolis Impact on Surface Salinity in the English Bay

It is robust that the Coriolis force results in a fresher surface plume in English Bay and maximum salinity difference can reach 15 in May (Figure F.1).

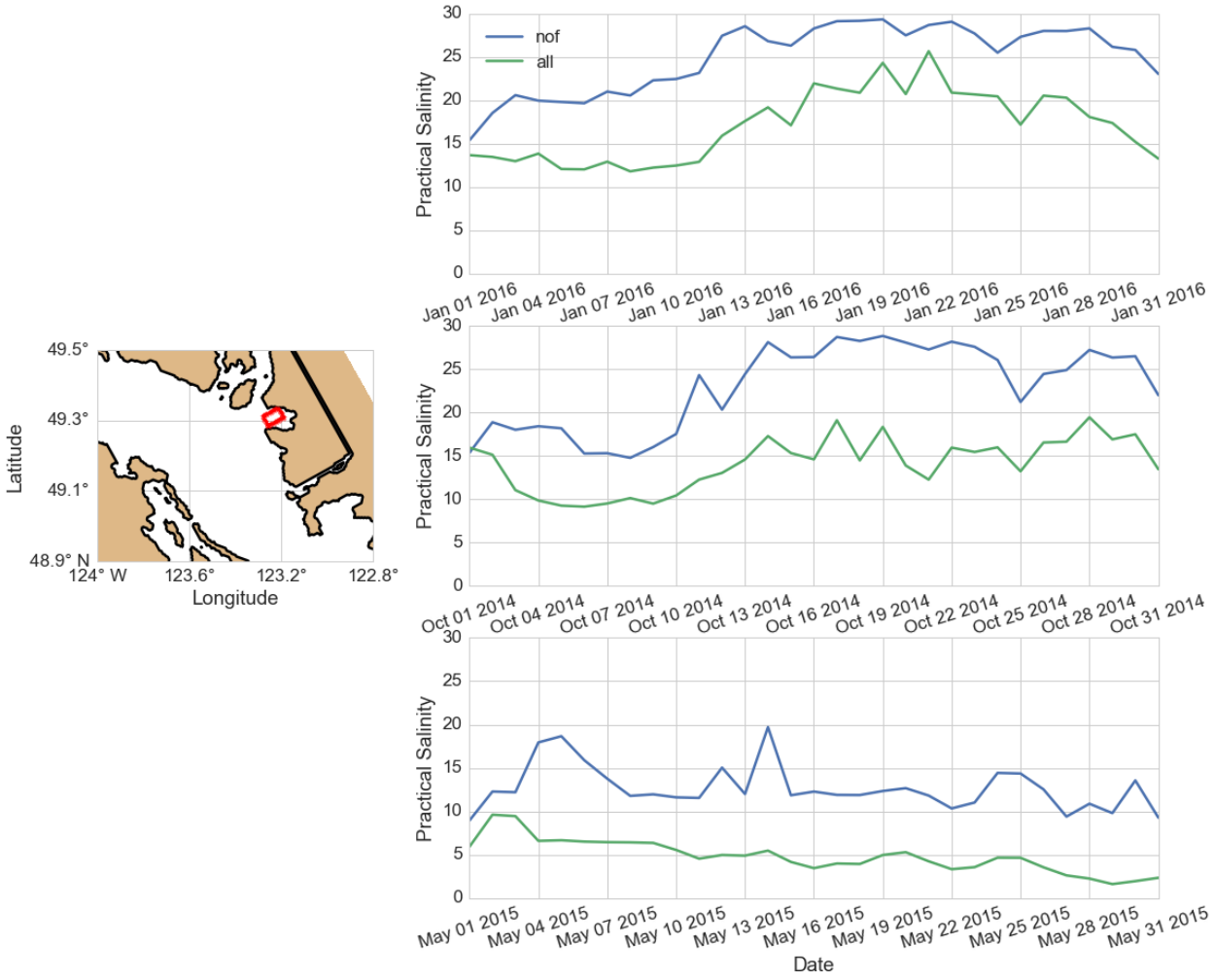

Figure F.1: Time series of averaged surface salinity in the English Bay. Left panel: map of part of the SoG and the red box is where surface salinity is averaged over in English Bay. Right panel: time series of averaged surface salinity within the red box in English Bay at instantaneous peak ebbs with the Coriolis force (all, green) and without the Coriolis force (nof, blue) during low (Jan, 2016), moderate (October, 2014) and high (May, 2015) river flow periods.

Appendix G

Centre Plume Location for the Other Two River Flow Periods

Wind impacts on the plume centre location during low and high river flow periods are shown (Figure G.1 and G.2). Similar with Figure 2.27, the movement of the centre of the plume location follows the winds and is significant when wind magnitude is stronger than 5 m s^{-1}.

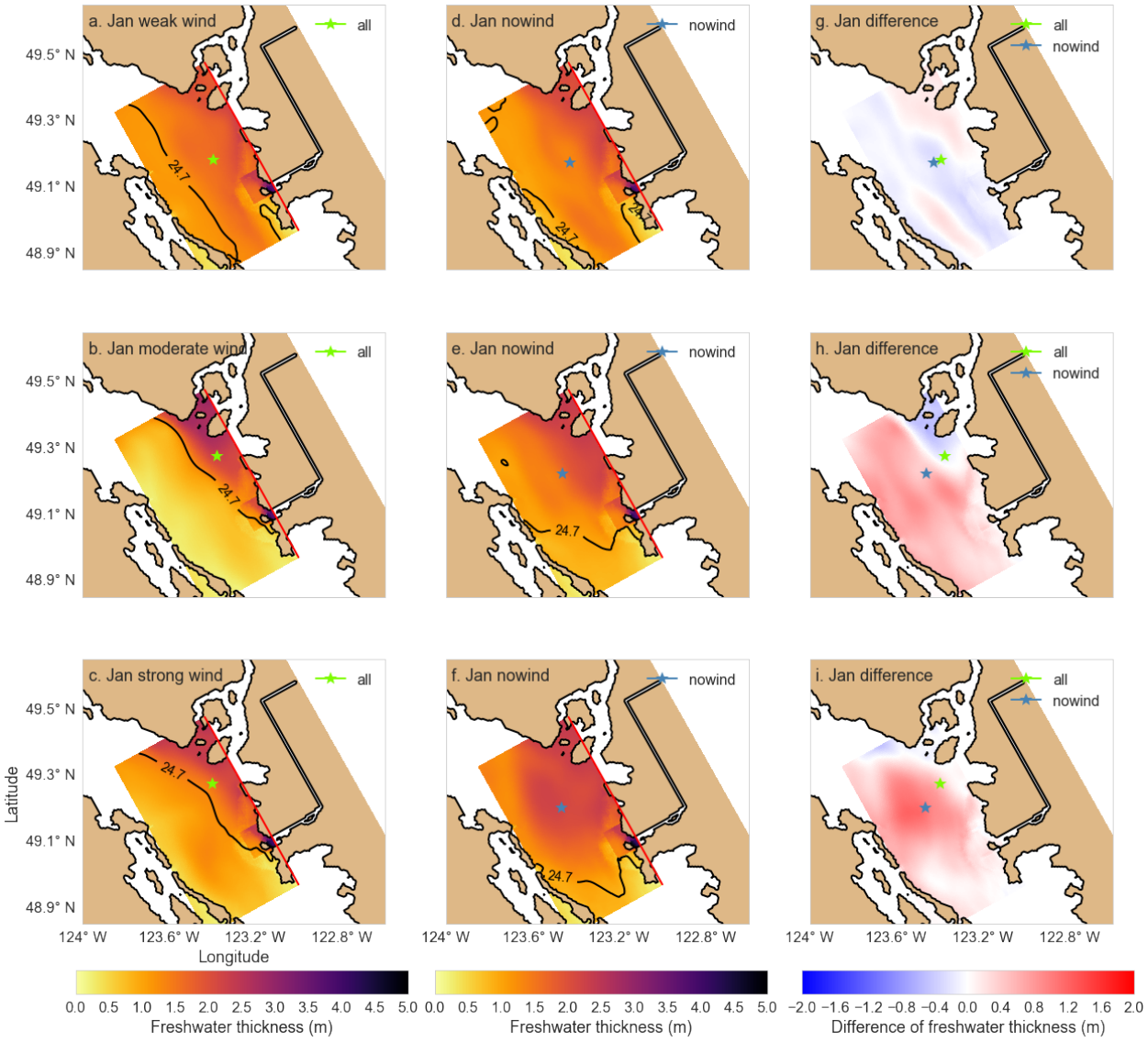

Figure G.1: Plume centre location with wind forcing and without wind forcing of wind events in January, 2016. Plume centre location (star) as well as freshwater thickness (2.15) spatial distribution for weak, moderate and strong wind events in January from top to bottom, and with wind forcing, without wind forcing, and their difference (With wind - without wind) from left to right. The change of the centre of the plume under weak wind conditions is small. Large changes occur during moderate and strong wind events.

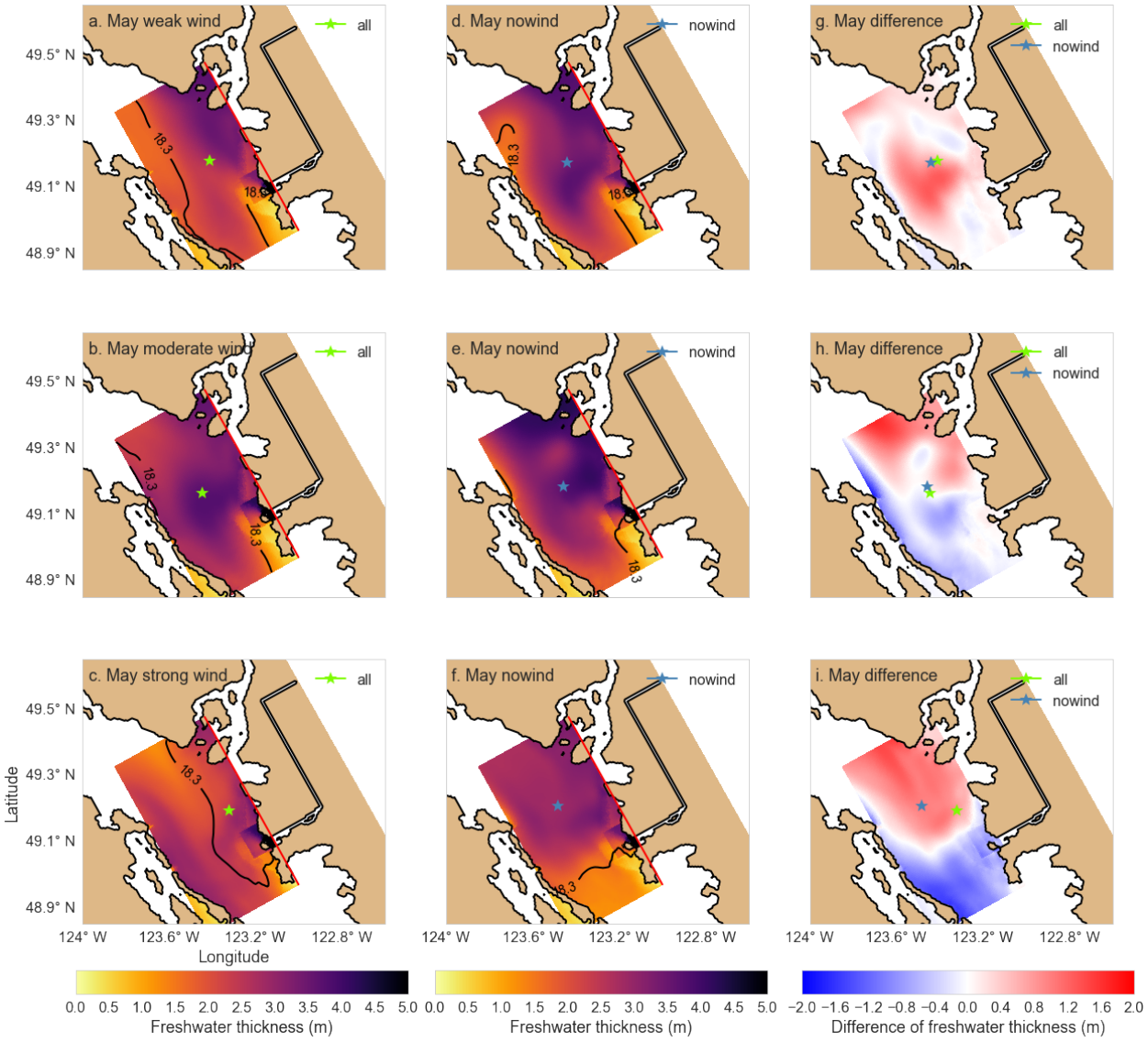

Figure G.2: Plume centre location with wind forcing and without wind forcing of wind events in May, 2015. Plume centre location (star) as well as freshwater thickness (2.15) spatial distribution for weak, moderate and strong wind events in May from top to bottom, and with wind forcing, without wind forcing, and their difference (With wind - without wind) from left to right. The change of the centre of the plume under weak wind conditions is small. Large changes occur during moderate and strong wind events.

Appendix H

Surface Drifter Tracks

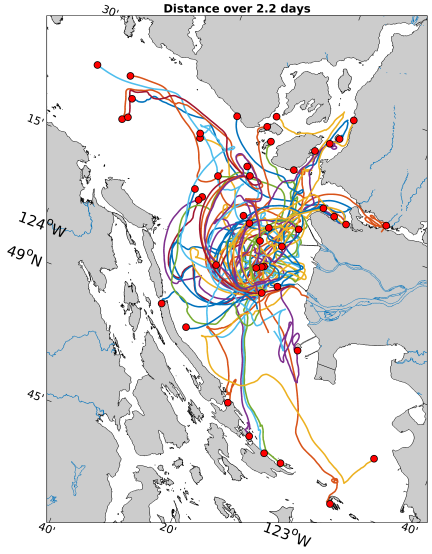

Figure H.1: 47 surface drifter tracks after 2.2 days released at Sand Heads. Red circle denotes the end position after 2.2 days duration. The drifters are released at random time during a tidal cycle. The tendency for most of the drifters is northward and the tracks pattern resemble a bulge-like circulation. Figure credit: Romain Di Costanzo and Rich Pawlowicz.